Bayesian shape optimisation of complex structures under stability criteria applied to brake systems

Pradeep Mohanasundaram

N°d'ordre NNT : 2021LYSEC26

THÈSE de DOCTORAT DE L'UNIVERSITÉ DE LYON

opérée au sein de
L'École Centrale de Lyon

École Doctorale ED 162
Mécanique - Énergétique - Génie Civil – Acoustique

Spécialité de doctorat : **Génie Mécanique**

Soutenue publiquement le 12/07/2021, par :
Pradeep Mohanasundaram

Bayesian shape optimisation of complex structures under stability criteria applied to brake systems

Optimisation de forme bayesienne de structures complexes sous critères de stabilité : application aux systèmes de freinage

---

Devant le jury composé de :

Baranger, Thouraya	Professor - Polytech Lyon, Université Claude Bernard Lyon 1 - President
Sébastien Berger	Professor - INSA Centre Val de Loire - Reviewer
Obayashi, Shigeru	Professor - Aerospace Fluid Engineering Laboratory, IFS, Tohoku University - Reviewer
Besset, Sébastien	Associate Professor - Laboratoire de Tribologie et Dynamique des Systèmes, École Centrale de Lyon – Supervisor
Shimoyama, Koji	Associate Professor - Fluid Engineering with Data Science Laboratory, IFS, Tohoku University – Supervisor
Gillot, Frédéric	Associate Professor - Laboratoire de Tribologie et Dynamique des Systèmes, École Centrale de Lyon – Supervisor

Université Claude Bernard – LYON 1

Président de l'Université	M. Frédéric FLEURY
Président du Conseil Académique	M. Hamda BEN HADID
Vice-Président du Conseil d'Administration	M. Didier REVEL
Vice-Président du Conseil des Etudes et de la Vie Universitaire	M. Philippe CHEVALLIER
Vice-Président de la Commission de Recherche	M. Petru MIRONESCU
Directeur Général des Services	M. Pierre ROLLAND

COMPOSANTES SANTE

Département de Formation et Centre de Recherche en Biologie Humaine	Directrice : Mme Anne-Marie SCHOTT
Faculté d'Odontologie	Doyenne : Mme Dominique SEUX
Faculté de Médecine et Maïeutique Lyon Sud - Charles Mérieux	Doyenne : Mme Carole BURILLON
Faculté de Médecine Lyon-Est	Doyen : M. Gilles RODE
Institut des Sciences et Techniques de la Réadaptation (ISTR)	Directeur : M. Xavier PERROT
Institut des Sciences Pharmaceutiques et Biologiques (ISBP)	Directrice : Mme Christine VINCIGUERRA

COMPOSANTES & DEPARTEMENTS DE SCIENCES & TECHNOLOGIE

Département Génie Electrique et des Procédés (GEP)	Directrice : Mme Rosaria FERRIGNO
Département Informatique	Directeur : M. Behzad SHARIAT
Département Mécanique	Directeur M. Marc BUFFAT
Ecole Supérieure de Chimie, Physique, Electronique (CPE Lyon)	Directeur : Gérard PIGNAULT
Institut de Science Financière et d'Assurances (ISFA)	Directeur : M. Nicolas LEBOISNE
Institut National du Professorat et de l'Education	Administrateur Provisoire : M. Pierre CHAREYRON
Institut Universitaire de Technologie de Lyon 1	Directeur : M. Christophe VITON
Observatoire de Lyon	Directrice : Mme Isabelle DANIEL
Polytechnique Lyon	Directeur : Emmanuel PERRIN
UFR Biosciences	Administratrice provisoire : Mme Kathrin GIESELER
UFR des Sciences et Techniques des Activités Physiques et Sportives (STAPS)	Directeur : M. Yannick VANPOULLE
UFR Faculté des Sciences	Directeur : M. Bruno ANDRIOLETTI

Contents

Résumé synthétique en Français

I - Introduction

Dans le cadre de cette thèse nous développons une approche générique pour définir l'optimisation de forme bayésienne de structures complexes sous critères de stabilité appliqués aux systèmes de freinage. L'idée de notre approche est qu'elle peut être facilement adaptée à tout problème d'optimisation de forme avec des fonctions de type boîte noire coûteuses pour lesquelles plusieurs fonctions objective peuvent être définies. Nous nous concentrons largement sur deux objectifs dans cette thèse, mais néanmoins, nous accordons une attention particulière à fournir des capacité à s'adapter à plus de deux objectifs. En référence au domaine d'étude complexe, l'objectif est par ailleurs de définir une stratégie de maillage automatisé robuste avec des formulations isogéométriques. Pour la définition préliminaire de l'approche isogéométrique, nous nous concentrons sur une simple approche de paramétrage qui peut être adaptée à un paramétrage plus complexe. Nous appliquons ensuite notre approche au problème de crissement de frein avec traitement nécessaire de la formule de contact et de friction sous formulation isogéométrique.

II - Modélisation

Les méthodes des éléments finis sont des méthodes numériques largement utilisées pour résoudre des équations différentielles, où physiquement une solution continue sur un domaine complexe Ω est discrètisée par éléments finis sur le domaine ${}_h\Omega \subset \Omega$. Cela nécessite la définition de formulation variationnelle/faible pour l'approximation de la solution. La formulation variationnelle affaiblit l'exigence de solution à définition intégrale plutôt que de satisfaire la solution au sens différentiel avec une forte continuité connue comme forme forte. Nous nous en tenons principalement au point de vue de l'approche de Galerkin définissant la forme faible où les fonctions de test peuvent également être considérées comme les fonctions associées au travail virtuel et généralise donc également le principe de travail virtuel. Pour notre application dans cette thèse qui implique le contact et le frottement, nous avons principalement traité la dynamique autour d'un point fixe où les perturbations autour de ce point sont considérées comme n'ayant pas de changement relatif à l'interface de contact. Cela signifie que nous traitons en grande partie l'hypothèse d'une petite déformation et d'aucun glissement relatif, d'où les non-linéarités spatio-temporelles associées aux coordonnées matérielles qui sont ignorés. Cela signifie également qu'il n'y a pas d'intérêt pour la variation temporelle de $\Omega \times [0, \mathfrak{T}]$ qui n'est donc pas prise en compte

dans les définitions suivantes qui sont données pour un temps arbitraire. Le but est également de définir la formulation faible du contact et du frottement qui modélise notre application.

III - Modélisation numérique du contact et du frottement

Les phénomènes de contact et de frottement sont de nature très discontinue. Cela peut être mathématiquement difficile pour gérer ces discontinuités et donc au travers de la régularisation de ces discontinuités, le modèle de contact et de frottement doit être capable de décrire un comportement réaliste. La prise en compte de telles considérations pour la modélisation numérique est également important pour les applications sensibles aux caractéristiques de contact et de frottement. Nous nous concentrons sur l'approximation des définitions de contact et de frottement avec des éléments finis dans ce chapitre. Nous donnons une brève introduction à la définition de la dimension finie de l'espace d'approximation ${}_hV$ dans le contexte à la fois de la des méthodes éléments finis classique et des méthodes isogéométriques. Nous nous concentrons principalement sur l'application à l'approche isogéométrique pour définir le contact et les formulations de friction, bien que des parallèles puissent être établis entre les deux. Nous discutons aussi de la formulation de contact nœud à nœud largement utilisée pour des éléments finis classiques pour étendre l'approche de collocation dans les formulations isogéométriques.

IV - Analyse de sensibilité

L'analyse de sensibilité définit essentiellement l'analyse de sensibilité d'une fonction par rapport à des variations de ses paramètres. L'analyse de sensibilité globale pour les paramètres de forme impliqués dans notre étude a été réalisée en utilisant la méthode basée sur la Variance qui vient de la décomposition de Hoeffding-Sobol. Cette méthode est basée sur la décomposition de la variance d'une fonction à sa variance associée aux paramètres et à l'interaction entre les paramètres. Par conséquent, plus la variance en sortie d'une fonction induite par un paramètre, plus sa sensibilité sera élevée. La méthode est appliquée via un échantillonnge de Monte-Carlo basé sur un plan latin hypercube pour l'efficacité. En effet, pour évaluer le comportement global et d'augmenter la précision pour la base de Monte-Carlo donnée l'estimation sur le cas asymptotique présumé demande un grand nombre de calcul, ce qui est tout simplement impossible à converger en temps raisonnable compte tenu du coût numérique pour évaluer les critères de stabilité C_s . Ainsi, un métamodèle basé sur une régression par processus gaussien a été utilisée. Les critères de stabilité donnés par le métamodèle peuvent donc être exprimés par $\hat{C}_s \approx C_s$.

V - Optimisation de forme - paramétrage

Dans cette section, nous détaillons le paramétrage de la forme définie par des NURBS. Nous précisions les contraintes posées sur le pad. Nous fournissons également une brève description du paramétrage et de la stratégie de raffinement pour le domaine du système disque-pad $\Omega^{(d-p)}$.

VI - Optimisation Bayesienne

L'optimisation bayésienne est une stratégie efficace pour réduire le coût des calculs des fonctions objectives coûteuses. Nous commençons les explications suivantes sans définir les spécificités de la modélisation de la probabilité $\mathcal{P}$ qui est donnée comme connu et on considère l'optimisation d'une seule fonction $f(x)$ tel que le problème revienne à $\min_{x \in \mathcal{X}} f(x)$. L'idée est basée sur la règle de Bayes où la connaissance a priori $\mathcal{P}(\mathcal{H})$ de l'hypothèse $\mathcal{H}$ et la probabilité de la preuve $\mathcal{E}$ étant donné l'hypothèse, $\mathcal{P}(\mathcal{E}|\mathcal{H})$, sont utilisés pour déduire la connaissance de l'hypothèse étant donné la preuve, $\mathcal{P}(\mathcal{H}|\mathcal{E})$, où la proportionnalité peut être exprimé comme

$$\mathcal{P}(\mathcal{H}|\mathcal{E}) \ \propto \ \mathcal{P}(\mathcal{E}|\mathcal{H})\mathcal{P}(\mathcal{H})$$

Par conséquent, $\mathcal{P}(\mathcal{H}|\mathcal{E})$ définit l'inférence bayésienne. Dans notre contexte, l'hypothèse $\mathcal{H}$ correspond à la fonction $f(x)$ et la preuve $\mathcal{E}$ correspond à

$$\mathcal{F}_{1:n} : \{f(x1), f(x2), ..., f(xn)\}$$

où $f(x)$ est échantillonné sur $\mathcal{X}_{1:n} : \{x1, x2, ..., xn\}$, avec $\mathcal{D}_{1:n} : \{X1 : n, F1 : n\}$. Ceci est typiquement connu sous le nom de paysage d'espace de fonctions, puisque la probabilité est définie sur l'espace des fonctions. Il peut être difficile de conceptualiser une tel paysage avec des fonctions, mais on peut imaginer l'existence d'une fonction au sens purement probabiliste telle qu'un tirage au sort de la distribution de probabilité est une fonction. La relation ci-dessus peut s'exprimer dans ce cas comme suit:

$$\mathcal{P}(f(x)|\mathcal{D}_{1:n}) \propto \mathcal{P}(\mathcal{D}_{1:n}|f(x))\mathcal{P}(f(x))$$

La connaissance à priori sur une fonction, $\mathcal{P}(f(x))$, est typiquement modélisé par des corrélations spatiales. En d'autres termes, une croyance a priori est définie sur l'espace des fonctions de telle sorte que les fonctions dans l'espace présentent en grande partie certaines caractéristiques de corrélation totale. Avec $\mathcal{P}(f(x))$ déjà défini, et étant donné la vraisemblance du points échantillonnés sur la fonction, $\mathcal{P}(\mathcal{D}_{1:n}|f(x))$, la connaissance a posteriori de la fonction, $\mathcal{P}(f(x)|\mathcal{D}_{1:n})$, peut être déduite de la relation ci-dessus. La connaissance postérieure $\mathcal{P}(f(x)|\mathcal{D}_{1:n})$ est ensuite utilisée pour déduire le prochain point x_{n+1} à échantillonner, en fonction de la stratégie définie pour l'échantillonnage en optimisation. Le point échantillonné x_{n+1} est alors utilisé pour mettre à jour la croyance de l'antérieur $\mathcal{P}(f(x))$ à la lumière

de $\mathcal{D}_{1:n+1}$, et avec la vraisemblance $\mathcal{P}(\mathcal{D}_{1:n+1}|f(x))$ pour en déduire un nouveau postérieur $\mathcal{P}(f(x)|\mathcal{D}_{1:n+1})$, qui caractérise l'apprentissage. Le processus est mené par la suite dans la perspective de trouver un point optimal pour la fonction grâce à l'apprentissage actif, modélisé par l'optimisation bayésienne.

VII - Optimisation de forme d'un système disque-pad

Tous les résultats présentés dans la section suivante ont été obtenus pour les objectifs définis plus haut. Le méta-modèle $\mathcal{GP}$ a été défini pour les calculs trop coûteux de la fonction objectif C_s où nous avons utilisé une fonction de tendance polynomiale linéaire pour définir la moyenne a priori, la fonction de covariance ayant été définie par le noyau Matern 5/2 considérant une corrélation spatiale anisotrope. Ainsi, dans le contexte de l'optimisation multiobjectifs (MOBO), les points de remplissage ont été déterminés principalement pour l'évaluation de la fonction C_s. Même si dans notre cas, le modèle $\mathcal{GP}$ pour MOBO n'a été défini que pour un des objectifs, il peut être étendu pour une résolution avec plusieurs $\mathcal{GP}$. Nous présentons une brève description des caractéristiques du front de Pareto obtenu pour MOBO via un critère EV. Les discontinuités apparaissent dans ce front de Pareto en raison de la définition locale de l'amélioration, puisque l'optimisation nécessite plusieurs valeurs de référence où les discontinuités se produisent, avec dans le même paramètre d'optimisation pour définir la référence de Nadir (NDS) pour l'algorithme NSGA-2. Cela signifie que les individus d'une génération donnée de NSGA-2 sont définis avec leur référence respective des valeurs à améliorer, et le tri et le critère de nichage (niching) non dominés sont définis sur l'espace objectif dans son ensemble - ce qui est moins coûteux en calcul étant donné la définition simultanée de l'amélioration qui utilise plusieurs valeurs de référence.

VIII - Conclusion

Nous avons proposé une stratégie efficace pour gérer l'optimisation de la forme des systèmes de freinage au travers d'une simple représentation disque-pad pour la réduction du bruit de crissement. La formulation faible du contact et du frottement spécifique pour la modélisation des instabilités induites par le frottement par la CEA a été défini avec une approche isogéométrique pour la discrétisation. Ce type d'étude peut être envisagée pour les systèmes de freinage tels qu'on les trouve dans l'automobile ou l'industrie aéronautique, mais aussi pour d'autres applications avec des phénomènes de frottement, comme les systèmes d'embrayage. Grâce à la CEA, le critère de stabilité C_s a été défini comme une fonction de type boîte noire pour caractériser les instabilités indépendantes du coefficient de frottement pour l'optimisation de forme, où des techniques de calcul parallèle et de réduction de modèle dynamique ont été utilisées pour réduire le coût de calcul du critère de stabilité.

1 Introduction

As the main objective of this thesis, we develop a generic framework to define Bayesian shape optimisation of complex structures under stability criteria applied to brake systems. The idea of generic framework is that it can be easily adapted to any shape optimisation problem with expensive black-box functions for which multi-objective Bayesian optimisation can be defined. We largely focus on two objective problems in this thesis, but nevertheless, we give careful attention to provide flexibility in adapting to more than two objectives. With reference to complex domain, the focus was to define a robust automated meshing strategy with Isogeometric approach. For the preliminary definition of Isogeometric approach, we focus on a simple parameterisation approach which can be adapted to more complex parameterisation strategies for the evolution of the frame-work. We then apply the framework to the problem of brake-squeal with necessary treatment of contact and friction formulations with Isogeometric approach.

Typically in structural dynamics, characteristics of a system can be largely described by its mass and stiffness properties which are in turn defined by its underlying material and geometric properties. Hence, to optimise a system from the perspective of structural dynamics requires optimisation of its material and geometric properties. Optimising geometric properties can be largely defined by shape optimisation or topology optimisation, where if a geometry is parameterised, parametric optimisation can also be achieved. The idea of shape optimisation is intuitive, where we optimise the boundary $\partial\Omega$ of a domain Ω for some optimum outcome, given that the topology of Ω is fixed. Given a topology, admissible Ω can be expressed by the set $\mathcal{X}_{ad}$. Mathematically, the problem of shape optimisation can be expressed as $\underset{\partial\Omega\in\mathcal{X}_{ad}}{min}\ f(\partial\Omega)$ where it defines functional optimisation over admissible domains. With classical gradient-based methods, this requires the definition of $\frac{\delta f(\partial\Omega)}{\delta\partial\Omega}$ which expresses the derivative of $f(\partial\Omega)$ with respect to the domain boundary variation $\delta\partial\Omega$ – typically called as shape derivative. This is essentially the idea of non-parametric shape optimisation which involves the notion of optimising $\partial\Omega$ in a continuum sense, where Hadamard boundary variation method is typically considered [1, 2, 3]. Hadamard boundary variation models the continuum variation of $\partial\Omega$ by defining perturbation on $\partial\Omega$ through continuous vector field such that the shape variation is homeomorphic. Hence, $\delta\partial\Omega$ can be defined from the first-order Taylor approximation for the perturbation of $\partial\Omega$. The mathematical definition of continuous domain eventually needs to be discretised by numerical methods, where the shape derivative of $f(\partial\Omega)$ can then be evaluated to infer variation on $\partial\Omega$ at every iteration. Typically, Ω is

discretised by finite element methods as ${}_h\Omega = \bigcup {}_{el}\Omega$[1] to solve f and hence, the variation of $\partial\Omega$ evaluated from gradient descent is defined on the vertices of the mesh boundary. This means that it can be convenient to use the same mesh for defining $\frac{\delta f(\partial\Omega)}{\delta\partial\Omega}$ and for solving f. The method is mathematically rigorous and the definition of $\frac{\delta f(\partial\Omega)}{\delta\partial\Omega}$ may not be often straight-forward with f expressed as partial differential equation. In contrary, Ω can be parameterised as part of CAD description or by discretisation of Ω as ${}_h\Omega$, where a domain can be expressed in a discrete sense with finite parameters. Typically, the description of ${}_h\Omega$ follows from the natural extension of finite element approach in solving differential equations, where the coordinates of the boundary nodes are interpreted as shape parameters [4]. Given a finite set of parameters $\boldsymbol{p}$ parameterising $\partial\Omega$, the shape optimisation problem can be expressed as $\underset{\boldsymbol{p}\in\mathcal{X}_{\boldsymbol{p}}}{min} f(\boldsymbol{p})$. Hence, the definition of shape derivative in finite dimension is defined by $\partial\boldsymbol{p}$ [5, 6]. The definition of shape through parameters limits the optimisation of shape to $\mathcal{X}_{\boldsymbol{p}} \subset \mathcal{X}_{ad}$, where non-parametric shape optimisation is relatively less bounded.

With gradient descent, naturally the question of local optimum occurs, where it may not be a suitable strategy to explore large design space efficiently in directly optimising a function for global optimum. While this can be overcome by multiple initialisations, the population based nature of evolutionary algorithms have intrinsic advantage to overcome local optimum [7, 8]. One can argue that the meta-heuristic characteristics of evolutionary algorithms can demand more number of evaluations for convergence to optimum. This is where the idea of Bayesian optimisation [9, 10] can be helpful, where evolutionary algorithms can be made to be efficient by avoiding direct evaluation of an expensive function through metamodels. Further, gradient information for black-box functions cannot be well defined, where for gradient descent to be efficient, this demands the function to have certain characteristics of smoothness and continuity. In conclusion, gradient-based methods directly defined for optimising a function in shape optimisation can be very restrictive to be called a generic strategy. Hence, we focus on evolutionary algorithms which are very robust and suitable for optimising black-box functions. The extension of evolutionary algorithms to multi-objective problems is also straight-forward when fitness is defined for optimality in multi-objective context [11, 12, 13, 14]. The population based nature of evolutionary algorithms allow to consider a set of optimal individuals, where individuals may not be necessarily from the same part of the design space. This allows multiple optimal designs to be considered as population to represent wider spread of design variations in a design space. Nevertheless, optimality in the context of multi-objective optimisation is defined with Pareto-optimal set of solutions where in this case, population based evolutionary algorithms have intrinsic advantage to deal with set of solutions.

[1] ${}_{el}\Omega$ represents an element discretising Ω

Though the idea of non-parametric shape optimisation using evolutionary algorithms is not clear or largely considered, definition of parametric shape optimisation is straightforward where cross-over and mutation operations can be defined on finite discrete set of parameters. This demands parameterisation of a domain Ω or at least its boundary $\partial\Omega$ by parameters as part of CAD description or considering finite element discretisation ${}_h\Omega$. With classical finite element methods, CAD description of Ω and its subsequent finite element discretisation ${}_h\Omega$ are completely different representations, where Ω is typically defined by splines parameterisation purely in the perspective of CAD and ${}_h\Omega \subseteq \Omega$ follows the description of Ω with discrete set of elements defined typically with Lagrange polynomials. [2]

With shape optimisation of Ω defined by parameters of CAD description, this demands a robust meshing strategy to achieve ${}_h\Omega$ from Ω at every iteration. Depending on the domain and the function to be approximated on the domain, this can be time-consuming and often involves manual intervention. With shape optimisation defined directly on ${}_h\Omega$ for coordinates of the nodes, this requires adapting mesh with the variation of boundary nodes, where mesh distortion can be a challenging issue. The later approach was largely found to be inefficient since finite element models can have large number of nodes to curtail approximation error, where taking in to account of the boundary nodes can lead to large number of parameters in optimisation. Further, C_0 continuity between the elements can lead to non-smooth boundary in optimisation [15]. Hence, the idea of defining shape optimisation with parameters of smooth CAD description was found to be a more robust approach. Early efforts of CAD description were primarily focused on polynomial representation for smooth definition of domain boundary [16]. This method has its limitations especially when design representation is restricted to family of polynomials where higher order polynomials can lead to spurious oscillation, and further, it also lacks local control of design for a given polynomial representation. The development of spline parameterisation was soon found to be very efficient for CAD description with its mathematical properties [5, 17]. Most of the advantages of splines stem from the property of piece-wise polynomials with possible continuity definition higher than C_0, where complicated shapes can be defined with low-order polynomials. Further, the mathematical properties of spline basis have less oscillation between interpolations, where this property is preserved even for higher order splines. This is unlike the classical Lagrange polynomials where oscillations become more severe as order of the polynomials grow. The piece-wise representation also allows for local control of geometry which is very advantageous for iterative design optimisation, while preserving continuity at intersection between

[2] The definition of Ω in a discrete sense as ${}_h\Omega$ is purely considered from the perspective of domain definition. Even though the parameterisation in CAD with NURBS can be interpreted in a discrete sense with finite number of knots and control points as respectively equivalent to elements and nodes of classical finite elements, given that the NURBS parameterisation completely encompasses the domain Ω, we consider ${}_h\Omega = \Omega$ with NURBS parameterisation. Nevertheless, from function space point of view, parameterisation of Ω with NURBS is defined by finite number of basis functions.

piece-wise polynomials. Hence, splines are largely considered as suitable choice for parameterising geometry and widely adapted in CAD community, which is followed by wide adaptation for shape optimisation. This still means lack of coherence between CAD description of geometry defined by splines and analysis description of geometry defined by piece-wise Lagrange polynomials. This lack of coherence is inconvenient in optimisation, since solution evaluated at nodes has no relation with CAD parameters unless explicitly defined, along with the lack of robustness in achieving ${}_h\Omega$ from Ω. This can be largely attributed to wide adaptation of Lagrange polynomials in finite element method community.

Finite element method is principally based on approximation of solution in finite dimensional function space which is classically defined by Lagrange polynomials that parameterises ${}_h\Omega$. This brings the idea of Isogeometric approach [18], where instead of replacing CAD description of Ω parameterised by splines with completely different representation of ${}_h\Omega$ through Lagrange polynomials to define function space for approximation, the basis functions of splines can be directly defined for approximation given that sufficient refinement is made over initial CAD parameterisation to curtail approximation error, where refinement over initial CAD parameterisation to define analysis-suitable parameterisation can be easily achieved in the same parametric space of CAD description. This completely preserves the geometry and hence, ${}_h\Omega = \Omega$. The definition of function space with splines is mainly possible because the underlying polynomials of splines are well-suited to define function space as subset of Sobolev space for energy functionals. Further, the advantages of splines over Lagrange polynomials in CAD are also reflected in approximation properties of solution, such as reduced oscillation in interpolation and providing higher solution continuity between knots[3]. This also means that optimisation can be defined directly over the control points of analysis-suitable parameterisation in relation to solution at the control points, where with higher-order continuity, it can avoid non-smooth shape definition of boundary that classical finite element methods with C_0 continuity suffer from.

The parameterisation with splines can be expressed as $\boldsymbol{X} : \hat{\Omega} \rightarrow \Omega$ which defines mapping from parametric space $\hat{\Omega}$ to physical space Ω, where isoparametric approach of classical FEM comes as an intrinsic property with Isogeometric approach. Hence, given a CAD description with suitable NURBS parameterisation, analysis-suitable parametrisation can be defined robustly. But the notion of suitable initial parameterisation to define analysis-suitable parameterisation is important and can be said as major limitation of at least body-fitted Isogeometric approach which we consider in this thesis [19]. In reality, initial parameterisation of CAD description cannot always be suitable to define analysis-suitable parameterisation, since there can be more efficient ways to parameterise a geometry in the perspective of CAD which necessarily may not be suited to define analysis-suitable parameterisation. One of the fundamental properties with body fitted approach to achieve analysis-suitable

[3]Knots can be interpreted as equivalent to elements of classical FEM.

parameterisation is that the initial parameterisation of the domain should be defined by complete mapping from the parametric space, which can be very restrictive for CAD description of complex domains. Hence, often in CAD, complex domains are defined through union of trimmed domains or expressing a domain as a trimmed domain, where with a trimmed domain, the mapping from parametric space is not completely defined over the domain [20]. Large part of research in Isogeometric community has been focused to take in to account of trimmed domains directly through Immersed methods rather than to define suitable initial parameterisation with which refinement could be achieved [21, 22]. The flexibility of immersed methods which can be generic to consider any arbitrary topology comes at the cost of accuracy, while the accuracy of body-fitted approach comes at the cost of flexibility, where body-fitted approach can be hard to generalize for arbitrary topology. This is nothing less to say that advanced parameterisation strategies are also being developed with body-fitted approach, typically by non-linear optimisation to achieve injective mapping [23, 24] or decomposing a topology with patches [25, 26]. We do not focus on the scope of defining advanced parameterisation strategies with body-fitted Isogeometric approach, where we use the explicit linear discrete Coon's patch method [27] in this thesis. This means that only shapes which satisfy injective mapping from parametric space with Coon's patch method is considered for shape optimisation in this thesis. We are aware that this can downsize the design space, but on the other hand, this also implicitly helps to avoid shapes which are too conceptual in our application, which stems from the nature of linear Coon's patch method. The idea is that for future evolution of the frame work, more advanced parameterisation can be adapted and hence also more conceptual shapes can be considered.

For this thesis, we consider the frame work of Bayesian optimisation, where we also discussed the limitations of direct gradient descent for shape optimisation. Given a design space with $\mathfrak{l}$ parameters, if $\mathfrak{n}$ discrete values are considered with each parameters to define combinations, it leads to $\mathfrak{l}^{\mathfrak{n}}$ combinations, where the idea is to show the scale of increase in design space. Firstly, the idea of parametric shape optimisation restricts the design space to subset of admissible shapes as $\mathcal{X}_{\boldsymbol{p}} \subset \mathcal{X}_{ad}$. Even with finite set of parameters that parameterises a shape to define sufficient shape variations in optimisation, it can be difficult to explore the set $\mathcal{X}_{\boldsymbol{p}}$ efficiently with computationally expensive functions. Further the idea of gradient-descent in multi-objective optimisation can be even more limiting for the definition of Pareto-optimal solutions, where it demands a multi-objective optimisation problem to be posed as multiple single-objective optimisation problems which can be optimised with gradient descent [28, 29, 30]. The expression of multi-objective optimisation problem as set of single-objective optimisation problems looses the explicit definition of optimality in multi-objective context, where Pareto-optimal solutions are implicitly achieved with single-objective optimisations. This implicit nature of optimising for Pareto-optimal solutions typically demands prior idea of the Pareto-front to select parameters for expressing a multi-objective optimisation problem as single-objective optimisation problems, especially for diversity of Pareto-optimal solutions. The single-objective

optimisation problems can also be solved by evolutionary algorithms which can help for global convergence, but nevertheless, it still preserves the limitations owing to the implicit nature of optimising for Pareto-optimal solutions[31, 32]. But instead of using evolutionary algorithms in solving for Pareto-optimal solutions implicitly with multiple single objective optimisations, evolutionary algorithms can be defined to explicitly solve for Pareto-optimal solutions [33]. This is mainly because the population based nature of evolutionary algorithms can handle set of solutions, where the fitness of individuals can be selected to favour Pareto optimality in multi-objective context. We consider NSGA-2 in this thesis as the evolutionary algorithm for multi-objective optimisation[11].

The major limitation with evolutionary algorithms is the stochastic nature of genetic operators to advance solutions towards optimum at least in the context of single objective optimisation, rather than a more mathematically sounding approach of gradient-descent. The stochastic nature of genetic operators typically crave more iterations in evolutionary algorithms to converge, which can be unrealistic with expensive functions, for which the idea of Bayesian optimisation can be helpful. Bayesian optimisation is essentially based on Bayes probability of prior and posterior probabilistic inference, where the idea is that a function can be approximated with some prior knowledge and given the observed data on the function, posterior knowledge can be inferred over the function with Bayes theorem [9, 10]. With the inference of posterior knowledge, a new infill point can be sampled to move towards optimum. The new evaluation is then used to update the prior belief to infer a new posterior, where eventually with several iterations, the idea is to find global optimum. The probabilistic inference of prior and posterior are achieved through meta-modelisation where we focus on Gaussian-process regression/Kriging [34, 35]. With Gaussian-process regression, prior and posterior inference for a given argument is defined by univariate Gaussian distribution, where the mean reflects the prediction and the variance to the uncertainty of the prediction in the metamodel. With the inference of posterior, naturally choice between exploration and exploitation arises given the prediction and the variance of the prediction, where wide range of acquisition functions exist with different sampling characteristics, typically to balance between exploration and exploitation [36]. In essence, acquisition functions define improvement with respect to a reference point which is typically the known optimum of the function, where at every iteration of Bayesian optimisation, typically an acquisition function is optimised to choose an infill point. For single objective Bayesian optimisation, optimising an acquisition function typically involves univariate Gaussian distribution and improvement is simply given by distance metric. Acquisition functions in multi-objective Bayesian optimisation focus on sampling for improvement with respect to empirical Pareto-front, where for higher dimensions of objective space, the natural extension of distance metric in one dimension corresponds to hypervolume metric [37, 38]. While most state-of-the-art acquisition functions in multi-objective Bayesian optimisation scalarize the measure of improvement with hypervolume metric, it is well known that the evaluation of hypervolume in higher dimensions is computationally demanding

[39]. The definition of improvement with scalar value also looses the expression of optimality in multiobjective context, even though the scaler value implicitly defines improvement in multi-objective context. We choose the approach of expressing improvements in multi-objective context directly with Pareto-optimal solutions where infills points can be chosen explicitly for parallelisation in the scope of improving diversity simultaneously with each iteration [40].

We consider the application of brake-squeal in this thesis. Brake squeal phenomenon is one of the major challenges in the development of brakes concerning NVH, where squeal noise is typically characterised by a frequency range of 1-16 KHz. The problem of brake squeal analysis has been studied for a very long time with one of the early reviews from [41] and is still a challenging issue due to the immense complexities involved, where it constitutes factors from tribology of contact interface to stability in the context of non-linear and non-smooth dynamics. It is because of this very nature, it is widely accepted that there may not be a single unified theory to define brake squeal phenomenon. Some of the complexities can be attributed to modelling friction [42], where even models based on simple macroscopic view (Coulomb's law) can give rise to non-smooth non-linearities which can be hard to model analytically and numerically. The early analyses were largely based on lumped models (mass-spring) where the discussions were primarily based on analytical solutions [43, 44]. These models were quite sophisticated and some with large degrees of freedom, which greatly improved the understanding of friction induced vibration. One of the conclusive evidence was that instability occurs even at constant coefficient of friction with the coupling of at least two degrees of freedom by friction, where the nature of instability was known to be flutter instability [45]. Flutter-type dynamic instability defines self-excitation behaviour in the presence of non-conservative force. In structural dynamics, this is understood as coalescence of modes, where two modes exist at a same frequency leading to self-excitation between the modes under favourable conditions in the presence of non-conservative force. Friction-induced dynamic instabilities are highly nonlinear phenomena which can be computationally expensive when defined through transient analyses and hence, unrealistic to be considered for optimisation. Instead of explicitly modelling instability inferred as limit-cycle with transient analysis, instability can be modelled through analysing the stability of fixed point for the dynamical system. This is mainly possible with the hypothesis of modelling the dynamical system with contact and friction as time-independent linear dynamical system around a fixed point, which otherwise requires satisfying non-holonomic constraints with strong time dependence [46, 47]. Hence, the stability of such linearized systems around a fixed point can be defined through its eigenvalues, commonly known as Complex-Eigenvalue Analysis (CEA) [48, 49, 50]. As a complex phenomenon, many parameters can be studied and optimized for squeal noise during its design phase [51, 52]. We focus on shape of the system [3], which has not been widely considered. Through CEA, we define a black-box function which is adversely expensive for computation, to describe a criterion for stability in shape optimization. For evaluation of the expensive black-box function,

we define a parallel computation strategy through dynamic model reduction. In this thesis, we consider shape optimisation of braking system through a simple disc-pad representation, where the simple system allows to make interesting studies by avoiding the complexity of boundary conditions present in a real braking systems.

Following introduction, in the second chapter, we detail continuum description in the scope of structural dynamics for modelling flutter-ype dynamic instability induced by friction. We also extend the definitions to brake squeal applications and define a criteria to characterise squeal for optimisation. In the third chapter, we focus on modelling contact and friction definitions with Isogeometric approach. We also provide a brief discussion of Isogeometric approach in relation to classical finite element approximation space. In the fourth chapter, we discuss sensitivity analysis with the considered approach and expose results for the application of brake-squeal. In the fifth chapter, we define shape parametrisation with NURBS for achieving shape optimisation, where the idea is to extend the NURBS parameterization for Isogeometric analysis. We introduce Bayesian optimisation in the seventh chapter and it's extension to multi-objective Bayesian optimisation, followed by seventh chapter for optimised results in our application and with the last chapter being the conclusion.

2 Modelisation

Finite element methods[1] are widely used numerical methods in solving differential equations, where physically a continuum solution on a complex domain Ω is discretised through finite elements, where the discretised domain ${}_h\Omega \subset \Omega$. This requires the definition of variational/weak formulation for the approximation of solution. The variational formulation weakens the requirement of solution with integral definition rather than satisfying the solution in differential sense with strong continuity known as strong form. We primarily stick with the view point of Galerkin's approach for defining the weak form where the test functions can also be considered to be the functions associated with virtual work and hence also generalises for the principle of virtual work.

For our application in this thesis which involves contact and friction, we primarily deal with dynamics around fixed point where perturbations around a fixed point are considered to have no relative change at the contact interface. This means that we largely deal with the assumption of small deformation and no relative sliding, and hence, the spatio-temporal non-linearities associated with the material coordinates are ignored. This also means that there is no interest in temporal variation of $\Omega \times [0, \mathfrak{T}]$ and hence not considered in the following definitions which are given for an arbitrary time. Further, the goal is also to define weak formulation of contact and friction which models our application.

2.1 Initial-boundary value problem

The continuum description of an initial-boundary value problem in structural dynamics can be expressed as

$$\begin{aligned} \rho\ddot{\boldsymbol{u}} + \nabla.\boldsymbol{\sigma}(\boldsymbol{u}) &= \boldsymbol{f} \quad \text{in} \quad \Omega \\ \boldsymbol{u} &= 0 \quad \text{on} \quad \Gamma_D \\ \boldsymbol{\sigma}(\boldsymbol{u}).\hat{\mathbf{v}}_n &= \boldsymbol{t}_N \quad \text{on} \quad \Gamma_N \end{aligned} \tag{2.1}$$

where $\boldsymbol{u} : \Omega^3 \to \mathbb{R}^3$, $\{\Gamma_N, \Gamma_D\} \subset \partial\Omega$, $\Gamma_N \bigcap \Gamma_D = \emptyset$, with $\partial\Omega$ defining the boundary of Ω, and $\hat{\mathbf{v}}_n$ defining the normal unit vector on $\partial\Omega$. Under Isotropic material consideration, the constitutive equations can be defined as

[1] By the definition of finite element methods, we also include Isogeometric method as a class of finite element methods unless specifically stated as classical finite element methods by which we distinguish the two approaches.

$$\boldsymbol{\sigma} = 2\mu_L \boldsymbol{\varepsilon} + \lambda_L tr(\boldsymbol{\varepsilon})\boldsymbol{I} \tag{2.2}$$

where $\mu_L = \frac{E}{2(1+\nu)}$ and $\lambda_L = \frac{\nu E}{(1+\nu)(1-2\nu)}$ are 3D Lamé parameters expressed in terms of young's modulus E and Poisson's ratio ν. The kinematic relation for the strain tensor $\boldsymbol{\varepsilon}$ under infinitesimal displacement is defined to be the symmetric part of the displacement gradient as

$$\boldsymbol{\varepsilon} = \frac{1}{2}(\nabla \boldsymbol{u} + \nabla \boldsymbol{u}^T) \tag{2.3}$$

where $\nabla \boldsymbol{u}$ is the second-order tensor.

The Eq.(2.1) is multiplied by a weighting function $\delta \boldsymbol{u}$, which also generalises for the principle of virtual work, as follows

$$\int_\Omega \rho \ddot{\boldsymbol{u}}.\delta \boldsymbol{u}\ d\Omega + \int_\Omega \nabla.\boldsymbol{\sigma}(\boldsymbol{u}).\delta \boldsymbol{u}\ d\Omega = \int_\Omega \boldsymbol{f}.\delta \boldsymbol{u} \qquad \forall \delta \boldsymbol{u} | \boldsymbol{u} = 0 \text{ on } \Gamma_D \tag{2.4}$$

Applying Green's theorem for the term $\int_\Omega \nabla.\boldsymbol{\sigma}(\boldsymbol{u}).\delta \boldsymbol{u}\ d\Omega$, the weak form of the problem (2.1) can be defined as follows

$$\int_\Omega \rho \ddot{\boldsymbol{u}}.\delta \boldsymbol{u}\ d\Omega + \int_\Omega \boldsymbol{\sigma}(\boldsymbol{u}) : \nabla \delta \boldsymbol{u}\ d\Omega - \int_{\Gamma_N} \boldsymbol{t}_N.\delta \boldsymbol{u}\ d\Gamma_N = \int_\Omega \boldsymbol{f}.\delta \boldsymbol{u} \qquad \forall \delta \boldsymbol{u} | \boldsymbol{u} = 0 \text{ on } \Gamma_D \tag{2.5}$$

where $\nabla \delta \boldsymbol{u} = \delta \boldsymbol{\varepsilon} + \delta \boldsymbol{\omega}$, with $\boldsymbol{\omega}$ being the anti-symmetric rotation tensor. Since $\boldsymbol{\sigma}$ is symmetric, $\boldsymbol{\sigma}(\boldsymbol{u}) : \nabla \delta \boldsymbol{u} = \boldsymbol{\sigma}(\boldsymbol{u}) : \delta \boldsymbol{\varepsilon}$.

The displacement $\boldsymbol{u}$ and the stress field $\boldsymbol{\sigma}(\boldsymbol{u}).\hat{\mathbf{v}}_n$ on $\partial\Omega$ can be decomposed as

$$\boldsymbol{u} = u_n \hat{\mathbf{v}}_n + u_t \hat{\mathbf{v}}_t = \boldsymbol{u}_n + \boldsymbol{u}_t \quad \text{and} \quad \boldsymbol{\sigma}(\boldsymbol{u}).\hat{\mathbf{v}}_n = \sigma_n \hat{\mathbf{v}}_n + \sigma_t \hat{\mathbf{v}}_t = \boldsymbol{\sigma}_n + \boldsymbol{\sigma}_t$$

The above decomposition helps to prescribe normal and tangential stresses on $\partial\Omega$ for Neumann boundary conditions and contact boundary conditions. The contact boundary conditions on $\Gamma_C \subset \partial\Omega : \Gamma_N \bigcap \Gamma_D \bigcap \Gamma_C = \emptyset$ will be introduced in the following definitions.

2.2 Modelling contact and friction

In this section, we define a short description of the concepts related to contact mechanics, which are important for the formulation in our application. The structural mechanics problem with contact can be viewed as constraints imposed on boundary of a domain, which leads to the definition of contact boundary conditions. Unlike the

classical Dirichlet and Neumann boundary conditions which are known a priori and hence can be prescribed directly in the Eq. (2.1), the contact boundary conditions are unknown a priori. Given in its basic form, it can be seen as boundary nonlinearity from the non-linear kinematic relations which are also non-smooth with multi-valued mapping, giving rise to numerical complications. Hence, to satisfy the contact boundary conditions, different formulations exist with diverse approximations based on set of assumptions depending on the application. Nevertheless, we give the basic contact kinematic relations on which the approximations will be defined for our application.

For simplicity, we consider a system with domains $\Omega^{(\mathrm{a})}$ and $\Omega^{(\mathrm{b})}$ in contact. We start with the definition of gap function defined between the domains as follows,

$$g_n = [\boldsymbol{X}^{(\mathrm{a})} - \overleftarrow{\boldsymbol{X}}^{(\mathrm{b})}].\hat{\mathbf{v}}_n \tag{2.6}$$

where several methods exist for determining $\overleftarrow{\boldsymbol{X}}^{(\mathrm{b})}$ and $\hat{\mathbf{v}}_n$. The most easiest is to define $\hat{\mathbf{v}}_n$ as outward normal projection from the slave surface $\partial\Omega^{(\mathrm{a})}$ to the master surface $\partial\Omega^{(\mathrm{b})}$ which determines the corresponding $\overleftarrow{\boldsymbol{X}}^{(\mathrm{b})}$ for any given $\boldsymbol{X}^{(\mathrm{a})}$. Distinguish between master and slave is made depending on the mesh density where typically slave surface has more elements than the master surface. Classically, the method of closest point projection is widely used where $\overleftarrow{\boldsymbol{X}}^{(\mathrm{b})}$ is defined as follows

$$\overleftarrow{\boldsymbol{X}}^{(\mathrm{b})} = \underset{\boldsymbol{X}^{(\mathrm{b})} \in \partial\Omega^{(\mathrm{b})}}{arg\,min}\ ||\boldsymbol{X}^{(\mathrm{a})} - \boldsymbol{X}^{(\mathrm{b})}|| \tag{2.7}$$

where $\hat{\mathbf{v}}_n$ is chosen as an outward normal of $\partial\Omega^{(\mathrm{b})}$. Concerning our application, we mostly deal with contact between flat surfaces with finite deformation, and hence the two approaches result in nearly the same value of $\overleftarrow{\boldsymbol{X}}^{(\mathrm{b})}$ for a given $\boldsymbol{X}^{(\mathrm{a})}$, where the problem of non-uniqueness which the closest point projection method suffers doesn't concern us. This is mostly achieved by projection through parameterisation of domains using Isoparametric approach of FEM, where in Isogeomteric approach the parametrisation is intrinsic. More on these definitions are discussed in §3.2.

Given the definition of gap function, the contact constraints can be defined unilaterally for a domain in contact through the set of following conditions which are commonly known as Signorini or Karush-Kuhn-Tucker (KKT) conditions.

$$g_n \geq 0 \tag{2.8a}$$

$$\sigma_n \leq 0 \tag{2.8b}$$

$$g_n \sigma_n = 0 \tag{2.8c}$$

From the conditions, the physical interpretations are apparent, the Eq. (2.8a) states that no penetration is allowed between the domains in contact, while the Eq.

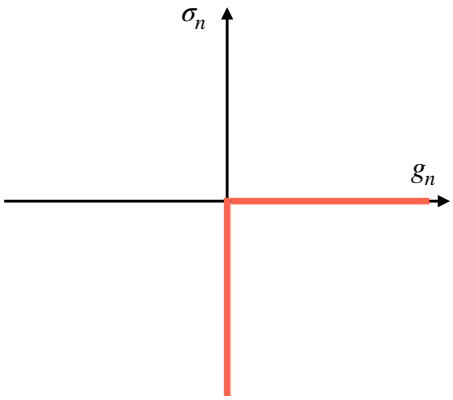

Figure 2.1: Illustration of Signorini conditions

(2.8b) states that only compressive stress is allowed at the contact boundary, where the adhesive effects are classically ignored. The Eq. (2.8c) is given as complementary condition which relates the first two constraints where it can be understood that when the compressive stress is nonzero, the gap function should be zero. It should be noted that the above set of constraints define multi-valued mapping, shown in Fig. 2.1.

For small deformation problems, the gap function (2.9) can be linearised as follows

$$\Delta g_n = [\boldsymbol{u}^{(\mathrm{a})} - \overleftarrow{\boldsymbol{u}}^{(\mathrm{b})}].\hat{\mathbf{v}}_n + g_0 = u_n + g_0 \tag{2.9}$$

where g_0 represents the gap function in the reference configuration. Hence, for any incremental time, the linearized expression of the gap function will be used for the following definitions where the condition (2.8a) can be expressed as

$$u_n + g_0 \geq 0 \quad \text{or} \quad u_n - g_0 \leq 0 \tag{2.10}$$

We use the later convention $u_n - g_0 \leq 0$ for the following definitions.

Friction is defined through Coulomb-Amonton's law which is based on threshold conditions to define stick and slip characteristics, where no motion is allowed until $||\boldsymbol{\sigma}_t||$ satisfies the threshold $\mu||\boldsymbol{\sigma}_n||$, expressed as follows

$$||\dot{\boldsymbol{u}}_t|| \geq 0 \tag{2.11a}$$

$$||\boldsymbol{\sigma}_t|| - \mu|\sigma_n| \leq 0 \tag{2.11b}$$

$$(||\boldsymbol{\sigma}_t|| - \mu|\sigma_n|)||\dot{\boldsymbol{u}}_t|| = 0 \tag{2.11c}$$

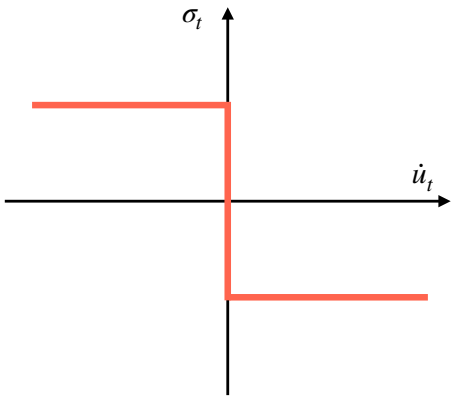

Figure 2.2: Illustration of Coulomb-Amonton's law

where μ is the classical coefficient of friction. The above conditions can be interpreted as follows, for the stick condition $||\dot{\boldsymbol{u}}_t|| = 0$, $||\boldsymbol{\sigma}_t|| \leq \mu|\sigma_n|$ where $||\boldsymbol{\sigma}_t||$ is inside Coulomb's cone in the space of traction stresses and contrarily, for the slip condition $||\dot{\boldsymbol{u}}_t|| > 0$, $||\boldsymbol{\sigma}_t|| = \mu|\sigma_n|$ where $||\boldsymbol{\sigma}_t||$ is on the Coulomb's cone. The conditions are graphically shown in Fig. 2.2, where similar to Signorini conditions, the conditions define multi-valued mapping.

2.3 Initial-boundary value problem with contact and friction

The initial boundary value problem Eq.(2.1) with unilateral conditions for contact and friction can be given as follows

$$\begin{aligned} \rho\ddot{\boldsymbol{u}} + \nabla.\boldsymbol{\sigma}(\boldsymbol{u}) = \boldsymbol{f} \quad &\text{in} \quad \Omega \\ \boldsymbol{u} = \boldsymbol{u}_D \quad &\text{on} \quad \Gamma_D \\ \boldsymbol{\sigma}(\boldsymbol{u}).\hat{\mathbf{v}}_n = \boldsymbol{t}_N \quad &\text{on} \quad \Gamma_N \end{aligned}$$

$$\begin{aligned} g_n \geq 0, \quad \sigma_n \leq 0, \quad g_n\sigma_n = 0 \\ ||\dot{\boldsymbol{u}}_t|| = 0 \implies ||\boldsymbol{\sigma}_t|| - \mu|\sigma_n| \leq 0 \\ ||\dot{\boldsymbol{u}}_t|| \neq 0 \implies \boldsymbol{\sigma}_t - \mu|\sigma_n|\frac{\dot{\boldsymbol{u}}_t}{||\dot{\boldsymbol{u}}_t||} = 0 \\ \text{on} \quad \Gamma_C \end{aligned} \tag{2.12}$$

Unlike the classical weak form (2.5) which can be obtained through principle of stationary action, with the action defined by Lagrangian energy functional. The

presence of inequalities from contact and friction defines the problem in the context of convex optimisation. Hence, the weak form of the problem has the form of variational inequality, expressed as

$$\int_\Omega \rho\ddot{\boldsymbol{u}}.(\delta\boldsymbol{u}-\dot{\boldsymbol{u}})\ d\Omega+\int_\Omega \boldsymbol{\sigma}(\boldsymbol{u}):(\nabla\delta\boldsymbol{u}-\nabla\dot{\boldsymbol{u}})\ d\Omega \\ -\int_{\Gamma_C}\sigma_n(\delta u_n-\dot{u}_n)\ d\Gamma_C-\int_{\Gamma_C}\sigma_t(||\delta\boldsymbol{u}_t||-||\dot{\boldsymbol{u}}_t||)\ d\Gamma_C \\ -\int_{\Gamma_N}\boldsymbol{t}_N.(\delta\boldsymbol{u}-\dot{\boldsymbol{u}})\ d\Gamma_N-\int_\Omega \boldsymbol{f}.(\delta\boldsymbol{u}-\dot{\boldsymbol{u}})\ d\Omega\geq 0 \quad (2.13)$$

where the weak form contains the simultaneous presence of two inequalities modelling contact and friction. To make it complete as an initial boundary value problem, the initial conditions can be defined as $\boldsymbol{u}_0$ and $\dot{\boldsymbol{u}}_0$ which satisfies the above equation at the initial time.

The solution to the above dynamical problem is often discussed in the context of non-smooth mechanics which we do not focus here. The existence and uniqueness of solution to the above problem under static notion without friction was proved by optimising the resulting convex functional over a convex domain [53, 54, 55]. Also with the static notion of friction, existence and uniqueness of solution was proved for small friction coefficient [56]. For the above dynamic problem, time integration can be achieved through regularisation of the multi-valued mappings from the Signorini conditions (2.8) and the Coulomb-Amonton's law (2.11) [57, 58, 59]. Such multi-valued mapping are also seen as fundamental in defining some of the friction-induced dynamic instabilities such as stick-slip phenomenon [60, 50]. Hence, the model for regularization and the parameters in modelling the regularization are important depending on the hypotheses that model the nature of a given instability. With regularisation of the non-differentiable terms, the equation can be integrated over time to determine instabilities which are typically of divergent or flutter type in nature. Flutter instability is defined by self-excited oscillation, typically in the presence of non-conservative force, which is characterised by limit cycle in the Phase-plane. This is a very expensive strategy of determining instability, since it can require solving the equation for several time-steps until a limit cycle could be reached. Nevertheless, it can be the most precise way to mathematically model and analyse the nature of instability [61].

We focus on modelling flutter-type dynamic instability through classical theories of linear analysis, where the first-order effect of perturbation around a fixed point is analysed. Hence, the stability of the dynamical system with frictional contact (2.13) can be characterized by determining the fixed point which is typically quasi-static or steady-sliding equilibrium, depending on the characteristics of the external forces, and defining the dynamics for the perturbation around the fixed point. For non-linear systems such as the system with frictional contact, the stability can be defined

through linearizing the perturbation around a fixed point, which brings the question of modelling the multi-valued mappings to be linear. This is possible through regularization of the multi-valued mappings with functions through normal-compliance approach [62] which will be discussed in detail with the case of steady-sliding equilibrium [63]. The linear expression of perturbation around a fixed point means that it can only characterise the nature of instability very close to the fixed point, while the non-linear evolution of instability away from the fixed point can only be defined by transient analysis [61]. Nevertheless, the linear definition can provide insight in to the nature of the system, so as to have an overview of the instabilities present which can be achieved through a single evaluation of eigenvalue analysis. As an intermediate step in realizing the stability analysis for the steady-sliding equilibrium, we discuss the quasi-static insight for the above dynamical system (2.13).

2.3.1 Quasi-static equilibrium

The dynamical problem can be expressed as quasi-static problem when the inertial effects can be ignored, given as

$$\begin{aligned}\int_{\Omega} \boldsymbol{\sigma}(\boldsymbol{u}) : (\nabla \delta \boldsymbol{u} - \nabla \dot{\boldsymbol{u}})\ d\Omega \\ - \int_{\Gamma_C} \sigma_n(\delta u_n - \dot{u}_n)\ d\Gamma_C - \int_{\Gamma_C} \sigma_t(||\delta \boldsymbol{u}_t|| - ||\dot{\boldsymbol{u}}_t||)\ d\Gamma_C \\ - \int_{\Gamma_N} \boldsymbol{t}_N.(\delta \boldsymbol{u} - \dot{\boldsymbol{u}})\ d\Gamma_N - \int_{\Omega} \boldsymbol{f}.(\delta \boldsymbol{u} - \dot{\boldsymbol{u}})\ d\Omega \geq 0 \quad (2.14)\end{aligned}$$

The quasi-static frictional problem characterizes the time-dependent variation of $\boldsymbol{u}_t$ with Coulomb's conditions, which implies the presence of time-dependent external forces $\boldsymbol{t}_N$ and $\boldsymbol{f}$. Hence, the evolution of the system can be considered as a series of quasi-static equilibrium states, where the stability of the dynamical system can be characterized around such equilibrium states. This means that the stability could be defined taking in to account of the time-dependent external forces, or also velocity-dependent friction coefficient, where the history of loading is important for such applications. The solution to the quasi-static problem with non-uniqueness is proved to exist under strict conditions[64].

2.3.2 Steady-sliding equilibrium

The quasi-static equilibrium can be expressed as a steady-sliding equilibrium between at least two half-spaces when no net acceleration is present [60, 50, 63]. Similar to quasi-static equilibrium, this can be seen as a series of equilibrium states with respect to time where the equilibrium characteristics remain the same, except for the change

in contact domain. Since the equilibrium characteristics remain the same for all the time, the equilibrium state could be expressed with no time dependent forces but purely by static forces. This also means that the knowledge of $\hat{\mathbf{v}}_t$ for $\sigma_t \hat{\mathbf{v}}_t$ at Γ_C is known a priori, where the general notion of $\hat{\mathbf{v}}_t$ could be given as $\hat{\mathbf{v}}_k$ for the known sliding direction. Hence, the time-independent definition of Coulomb's law could be expressed for the so-called static state as follows

$$||\boldsymbol{u}_t|| \geq 0 \tag{2.15a}$$

$$||\boldsymbol{\sigma}_t|| - \mu|\sigma_n| \leq 0 \tag{2.15b}$$

$$(||\boldsymbol{\sigma}_t|| - \mu|\sigma_n|)||\boldsymbol{u}_t|| = 0 \tag{2.15c}$$

The steady-sliding equilibrium explicitly defines the slip condition where the sliding velocity is constant and hence, at the equilibrium, $\sigma_t = \mu\sigma_n$ on Γ_C. For simplicity, we consider only one half-space of the sliding contact where the half-space is considered to be fixed relative to the other half-space, while the other half-space moves parallel to $\hat{\mathbf{v}}_t$ creating a sliding contact. Hence, at any time, the equilibrium state could be expressed as

$$\begin{aligned}\int_\Omega \boldsymbol{\sigma}(\boldsymbol{u}) : (\nabla\delta\boldsymbol{u} - \nabla\boldsymbol{u})\ d\Omega - \int_{\Gamma_C} \mu\sigma_n(||\delta\boldsymbol{u}_t|| - ||\boldsymbol{u}_t||)\ d\Gamma_C \\ - \int_{\Gamma_N} \boldsymbol{t}_N.(\delta\boldsymbol{u} - \boldsymbol{u})\ d\Gamma_N - \int_\Omega \boldsymbol{f}.(\delta\boldsymbol{u} - \boldsymbol{u})\ d\Omega \geq 0\end{aligned} \tag{2.16}$$

Since the knowledge of $\hat{\mathbf{v}}_t$ for $u_t\hat{\mathbf{v}}_t$ at Γ_C is known a priori as $\hat{\mathbf{v}}_k$, and with the slip condition for friction, the above formulation can be defined as

$$\begin{aligned}\int_\Omega \boldsymbol{\sigma}(\boldsymbol{u}) : (\nabla\delta\boldsymbol{u} - \nabla\boldsymbol{u})\ d\Omega - \int_{\Gamma_C} \mu\sigma_n(\delta\boldsymbol{u} - \boldsymbol{u}).\hat{\mathbf{v}}_k\ d\Gamma_C \\ - \int_{\Gamma_N} \boldsymbol{t}_N.(\delta\boldsymbol{u} - \boldsymbol{u})\ d\Gamma_N - \int_\Omega \boldsymbol{f}.(\delta\boldsymbol{u} - \boldsymbol{u})\ d\Omega \geq 0\end{aligned} \tag{2.17}$$

where the multi-valued mapping of friction is replaced by a smooth definition. We now introduce the function space for defining $\delta\boldsymbol{u}$ and $\boldsymbol{u}$, where $\delta\boldsymbol{u}$ and $\boldsymbol{u}$ are defined to be from the same space $\boldsymbol{K} \subset \boldsymbol{V}$, with $\boldsymbol{K}$ being the convex subset of $\boldsymbol{V}$, given as

$$\boldsymbol{V} := \{\delta\boldsymbol{u} \in (H^1(\Omega))^3 | \delta\boldsymbol{u} = \boldsymbol{u}_D \text{ on } \Gamma_D\}$$

$$\boldsymbol{K} := \{\delta\boldsymbol{u} \in \boldsymbol{V} | \delta\boldsymbol{u}_n \leq g_n\}$$

$$\boldsymbol{f} \in (L^2(\Omega))^3 \text{ and } \boldsymbol{t} \in (H^{-1/2}(\partial\Omega))^3$$

where $(H^1(\Omega))^3$ is the Sobolev space of functions, given with the property

$$(H^1(\Omega))^3 := \{\delta \boldsymbol{u} \in (L^2(\Omega))^3, \nabla \delta \boldsymbol{u} \in (L^2(\Omega))^3\}$$

Hence, the Hilbert space induced by inner product is given through L^2 norm: $\|\delta \boldsymbol{u}\|_{L^2} = \langle \delta \boldsymbol{u}, \delta \boldsymbol{u} \rangle = \int_\Omega \delta \boldsymbol{u}^2 d\Omega < \infty$. A subspace $(H^{1/2}(\partial\Omega))^3$ can be defined as the restriction of $(H^1(\Omega))^3$ on $\partial\Omega$, where $(H^{-1/2}(\partial\Omega))^3$ is the dual of the space $(H^{1/2}(\partial\Omega))^3$. Even though $\boldsymbol{t}$ is typically defined to be in $L^2(\Omega)$, the unknown a priori conditions of $\boldsymbol{t}$ for σ_n on Γ_C results in the space to be $H^{1/2}(\partial\Omega)$. Unlike the case for the dynamical problem or quasi-static problems which are characterized by the presence of two simultaneous inequalities, the above problem is characterized purely by the inequalities of the Signorini conditions, when friction is defined for the slip condition with equality.

Regularisation through normal compliance

The Signorini and Coulomb's conditions (2.8) (2.11) represent the mathematical model for contact and friction in macroscopic view, where such conditions have been found through experiments to be far from the physical reality [60]. This leads to the view of normal compliance approach to define a better approximation of the contact interface, also through which regularization for the muti-valued mapping can be achieved. Normal compliance is defined by σ_n as the function of gap function g_n with a set of parameters determined largely by experiments, given as

$$-\sigma_n = c_n(u_n - g_n)_+^{m_n} \tag{2.18}$$

where $(.)_+$ allows only positive value. This can be extended to friction as follows

$$||\dot{\boldsymbol{u}}_t|| \geq 0 \tag{2.19a}$$

$$||\boldsymbol{\sigma}_t|| - c_t(u_n - g_n)_+^{m_t} \leq 0 \tag{2.19b}$$

$$||\boldsymbol{\sigma}_t|| - c_t(u_n - g_n)_+^{m_t}||\dot{\boldsymbol{u}}_t|| = 0 \tag{2.19c}$$

where the parameters c_n, m_n, c_t and m_t are determined from the experiments. The normal compliance can also be applied to the previously defined quasi-static case, where existence of a solution was proved through regularisation from normal compliance. For steady-sliding equilibrium, $||\dot{\boldsymbol{u}}_t||$ can be expressed as $||\boldsymbol{u}_t||$.

The Eq. (2.17) can hence be defined through normal compliance as follows

$$\int_{\Omega} \boldsymbol{\sigma}(\boldsymbol{u}) : (\nabla \delta \boldsymbol{u} - \nabla \boldsymbol{u})\ d\Omega - \int_{\Gamma_C} c_t (u_n - g_n)_+^{m_t} (\delta \boldsymbol{u} - \boldsymbol{u}).\hat{\mathbf{v}}_k\ d\Gamma_C$$
$$- \int_{\Gamma_N} \boldsymbol{t}_N.(\delta \boldsymbol{u} - \boldsymbol{u})\ d\Gamma_N - \int_{\Omega} \boldsymbol{f}.(\delta \boldsymbol{u} - \boldsymbol{u})\ d\Omega \geq 0 \quad (2.20)$$

The above variational inequality can be expressed as variational equality through active set strategy, where instead of looking for the admissible displacement field that satisfies the condition $u_n \leq g_n$ on Γ_C, as the minimizer of the above functional in the convex set $\boldsymbol{K}$ if there exists a unique solution in the set, the set Γ_C is defined a priori, called active set, at least for an incremental time in which $u_n - g_n \to 0$, provided that $u_n \leq g_n$ was satisfied prior to the given time. With the knowledge of active set, the displacement field u_n on Γ_C could be satisfied by normal compliance given in Eq. (2.18). Hence, the above functional with inequality can be expressed through equality as follows

$$\int_{\Omega} \boldsymbol{\sigma}(\boldsymbol{u}) : \nabla \delta \boldsymbol{u}\ d\Omega - \underbrace{\int_{\Gamma_C} c_t (u_n - g_n)_+^{m_t} \delta \boldsymbol{u}.\hat{\mathbf{v}}_k\ d\Gamma_C}_{\langle \boldsymbol{\sigma}_n, \delta \boldsymbol{u} \rangle} + \underbrace{\int_{\Gamma_C} c_n (u_n - g_n)_+^{m_n} \delta \boldsymbol{u}.\hat{\mathbf{v}}_n\ d\Gamma_C}_{\langle \boldsymbol{\sigma}_t, \delta \boldsymbol{u} \rangle}$$
$$- \int_{\Gamma_N} \boldsymbol{t}_N.\delta \boldsymbol{u}\ d\Gamma_N - \int_{\Omega} \boldsymbol{f}.\delta \boldsymbol{u}\ d\Omega = 0 \quad (2.21)$$

where the inner products $\langle \boldsymbol{\sigma}_n, \delta \boldsymbol{u} \rangle$ and $\langle \boldsymbol{\sigma}_t, \delta \boldsymbol{u} \rangle$ define the weak form of contact and friction respectively. The definition of Γ_C through the active set strategy means that $\boldsymbol{t}_N \in (L^2(\Omega))^3$. When $m_n \neq 1$ and $m_t \neq 1$, the steady-sliding equilibrium can be solved through non-linear programming like Newton-Rhapson for $\boldsymbol{u}_{eq}$.

We do not relate to the experimental determination of the parameters c_n, m_n, c_t and m_t. Hence, c_n is purely given as the penalty parameter p considering numerical stability, which implies that for any $(u_n - g_0) > 0$ defined by $(u_n - g_0)_+$ is penalized by a factor p, where the ideal would be $p \to \infty$. While c_t is given for the ideal slip state of the steady-sliding equilibrium as $c_t = \mu p$. The normal compliance approach can be viewed in general as modelling springs with certain stiffness c_n which resist penetration at the contact interface. We consider $m_n = m_t = 1$, where the parameters m_n and m_t for any value other than 1 can be physically interpreted as non-linear springs. With the above consideration of the parameters for the normal compliance, the above functional can be expressed as follows

$$\int_{\Omega} \boldsymbol{\sigma}(\boldsymbol{u}) : \nabla \delta \boldsymbol{u}\ d\Omega - \int_{\Gamma_C} \mu p (u_n - g_n)_+ \delta \boldsymbol{u}.\hat{\mathbf{v}}_k\ d\Gamma_C + \int_{\Gamma_C} p (u_n - g_n)_+ \delta \boldsymbol{u}.\hat{\mathbf{v}}_n\ d\Gamma_C$$
$$- \int_{\Gamma_N} \boldsymbol{t}_N.\delta \boldsymbol{u}\ d\Gamma_N - \int_{\Omega} \boldsymbol{f}.\delta \boldsymbol{u}\ d\Omega = 0 \quad (2.22)$$

where for finite deformation, the problem can be solved for $\boldsymbol{u}_{eq}$ with one incremental time step. It should be noted that non-unique solutions may exist for steady-sliding equilibrium [63, 45]. On the other hand, it is also possible to define the dynamics of the perturbation explicitly without inferring $\boldsymbol{u}_{eq}$, at least for linear case.

2.3.3 Perturbation around steady-sliding equilibrium

The perturbed state of the displacement field for any excitation of the steady-sliding equilibrium can be given as

$$\boldsymbol{u} = \boldsymbol{u}_{eq} + \widetilde{\boldsymbol{u}} \tag{2.23}$$

where $\widetilde{\boldsymbol{u}}$ corresponds to the perturbed displacement field. The idea is to analyse the dynamics of the perturbation such that the stability of the dynamical system can be determined through the onset evolution of the dynamics for the perturbation, where it is hypothesized that the onset evolution of the dynamics can be expressed linearly. This brings the question of linearization for the non-linear frictional contact problem, with the sufficient approximation made in Eq. (2.22) with normal compliance.

Linearization of the perturbation around steady-sliding equilibrium

As a detour for generalization, we discuss the linearization of the normal compliance terms. The contact and friction terms in Eq. (2.21) with $c_n = p, c_t = \mu p$, $0 < m_n \neq 1$ and $0 < m_t \neq 1$, can be expressed as

$$\langle \boldsymbol{\sigma}_n, \delta\boldsymbol{u} \rangle_{\Gamma_C} = \int_{\Gamma_C} p(u_n - g_0)_+^{m_n} \delta\boldsymbol{u}.\hat{\mathbf{v}}_n \; d\Gamma_C \tag{2.24a}$$

$$\langle \boldsymbol{\sigma}_t, \delta\boldsymbol{u} \rangle_{\Gamma_C} = \int_{\Gamma_C} \mu p(u_n - g_0)_+^{m_t} \delta\boldsymbol{u}.\hat{\mathbf{v}}_k \; d\Gamma_C \tag{2.24b}$$

The perturbation of the normal compliance can hence be expressed as

$$p(\widetilde{u}_n + u_n - g_0)_+^{m_n} - p(u_n - g_0)_+^{m_n} \approx p(\widetilde{u}_n)_+^{m_n} \tag{2.25a}$$

$$\mu p(\widetilde{u}_n + u_n - g_0)_+^{m_t} - \mu p(u_n - g_0)_+^{m_t} \approx \mu p(\widetilde{u}_n)_+^{m_t} \tag{2.25b}$$

if it can be assumed that the parameters of the normal compliance stay the same for the perturbation $\widetilde{\boldsymbol{u}}$ close to the equilibrium $\boldsymbol{u}_{eq}$. The linearization for the degree of the polynomial terms at $\boldsymbol{u}_{eq}$ can be defined as

$$\Delta p(\widetilde{u}_n)_+^{m_n}|_{\boldsymbol{u}_{eq}} = m_n p(\widetilde{u}_n)_+^{m_n-1}|_{\boldsymbol{u}_{eq}} \tag{2.26a}$$

$$\Delta \mu p(\widetilde{u}_n)_+^{m_t}|_{\boldsymbol{u}_{eq}} = \mu m_t p(\widetilde{u}_n)_+^{m_t-1}|_{\boldsymbol{u}_{eq}} \tag{2.26b}$$

where the expressions are still non-linear in the presence of $(.)_+$. It should be noted that the perturbation $\widetilde{u}_n$ on Γ_C may not result in the same active set as the equilibrium due to possible separation on Γ_C, which introduces non-linearities defined by $(.)_+$. This is because the separation leads to $u_n - g_0 < 0$ and hence $p(u_n - g_0)_+^{m_n} \to 0$ which can only be taken in to account nonlinearly. This is linearized with the hypothesis that the onset of instability occurs very close to the equilibrium $\boldsymbol{u}_{eq}$ such that Γ_C remains the same for the perturbation $\widetilde{\boldsymbol{u}}$. This means that if Γ_C must be constant for $\widetilde{\boldsymbol{u}}$, the separation $u_n - g_0 < 0$ must also be penalized which can simply be achieved by evading the operator $(.)_+$. The above hypothesis for the perturbation of $\widetilde{u}_n$ on Γ_C would have been impossible to define with Signorini conditions where $\widetilde{u}_n$ may lead to strict contact separation on Γ_C. While in the view of normal compliance, the perturbation $\widetilde{u}_n$ for no variation of Γ_C can be considered to define the variation of σ_n and hence also its subsequent effect on σ_t for friction.

With the above hypothesis, the linearized weak form of contact and friction for the dynamics of the perturbation $\widetilde{\boldsymbol{u}}$ close to $\boldsymbol{u}_{eq}$ can be defined as

$$\langle \boldsymbol{\sigma}_n, \delta \boldsymbol{u} \rangle_{\Gamma_C} = \int_{\Gamma_C} m_n p \widetilde{u}_n^{m_n-1}|_{\boldsymbol{u}_{eq}} \delta \boldsymbol{u}.\hat{\mathbf{v}}_n \; d\Gamma_C \tag{2.27a}$$

$$\langle \boldsymbol{\sigma}_t, \delta \boldsymbol{u} \rangle_{\Gamma_C} = \int_{\Gamma_C} \mu m_n p \widetilde{u}_n^{m_n-1}|_{\boldsymbol{u}_{eq}} \delta \boldsymbol{u}.\hat{\mathbf{v}}_k \; d\Gamma_C \tag{2.27b}$$

It should be noted that the above weak form is different from the classical weak form of contact and friction defined by normal compliance in Eq. (2.21). The above weak form essentially characterises force which is purely displacement-dependent, also known as follower force. The definition of follower force can be largely said as implicit for modelling flutter-type dynamic instability. In the case of flutter-type instability arising from friction between solids, the main hypothesis is that the onset of instability occurs at perturbations very close to $\boldsymbol{u}_{eq}$ such that the non-linearities of the classical contact and friction (2.21) can be effectively ignored and hence, friction phenomenon for a perturbed state $\widetilde{\boldsymbol{u}}$ can be modelled linearly with the contact state of $\boldsymbol{u}_{eq}$ purely by displacement-dependent forces. Hence, the hypothesis only characterises $\widetilde{\boldsymbol{u}}$ with the linearization of non-linearities very close to $\boldsymbol{u}_{eq}$, while the characteristics of non-linearities away from $\boldsymbol{u}_{eq}$ cannot be forseen. This essentially reflects on the possibility of utilising linear analysis such as CEA 2.5, where CEA can characterise instability of a system through eigenmodes in one computation, which would otherwise require expensive transient analysis to find a limit cycle. This defines the system to be holonomic and autonomous since the nature of follower force depends only on generalized coordinates without explicit time dependence.

We consider the case of $m_n = 1$ and $m_t = 1$ for the following discussions, where the linearization of Eqs. (2.24) can simply be expressed as

$$\langle \boldsymbol{\sigma}_n, \delta \boldsymbol{u} \rangle_{\Gamma_C} = \int_{\Gamma_C} p \widetilde{u}_n \delta \boldsymbol{u}.\hat{\mathbf{v}}_n \; d\Gamma_C \tag{2.28a}$$

$$\langle \boldsymbol{\sigma}_t, \delta \boldsymbol{u} \rangle_{\Gamma_C} = \int_{\Gamma_C} \mu p \widetilde{u}_n \delta \boldsymbol{u}.\hat{\mathbf{v}}_k \; d\Gamma_C \tag{2.28b}$$

Dynamics of the pertubation

The initial-boundary value problem for the dynamics of the perturbation can be given as

$$\begin{aligned} \rho^{(\mathrm{k})} \ddot{\widetilde{\boldsymbol{u}}}^{(\mathrm{k})} + \nabla . \boldsymbol{\sigma}^{(\mathrm{k})}(\widetilde{\boldsymbol{u}}^{(\mathrm{k})}) = 0 \quad &\text{in} \quad \Omega^{(\mathrm{k})} \\ \widetilde{\boldsymbol{u}}^{(\mathrm{k})} = \widetilde{\boldsymbol{u}}_D^{(\mathrm{k})} \quad &\text{on} \quad \Gamma_D^{(\mathrm{k})} \\ \sigma_n^{(\mathrm{k})}(\widetilde{\boldsymbol{u}}^{(\mathrm{k})}) \hat{\mathbf{v}}_n = -p \widetilde{u}_n^{(\mathrm{k})} \hat{\mathbf{v}}_n, \quad \sigma_t^{(\mathrm{k})}(\widetilde{\boldsymbol{u}}^{(\mathrm{k})}) \hat{\mathbf{v}}_k = \mu p \widetilde{u}_n^{(\mathrm{k})} \hat{\mathbf{v}}_k \quad &\text{on} \quad \Gamma_C^{(\mathrm{k})} \end{aligned} \tag{2.29}$$

It should be noted that for linear case, the problem can be explicitly defined without the fore knowledge of $\boldsymbol{u}_{eq}$, by defining Γ_C explicitly. For simplicity, we consider the parameters p and μ to be constant between the contact interface of all the domains in contact. The subscript k distinguishes the domains in contact. Similar to Eq. (2.5), the weak form of the differential formulation can be expressed as

$$\int_{\Omega^{(k)}} \rho^{(\mathrm{k})} \ddot{\widetilde{\boldsymbol{u}}}^{(\mathrm{k})} . \delta \boldsymbol{u}^{(\mathrm{k})} \; d\Omega^{(\mathrm{k})} + \int_{\Omega^{(k)}} \boldsymbol{\sigma}^{(\mathrm{k})}(\widetilde{\boldsymbol{u}}^{(\mathrm{k})}) : \nabla \delta \boldsymbol{u}^{(\mathrm{k})} \; d\Omega^{(\mathrm{k})} - \int_{\Gamma_C^{(k)}} \boldsymbol{t}_C^{(\mathrm{k})} . \delta \boldsymbol{u}^{(\mathrm{k})} \; d\Gamma_C^{(\mathrm{k})} = 0 \tag{2.30}$$

The traction force $\boldsymbol{t}_C \in H^{-1/2}(\Gamma_C)$ can be decomposed as follows

$$\begin{aligned} \int_{\Gamma_C^{(\mathrm{k})}} \boldsymbol{t}_C^{(\mathrm{k})} . \delta \boldsymbol{u}^{(\mathrm{k})} \; d\Gamma_C^{(\mathrm{k})} &= \int_{\Gamma_C^{(k)}} (\sigma_n^{(\mathrm{k})} \hat{\mathbf{v}}_n + \sigma_t^{(\mathrm{k})} \hat{\mathbf{v}}_k) . \delta \boldsymbol{u}^{(\mathrm{k})} \; d\Gamma_C^{(\mathrm{k})} \\ &= \int_{\Gamma_C^{(k)}} \sigma_n^{(\mathrm{k})} \hat{\mathbf{v}}_n . \delta \boldsymbol{u}^{(\mathrm{k})} \; d\Gamma_C^{(\mathrm{k})} + \int_{\Gamma_C^{(k)}} \sigma_t^{(\mathrm{k})} \hat{\mathbf{v}}_k . \delta \boldsymbol{u}^{(\mathrm{k})} \; d\Gamma_C^{(\mathrm{k})} \end{aligned} \tag{2.31}$$

Hence, the Eq. (2.30) for the $\mathrm{n_k}$ domains in contact can be defined as

$$\sum_{\mathrm{k}=1}^{\mathrm{n_k}} \Bigg\{ \int_{\Omega^{(k)}} \rho^{(\mathrm{k})} \ddot{\widetilde{\boldsymbol{u}}}^{(\mathrm{k})} . \delta \boldsymbol{u}^{(\mathrm{k})} \; d\Omega^{(\mathrm{k})} + \int_{\Omega^{(k)}} \boldsymbol{\sigma}^{(\mathrm{k})}(\widetilde{\boldsymbol{u}}^{(\mathrm{k})}) : \nabla \delta \boldsymbol{u}^{(\mathrm{k})} \; d\Omega^{(\mathrm{k})} \\ - \underbrace{\int_{\Gamma_C^{(k)}} \sigma_n^{(\mathrm{k})} \hat{\mathbf{v}}_n . \delta \boldsymbol{u}^{(\mathrm{k})} \; d\Gamma_C^{(\mathrm{k})}}_{\langle \boldsymbol{\sigma}_n^{(\mathrm{k})}, \delta \boldsymbol{u}^{(\mathrm{k})} \rangle_{\Gamma_C^{(\mathrm{k})}}} - \underbrace{\int_{\Gamma_C^{(k)}} \sigma_t^{(\mathrm{k})} \hat{\mathbf{v}}_k . \delta \boldsymbol{u}^{(\mathrm{k})} \; d\Gamma_C^{(\mathrm{k})}}_{\langle \boldsymbol{\sigma}_t^{(\mathrm{k})}, \delta \boldsymbol{u}^{(\mathrm{k})} \rangle_{\Gamma_C^{(\mathrm{k})}}} \Bigg\} = 0 \quad (2.32)$$

where $\boldsymbol{\sigma}_n, \boldsymbol{\sigma}_t \in (H^{-1/2}(\Gamma_C))^3$. The inner products can be expressed in $(H^{1/2}(\Gamma_C))^3$ space which is the restriction of $\boldsymbol{u} \in H^1(\Omega) \to H^{1/2}(\Gamma_C)$ through the normal compliance approach, where the above equation can be defined as

$$\sum_{\mathrm{k}=1}^{\mathrm{n_k}} \Bigg\{ \int_{\Omega^{(k)}} \rho^{(\mathrm{k})} \ddot{\widetilde{\boldsymbol{u}}}^{(\mathrm{k})} . \delta \boldsymbol{u}^{(\mathrm{k})} \; d\Omega^{(\mathrm{k})} + \int_{\Omega^{(k)}} \boldsymbol{\sigma}^{(\mathrm{k})}(\widetilde{\boldsymbol{u}}^{(\mathrm{k})}) : \nabla \delta \boldsymbol{u}^{(\mathrm{k})} \; d\Omega^{(\mathrm{k})} \\ + \underbrace{\int_{\Gamma_C^{(k)}} p \widetilde{u}_n^{(\mathrm{k})} \hat{\mathbf{v}}_n . \delta \boldsymbol{u}^{(\mathrm{k})} \; d\Gamma_C^{(\mathrm{k})}}_{\langle \boldsymbol{\sigma}_n^{(\mathrm{k})}, \delta \boldsymbol{u}^{(\mathrm{k})} \rangle_{\Gamma_C^{(\mathrm{k})}}} - \underbrace{\int_{\Gamma_C^{(k)}} \mu p \widetilde{u}_n^{(\mathrm{k})} \hat{\mathbf{v}}_k . \delta \boldsymbol{u}^{(\mathrm{k})} \; d\Gamma_C^{(\mathrm{k})}}_{\langle \boldsymbol{\sigma}_t^{(\mathrm{k})}, \delta \boldsymbol{u}^{(\mathrm{k})} \rangle_{\Gamma_C^{(\mathrm{k})}}} \Bigg\} = 0 \quad (2.33)$$

For simplicity in expansion of the contact and friction compliance terms, we consider contact between two domains $\Omega^{(a)}$ and $\Omega^{(b)}$, with the derivation of traction forces on $\Omega^{(a)}$. Hence, the inner products $\langle \boldsymbol{\sigma}_n^{(\mathrm{a})}, \delta \boldsymbol{u}^{(\mathrm{a})} \rangle_{\Gamma_C^{(\mathrm{a})}}$ and $\langle \boldsymbol{\sigma}_t^{(\mathrm{a})}, \delta \boldsymbol{u}^{(\mathrm{a})} \rangle_{\Gamma_C^{(\mathrm{a})}}$ can be expressed as

$$\langle \boldsymbol{\sigma}_n^{(\mathrm{a})}, \delta \boldsymbol{u}^{(\mathrm{a})} \rangle_{\Gamma_C^{(\mathrm{a})}} = \int_{\Gamma_C^{(\mathrm{a})}} p \widetilde{u}_n^{(\mathrm{a})} \hat{\mathbf{v}}_n . \delta \boldsymbol{u}^{(\mathrm{a})} \; d\Gamma_C^{(\mathrm{a})} = \int_{\Gamma_C^{(\mathrm{a})}} p[(\widetilde{\boldsymbol{u}}^{(\mathrm{a})} - \widetilde{\boldsymbol{u}}^{(\mathrm{b})}) . \hat{\mathbf{v}}_n] \delta \boldsymbol{u}^{(\mathrm{a})} . \hat{\mathbf{v}}_n \; d\Gamma_C^{(\mathrm{a})} \quad (2.34)$$

$$\langle \boldsymbol{\sigma}_t^{(\mathrm{a})}, \delta \boldsymbol{u}^{(\mathrm{a})} \rangle_{\Gamma_C^{(\mathrm{a})}} = \int_{\Gamma_C^{(\mathrm{a})}} \mu p \widetilde{u}_n^{(\mathrm{a})} \hat{\mathbf{v}}_n . \delta \boldsymbol{u}^{(\mathrm{a})} \; d\Gamma_C^{(\mathrm{a})} = \int_{\Gamma_C^{(\mathrm{a})}} \mu p[(\widetilde{\boldsymbol{u}}^{(\mathrm{a})} - \widetilde{\boldsymbol{u}}^{(\mathrm{b})}) . \hat{\mathbf{v}}_n] \delta \boldsymbol{u}^{(\mathrm{a})} . \hat{\mathbf{v}}_k \; d\Gamma_C^{(\mathrm{a})} \quad (2.35)$$

The traction forces on $\Omega^{(b)}$ can similarly be defined from the conservation of momentum as $\boldsymbol{\sigma}_n^{(\mathrm{a})} = -\boldsymbol{\sigma}_n^{(\mathrm{b})}$ and $\boldsymbol{\sigma}_t^{(\mathrm{a})} = -\boldsymbol{\sigma}_t^{(\mathrm{b})}$.

Finite element method for approximation

We defined a suitable function space $\boldsymbol{V} \subset (H^1(\Omega))^3$ on which the solution $\boldsymbol{u}$ of the functional in modelling the continuum is presumed to exist.The arbitrary variation $\delta \boldsymbol{u}$ in an infinite-dimensional function space $\boldsymbol{V}$ can be expressed as

$$\delta \boldsymbol{u} = \sum_{\mathrm{i}}^{\infty} \delta \boldsymbol{\vartheta}_{\mathrm{i}} \boldsymbol{v}_i \qquad \forall \boldsymbol{v}_i \in \boldsymbol{V} \tag{2.36}$$

Hence, the Eq. (2.3.3) can be defined for a system of two domains $\Omega^{(a)}$ and $\Omega^{(b)}$as

$$\sum_{\mathrm{k}}^{\mathrm{a,b}} \Bigg\{ \Bigg(\int_{\Omega^{(k)}} \rho^{(\mathrm{k})} \ddot{\widetilde{\boldsymbol{u}}}^{(\mathrm{k})} . \boldsymbol{v}_i^{(\mathrm{k})} \, d\Omega^{(k)} + \int_{\Omega^{(k)}} \boldsymbol{\sigma}^{(\mathrm{k})}(\widetilde{\boldsymbol{u}}^{(\mathrm{k})}) : \nabla \boldsymbol{v}_i^{(\mathrm{k})} \, d\Omega^{(\mathrm{k})} + \int_{\Gamma_C^{(k)}} p[(\widetilde{\boldsymbol{u}}^{(\mathrm{k})} - \widetilde{\boldsymbol{u}}^{(\sim \mathrm{k})}) . \hat{\mathbf{v}}_n] \boldsymbol{v}_i^{(\mathrm{k})} . \hat{\mathbf{v}}_n \, d\Gamma_C^{(k)} - \int_{\Gamma_C^{(k)}} \mu p[(\widetilde{\boldsymbol{u}}^{(\mathrm{k})} - \widetilde{\boldsymbol{u}}^{(\sim \mathrm{k})}) . \hat{\mathbf{v}}_n] \boldsymbol{v}_i^{(\mathrm{k})} . \hat{\mathbf{v}}_k \, d\Gamma_C^{(\mathrm{k})} \Bigg) \delta \boldsymbol{\vartheta} \Bigg\} = 0 \tag{2.37}$$

where the equation must be satisfied for any arbitrary variation of $\delta \boldsymbol{\vartheta}$. $\sim$ k defines the domain which is not k, i.e., k = a implies $\sim$ k = b and vice-versa.

With the finite element approach, we define a finite-dimensional function space ${}_h\boldsymbol{V} \subset \boldsymbol{V}$ and hence, there is some bound for ${}_h\boldsymbol{v}_{\mathrm{i}} \in {}_h\boldsymbol{V}$. We define the approximation of $\boldsymbol{u}$ in the same space ${}_h\boldsymbol{V}$ as $\boldsymbol{u} \approx {}_h\boldsymbol{u} \in {}_h\boldsymbol{V}$, where the above equation can be defined as

$$\sum_{\mathrm{k}}^{\mathrm{a,b}} \Bigg\{ \int_{\Omega^{(k)}} \rho^{(\mathrm{k})} {}_h\ddot{\widetilde{\boldsymbol{u}}}^{(\mathrm{k})} . {}_h\boldsymbol{v}_i^{(\mathrm{k})} \, d\Omega^{(\mathrm{k})} + \int_{\Omega^{(k)}} \boldsymbol{\sigma}^{(\mathrm{k})}({}_h\widetilde{\boldsymbol{u}}^{(\mathrm{k})}) : \nabla_h \boldsymbol{v}_i^{(\mathrm{k})} \, d\Omega^{(\mathrm{k})} + \int_{\Gamma_C^{(k)}} p[({}_h\widetilde{\boldsymbol{u}}^{(\mathrm{k})} - {}_h\widetilde{\boldsymbol{u}}^{(\sim \mathrm{k})}) . \hat{\mathbf{v}}_n] {}_h\boldsymbol{v}_i^{(\mathrm{k})} . \hat{\mathbf{v}}_n \, d\Gamma_C^{(k)} - \int_{\Gamma_C^{(k)}} \mu p[({}_h\widetilde{\boldsymbol{u}}^{(\mathrm{k})} - {}_h\widetilde{\boldsymbol{u}}^{(\sim \mathrm{k})}) . \hat{\mathbf{v}}_n] {}_h\boldsymbol{v}_i^{(\mathrm{k})} . \hat{\mathbf{v}}_k \, d\Gamma_C^{(\mathrm{k})} \Bigg\} = 0 \qquad \forall {}_h\boldsymbol{v}_i^{(\mathrm{k})} \in {}_h\boldsymbol{V}^{(\mathrm{k})} \tag{2.38}$$

We explain the definition of space ${}_h\boldsymbol{V}$ for classical finite elements in , but we mainly explain in detail for Isogeometric methods with focus on contact in , where the Isogeometric approach is new for the given application. But given a suitable choice of finite-dimensional space ${}_h\boldsymbol{V}$, the above equation can be defined in matrix form as

$$\mathbf{M}^{(\mathrm{a-b})} \ddot{\widetilde{\boldsymbol{U}}}^{(\mathrm{a-b})} + (\mathbf{K}^{(\mathrm{a-b})} + \mathbf{K}_C^{(\mathrm{a-b})} + \mathbf{K}_F^{(\mathrm{a-b})}) \widetilde{\boldsymbol{U}}^{(\mathrm{a-b})} = 0 \tag{2.39}$$

The properties of the matrices can be given as follows, where $\mathbf{M}$ and $\mathbf{K}$ are symmetric and positive definite. $\mathbf{K}_C$ is also symmetric which essentially defines the conservation of momentum at the interface, while $\mathbf{K}_F$ is non-symmetric with the non-conservative nature of friction at slip state. Often damping matrix $\mathbf{C}$ is also added purely in numerical context, typically through modal or Rayleigh damping. In the scope of modelling rotational inertia effects, gyroscopic matrix $\mathbf{G}$ can also be defined, where $\mathbf{C}$ and $\mathbf{G}$ are both velocity dependent. We do not consider damping

and gyroscopic effects for the following discussions, where we mainly focus on contact and friction definitions.

With the definition of finite-dimensional space ${}_h\boldsymbol{V}$, the steady-sliding problem can be expressed as

$$\sum_{\mathrm{k}}^{\mathrm{a,b}} \Bigg\{ \int_\Omega \boldsymbol{\sigma}^{(\mathrm{k})}({}_h\boldsymbol{u}^{(\mathrm{k})}) : \nabla_h \boldsymbol{v}_i^{(\mathrm{k})} \, d\Omega - \int_{\Gamma_C} \mu p({}_h u_n - {}_h g_n)_+ \, {}_h\boldsymbol{v}_i^{(\mathrm{k})}.\hat{\mathbf{v}}_k \, d\Gamma_C$$
$$+ \int_{\Gamma_C} p({}_h u_n - {}_h g_n)_+ \, {}_h\boldsymbol{v}_i^{(\mathrm{k})}.\hat{\mathbf{v}}_n \, d\Gamma_C - \int_{\Gamma_N} {}_h\boldsymbol{t}_N^{(\mathrm{k})}.{}_h\boldsymbol{v}_i^{(\mathrm{k})} \, d\Gamma_N - \int_\Omega {}_h\boldsymbol{f}^{(\mathrm{k})}.{}_h\boldsymbol{v}_i^{(\mathrm{k})} \, d\Omega = 0 \Bigg\}$$
$$\forall {}_h\boldsymbol{v}_i^{(\mathrm{k})} \in {}_h\boldsymbol{V}^{(\mathrm{k})} \quad (2.40)$$

where the solution to the problem corresponds to $\boldsymbol{u}_{eq}$. The matrix form of the problem can be expressed as

$$(\mathbf{K}^{(a-b)} + \mathbf{K}_C^{(a-b)} + \mathbf{K}_F^{(a-b)})\boldsymbol{U}_{eq}^{(a-b)} = \boldsymbol{F}^{(a-b)} \quad (2.41)$$

2.3.4 Hypothesis of contact stiffness

We do not focus on the physical characteristics of contact stiffness in the light of normal compliance, and its subsequent effect on CEA. It is widely known that contact stiffness is correlated to contact pressure and in fact the variation of pressure at the contact interface has been shown to be sensitive to squeal prediction. With node-to-node contact, such variation of contact pressure can not be considered since the strong form of contact is only satisfied discretely at nodes. In essence, contact stiffness models the interface characteristics in a differential sense by taking in to account of the so called asperities which are microscopic undulations in addition to other tribological characteristics. With determining contact stiffness experimentally in a differential sense for a contact interface, it can be extended mathematically to define contact characteristics on the whole interface, provided the interface characteristics are unvarying on the whole interface. This is not often the case with braking systems where interface characteristics largely vary within the contact interface. This is apparent, since in a typical braking system, contact pressure is known to be non-uniformly distributed in the process of braking, where such pressure variations can lead to variation in contact stiffness. But the correlation between contact pressure and contact stiffness is not often straightforward to model mathematically. Nevertheless, for a given contact formulation, contact stiffness can be determined to be at least close to the experimental results. But a detailed analysis of the sensitivity of contact formulation in relation to CEA has not been largely studied.

The other major question is characterising contact stiffness for the variation of shapes in shape optimisation, such that the characteristics of contact stiffness is

stationary given the considered setting in optimisation. With varying contact area in shape optimisation, either the setting of constant force or constant pressure can be considered at the interface. Since, the precise relation between contact pressure and contact stiffness is not mathematically known, one can only hypothesise with some intuition. For an applied force $\boldsymbol{t}$ at the contact interface Γ_C, we hypothesise that $\boldsymbol{t} \propto p_G = \int_{\Gamma_C} p_l \, d\Gamma_C$, where we can define p_G and p_l as global contact stiffness and local contact stiffness respectively. With regards to experiments, contact stiffness can be determined either from the perspective of p_G or p_l depending on the desired accuracy. With node-to-node contact formulation which can be interpreted as collocation with strong form, only constant force setting can be considered with non-varying p_G in optimisation, where contact stiffness between any two spatially corresponding nodes can be defined by p_l as

$$p_l = \frac{p_G}{\mathrm{m}} \tag{2.42}$$

with m being the number of contact nodes at the interface. With the weak form, either of the setting can be considered, which we define with Isogeometric approach in §3.2.2.

2.4 Craig & Bampton reduction

For the ease of computation, the dynamical model (2.39) can be reduced through model reduction where we used Craig & Bampton reduction [65]. This is essentially to take advantage of sub-structuring in shape optimisation, where only the matrices of the sub-structures defined for shape optimisation can be computed in every iteration. Craig & Bampton (C&B) reduction essentially captures the properties at the contact interface along with the internal dynamic properties. In accordance to the method, for a domain $\Omega^{(\mathrm{k})}$, the vector $\boldsymbol{U}^{(\mathrm{k})}$ and the matrices $\mathbf{K}^{(\mathrm{k})}$ and $\mathbf{M}^{(\mathrm{k})}$ are split between internal (u) and interface (v) degrees of freedom as follows

$$\boldsymbol{U}^{(\mathrm{k})} = \begin{bmatrix} \boldsymbol{U}_{\mathrm{u}}^{(\mathrm{k})} \\ \boldsymbol{U}_{\mathrm{v}}^{(\mathrm{k})} \end{bmatrix} \tag{2.43}$$

$$\mathbf{K}^{(\mathrm{k})} = \begin{bmatrix} \mathbf{K}_{\mathrm{uu}}^{(\mathrm{k})} & \mathbf{K}_{\mathrm{uv}}^{(\mathrm{k})} \\ \mathbf{K}_{\mathrm{vu}}^{(\mathrm{k})} & \mathbf{K}_{\mathrm{vv}}^{(\mathrm{k})} \end{bmatrix} \tag{2.44}$$

$$\mathbf{M}^{(\mathrm{k})} = \begin{bmatrix} \mathbf{M}_{\mathrm{uu}}^{(\mathrm{k})} & \mathbf{M}_{\mathrm{uv}}^{(\mathrm{k})} \\ \mathbf{M}_{\mathrm{vu}}^{(\mathrm{k})} & \mathbf{M}_{\mathrm{vv}}^{(\mathrm{k})} \end{bmatrix} \tag{2.45}$$

The transformation matrix $\mathbf{T}$ can be constructed from the composition of static transformation $\mathbf{\Theta}_s = \mathbf{K}_{\mathrm{uu}}^{-1}\mathbf{K}_{\mathrm{uv}}$ and the matrix of eigenvectors $\mathbf{\Theta}_d = [\Theta_1 \quad \Theta_2 \quad \cdots \quad \Theta_H]$ obtained by solving the problem $(\mathbf{K}_{\mathrm{uu}} - \lambda_{\mathrm{i}}^2\mathbf{M}_{\mathrm{uu}})\Theta_{\mathrm{i}} = 0$ for the first H modes, where the choice of H depends on the number of modes to be represented in the problem. The matrix $\mathbf{T}$ can hence be defined as

$$\mathbf{T}^{(\mathrm{k})} = \begin{bmatrix} \mathbf{\Theta}_d^{(\mathrm{k})} & \mathbf{\Theta}_s^{(\mathrm{k})} \\ \mathbf{0} & \mathbb{I} \end{bmatrix} \tag{2.46}$$

The transformation to define the reduced mass $\hat{\mathbf{M}}^{(\mathrm{k})}$ and stiffness $\hat{\mathbf{K}}^{(\mathrm{k})}$ matrices can be realized by $\hat{\mathbf{M}} = \mathbf{T}^T\mathbf{M}\mathbf{T}$ and $\hat{\mathbf{K}} = \mathbf{T}^T\mathbf{K}\mathbf{T}$, where the reduced matrices are expressed in the reduced coordinates $\mathbf{Z} = \begin{bmatrix} \mathscr{M} \\ \boldsymbol{U}_{\mathrm{v}} \end{bmatrix}$, with $\mathscr{M}$ representing the modal coordinates.

The composition of the matrices $\hat{\mathbf{M}}$ and $\hat{\mathbf{K}}$ can be expressed as

$$\hat{\mathbf{M}} = \begin{bmatrix} \hat{\mathbf{M}}_{\mathrm{uu}} & \hat{\mathbf{M}}_{\mathrm{uv}} \\ \hat{\mathbf{M}}_{\mathrm{vu}} & \hat{\mathbf{M}}_{\mathrm{vv}} \end{bmatrix} \tag{2.47}$$

$$\hat{\mathbf{K}} = \begin{bmatrix} \hat{\mathbf{K}}_{\mathrm{uu}} & \hat{\mathbf{K}}_{\mathrm{uv}} \\ \hat{\mathbf{K}}_{\mathrm{vu}} & \hat{\mathbf{K}}_{\mathrm{vv}} \end{bmatrix} \tag{2.48}$$

where for $\hat{\mathbf{M}}$, the sub-matrices can be expressed as $\hat{\mathbf{M}}_{\mathrm{uu}} = \mathbb{I}$, $\hat{\mathbf{M}}_{\mathrm{uv}} = \hat{\mathbf{M}}_{\mathrm{vu}}^T = {\mathbf{\Theta}_d}^T(\mathbf{M}_{\mathrm{uv}} - \mathbf{M}_{\mathrm{uu}}\mathbf{K}_{\mathrm{uu}}^{-1}\mathbf{K}_{\mathrm{uv}})$ and $\hat{\mathbf{M}}_{\mathrm{vv}} = \mathbf{M}_{\mathrm{vv}} - \mathbf{M}_{\mathrm{vu}}\mathbf{K}_{\mathrm{uu}}^{-1}\mathbf{K}_{\mathrm{uv}} - \mathbf{K}_{\mathrm{vu}}\mathbf{K}_{\mathrm{uu}}^{-1}\mathbf{M}_{\mathrm{uv}} + \mathbf{K}_{\mathrm{vu}}\mathbf{K}_{\mathrm{uu}}^{-1}\mathbf{M}_{\mathrm{uu}}\mathbf{K}_{\mathrm{uu}}^{-1}\mathbf{K}_{\mathrm{uv}}$. Similarly for $\hat{\mathbf{K}}$, the sub-matrices can be expressed as $\hat{\mathbf{K}}_{\mathrm{uu}} = {\mathbf{\Theta}_d}^T\mathbf{K}_{\mathrm{uu}}\mathbf{\Theta}_d = \hat{\mathcal{I}}$, $\hat{\mathbf{K}}_{\mathrm{uv}} = \hat{\mathbf{K}}_{\mathrm{vu}} = 0$ and $\hat{\mathbf{K}}_{\mathrm{vv}} = \mathbf{K}_{\mathrm{vv}} - \mathbf{K}_{\mathrm{vu}}\mathbf{K}_{\mathrm{vu}}^{-1}\mathbf{K}_{\mathrm{uv}}$, where $\hat{\mathcal{I}} = \begin{bmatrix} \lambda_1 & 0 & 0 \\ 0 & \ddots & 0 \\ 0 & 0 & \lambda_H \end{bmatrix}$.

Essentially, the interface degrees of freedom $\boldsymbol{U}_{\mathrm{v}}$ for a given domain is defined by contact and friction degrees of freedom, where the reduced contact $\hat{\mathbf{K}}_C$ and friction $\hat{\mathbf{K}}_F$ matrices defined by the coordinates $\boldsymbol{U}_{\mathrm{v}}^{(\mathrm{a-b})} = \begin{bmatrix} \boldsymbol{U}_{\mathrm{v}}^{(\mathrm{a})} \\ \boldsymbol{U}_{\mathrm{v}}^{(\mathrm{b})} \end{bmatrix}$, has the form

$$\hat{\mathbf{K}}_C^{(\mathrm{a-b})} = \begin{bmatrix} \hat{\mathbf{K}}_C^{(\mathrm{a})} & \hat{\mathbf{K}}_C^{(\mathrm{a,b})} \\ \hat{\mathbf{K}}_C^{(\mathrm{b,a})} & \hat{\mathbf{K}}_C^{(\mathrm{b})} \end{bmatrix} \tag{2.49}$$

$$\hat{\mathbf{K}}_F^{(\mathrm{a-b})} = \begin{bmatrix} \hat{\mathbf{K}}_F^{(\mathrm{a})} & \hat{\mathbf{K}}_F^{(\mathrm{a,b})} \\ \hat{\mathbf{K}}_F^{(\mathrm{b,a})} & \hat{\mathbf{K}}_F^{(\mathrm{b})} \end{bmatrix} \tag{2.50}$$

The reduced mass matrix of the system, $\hat{\mathbf{M}}^{(a-b)}$, can simply be expressed as

$$\hat{\mathbf{M}}^{(a-b)} = \begin{bmatrix} \hat{\mathbf{M}}^{(a)} & 0 \\ 0 & \hat{\mathbf{M}}^{(b)} \end{bmatrix} \tag{2.51}$$

where the mass matrix is essentially uncoupled between the domains. But it should be noted that, for $\hat{\mathbf{M}}^{(\mathrm{k})}$, the internal $\boldsymbol{U}_{\mathrm{u}}$ and interface $\boldsymbol{U}_{\mathrm{v}}$ degrees of freedom are coupled, i.e., $\hat{\mathbf{M}}^{(\mathrm{k})}_{\mathrm{uv}} = (\hat{\mathbf{M}}^{(\mathrm{k})}_{\mathrm{vu}})^T \neq 0$. This is not true in case of the reduced stiffness matrix of the system, $\hat{\mathbf{K}}^{(a-b)}$, where coupling exists through contact and friction. Hence, the sub-structuring of the domains are essentially coupled through the interface degrees of freedom $\boldsymbol{U}_{\mathrm{v}}$, where the stiffness matrix with the definition of contact and friction can be expressed with the matrix $\hat{\mathbf{K}}^{(\mathrm{a-b})}_{\uplus CF}$ in reduced coordinates as

$$\hat{\mathbf{K}}^{(\mathrm{a-b})}_{\uplus CF} = \begin{bmatrix} \hat{\mathcal{I}}^{(\mathrm{a})} & 0 & 0 & 0 \\ 0 & \hat{\mathbf{K}}^{(\mathrm{a})}_{\mathrm{vv}} + \hat{\mathbf{K}}^{(\mathrm{a})}_{C} + \hat{\mathbf{K}}^{(\mathrm{a})}_{F} & 0 & \hat{\mathbf{K}}^{(\mathrm{a,b})}_{C} + \hat{\mathbf{K}}^{(\mathrm{a,b})}_{F} \\ 0 & 0 & \hat{\mathcal{I}}^{(\mathrm{b})} & 0 \\ 0 & \hat{\mathbf{K}}^{(\mathrm{b,a})}_{C} + \hat{\mathbf{K}}^{(\mathrm{b,a})}_{F} & 0 & \hat{\mathbf{K}}^{(\mathrm{b})}_{\mathrm{vv}} + \hat{\mathbf{K}}^{(\mathrm{b})}_{C} + \hat{\mathbf{K}}^{(\mathrm{b})}_{F} \end{bmatrix} \tag{2.52}$$

where the coordinates of the matrix is defined by $\mathbf{Z}^{(\mathrm{a-b})} = \begin{bmatrix} \mathbf{Z}^{(\mathrm{a})} \\ \mathbf{Z}^{(\mathrm{b})} \end{bmatrix}$, which is also true for $\hat{\mathbf{M}}^{(\mathrm{a-b})}$. Unlike $\hat{\mathbf{M}}^{(\mathrm{k})}$, for $\hat{\mathbf{K}}^{(\mathrm{k})}$ there is no coupling between $\boldsymbol{U}_{\mathrm{u}}{}^{(\mathrm{k})}$ and $\boldsymbol{U}_{\mathrm{v}}{}^{(\mathrm{k})}$, but essentially it is only $\hat{\mathbf{K}}^{(\mathrm{a-b})}$ that couples the domains.

2.5 Brake squeal problem

Considering brake squeal, it is well known that squeal noise can be linked to modal behaviour. Hence, it seems quite obvious to build an optimisation criterion to characterise squeal noise on the presence of unstable modes which define flutter-type instability. Given a linear system, the most efficient is to use eigenvalue analysis where we can characterise modes through eigenvalues in one computation. The topic of linearisation of such systems has been the discussion with previous explanations, where we achieve linearisation of contact and friction around a fixed point.

2.5.1 Complex-eigenvalue analysis

For the following definitions, we consider an applicative example of disc-pad system $\mathrm{d}-\mathrm{p}$ as a simplified brake system, which essentially consists of two domains: a disc $\Omega^{(\mathrm{d})}$ and a pad $\Omega^{(\mathrm{p})}$. The disc is defined as a solid annulus geometry fixed at the inner cylindrical face. The pad is constrained to be in contact with the disc defined by $\boldsymbol{u}_{eq}$ and with additional constraints to avoid any rigid body modes in the system. The description of pad shapes in optimization is detailed in section 4. The idea of defining a simple system at least initially is to make focused studies on individual problems by avoiding the complexity of boundary conditions present in a real braking system, where we focus on defining a frame-work for shape optimisation of such systems. For the following explanations, we express the matrices in normal coordinates as

supposed to reduced coordinates where we later define a strategy for sub-structuring with reduced coordinates in optimisation. The problem (2.39) for d − p system can be defined as

$$\mathbf{M}^{(\mathrm{d-p})}\ddot{\widetilde{\boldsymbol{U}}}^{(\mathrm{d-p})} + (\mathbf{K}^{(\mathrm{d-p})} + \mathbf{K}_C^{(\mathrm{d-p})} + \mathbf{K}_F^{(\mathrm{d-p})})\widetilde{\boldsymbol{U}}^{(\mathrm{d-p})} = 0 \tag{2.53}$$

With the assumption of a feasible solution of the form $\Theta e^{\lambda t}$ for $\boldsymbol{U}$, the characteristics eigenvalue problem can be expressed as

$$(\lambda^2\mathbf{M}^{(\mathrm{d-p})} + (\mathbf{K}^{(\mathrm{d-p})} + \mathbf{K}_C^{(\mathrm{d-p})} + \mathbf{K}_F^{(\mathrm{d-p})}))\Theta = 0 \tag{2.54}$$

It is evident that the value of λ determines the state of the perturbed solution $\widetilde{\boldsymbol{U}}$. Since $\mathbf{K}_F$ is non-symmetric from the definition of friction at the slip state, this can lead to λ and Θ being a complex value and a complex vector respectively. For a complex value of λ, the imaginary part $\Im(\lambda)$ defines the oscillatory behaviour of $\widetilde{\boldsymbol{U}}$ and the real part $\Re(\lambda)$ characterizes the stability of $\widetilde{\boldsymbol{U}}$.

Hence, depending on the value of $\Re(\lambda)$, the stability of a mode can be categorized into one of the following:

- $\Re(\lambda) > 0$ unstable mode
- $\Re(\lambda) < 0$ stable mode
- $\Re(\lambda) = 0$ neutral

In our system, the coefficient of friction μ is the driving parameter which determines stability, such that increase in the value of μ can drive the system from stable to unstable behaviour. This type of instability is characterised by Hopf-bifurcation where the presence of a limit cycle is determined by the occurrence of a pair of eigenvalues $\pm\Re(\widehat{\lambda}_\mu) + \Im(\widehat{\lambda}_\mu)$, with $\widehat{\lambda}_\mu$ being the eigenfrequency of two modes undergoing coalescence at μ [66, 67]. The presence of this type of limit cycle defines a self-excitation behaviour leading to flutter-type instability. This is physically understood for our system as follows, the bifurcation leads to two modes with $\pm\Re(\widehat{\lambda}_{\mu_o})$ for a given frequency $\Im(\widehat{\lambda}_{\mu_o})$ at the point of bifurcation μ_o and when $\mu > \mu_o$, the two modes $+\Re(\widehat{\lambda}_{\mu>\mu_o}) + \Im(\widehat{\lambda}_{\mu>\mu_o})$ and $-\Re(\widehat{\lambda}_{\mu>\mu_o}) + \Im(\widehat{\lambda}_{\mu>\mu_o})$ characterize stable and unstable behaviours respectively, leading to mode-coalescence phenomenon [68]. The presence of this type of instability in the range of brake squeal frequency can indicate the presence of brake squeal noise. But, it should be noted that the magnitude of $+\Re(\widehat{\lambda})$ defines the rate of divergence which may not quantify noise level.

Example of mode shapes for the disc-pad system obtained through CEA are shown in the Figures 2.3 and 2.4.

We discuss the empirical observations from the post-processing of mode shapes, even though the results are highly subjective and depend on the value of p which is typically determined from experiments in the light of normal compliance. Typically

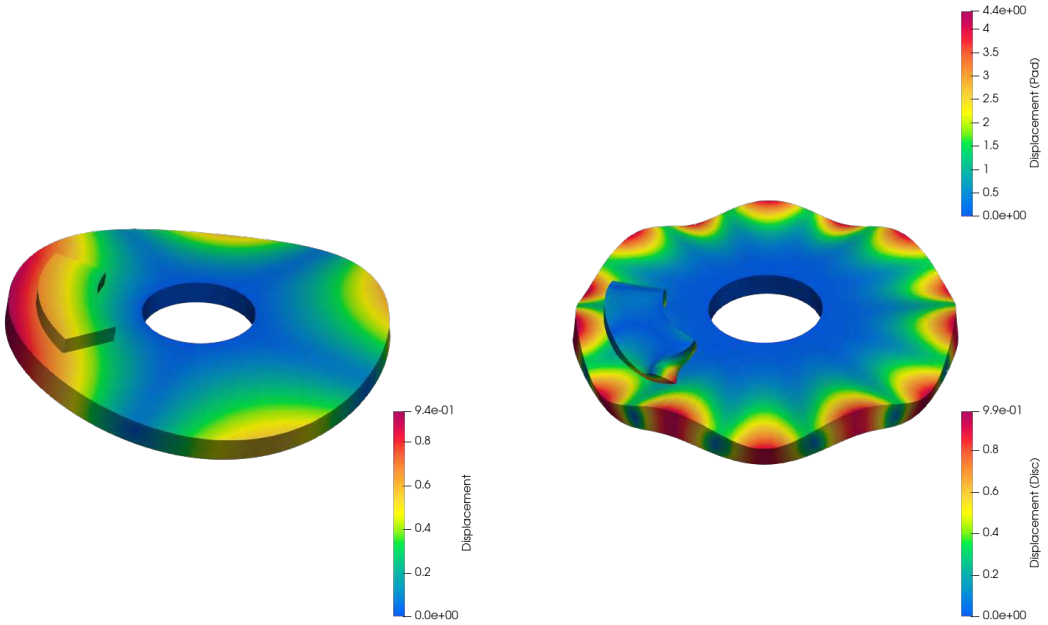

(a) Mode no. 5, Frequency:1476 Hz (b) Mode no. 26, Frequency:9245 Hz

Figure 2.3: Example of disc-pad stable modes (Achieved with Isogeometric method)

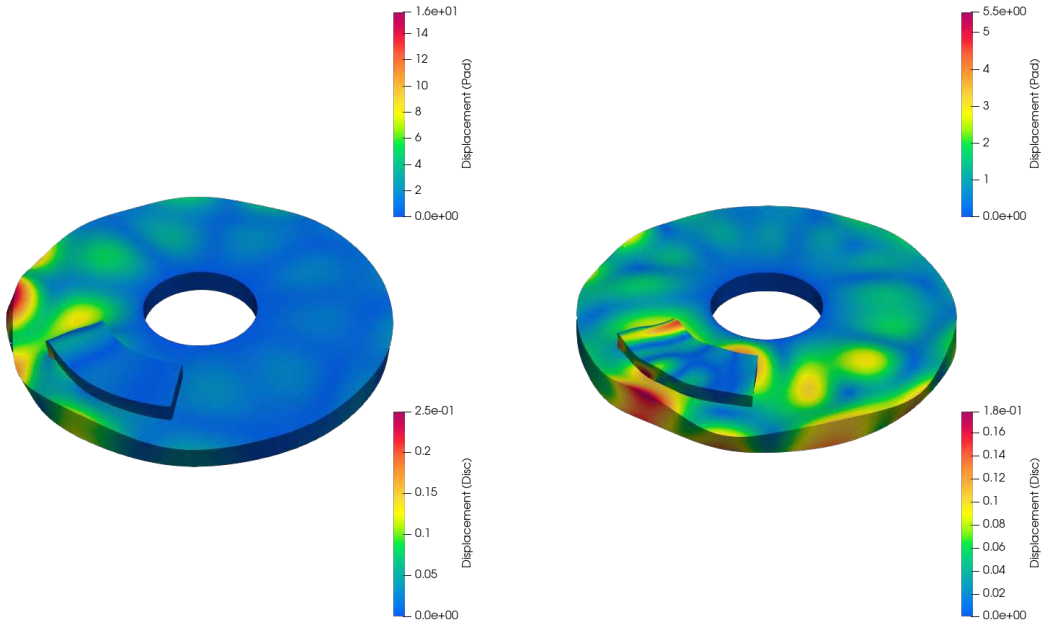

(a) Mode no. 45, Frequency:12236 Hz (b) Mode no. 82, Frequency:17259 Hz

Figure 2.4: Example of disc-pad unstable modes, where the displacement field is considered only for real-part of the eigenvector (Achieved with Isogeometric method)

at low frequencies, the mode shape of the pad follows the shape of the disc with correspondence in displacement field at the contact interface. While at higher frequencies, the behaviour is complicated to understand, but relatively large difference in magnitude of displacement field between the disc and the pad was observed. Further, the unstable modes lead to definition of eigenvectors in complex-plane for displacement field, which was not considered for representation in Figure 2.4. For intuition, a complex eigenvalue with non-zero real and imaginary parts, defines the phase-lag in the displacement field for an eigenvector and hence, the stable equilibrium position of the displacement field for an eigenvector is never achieved simultaneously.

2.5.2 Stability criterion in optimisation

In the context of shape optimization, the idea is to define a criterion for optimization independent of the coefficient of friction μ, such as to reduce the influence of μ in defining optimal shapes. This is because the parameter μ is mostly uncertain in real world[2] and also instabilities could be easily averted at lower values of μ. Hence, to define a criterion which characterizes instability for a geometric shape $\boldsymbol{X}$ independent of μ, we define the criterion as follows

$$C_{\mathsf{s}}(\boldsymbol{X}) = \int_{\mu} max\{\Re(\boldsymbol{\Lambda}_{\mu}(\boldsymbol{X}))\}\, d\mu \tag{2.55}$$

where $\boldsymbol{\Lambda} = \{\lambda^1 \cdots \lambda^{(.)}\}$ is a set of eigenvalues of the system. The criterion is essentially a black-box function defined by maximum of the real part in $\boldsymbol{\Lambda}_{\mu}(\boldsymbol{X})$ at a given value of μ, integrated over μ. Typically, it can be too unrealistic or optimistic to minimise the criterion over the whole range of squeal frequency (1 to 16 KHz) and hence, the set $\boldsymbol{\Lambda}$ can be chosen for a specific range of frequency. This can also be a better strategy in defining meta-model for C_{s}, since the meta-model can be more accurate in characterising the behaviour of modes over a specific range of frequency than the whole range. Even though, no correlation can be implied between $\max\{\Re(\boldsymbol{\Lambda}_{\mu}(\boldsymbol{X}))\}$ and noise level, choosing $\max\{\Re(\boldsymbol{\Lambda}_{\mu}(\boldsymbol{X}))\}$ is essential to define some smoothness for C_{s} in optimisation. Hence the choice of $\max\{\Re(\boldsymbol{\Lambda}_{\mu}(\boldsymbol{X}))\}$ does not necessarily characterise noise level but the presence of instability which can be accounted for squeal noise. Nevertheless, the Utopian goal of $C_{\mathsf{s}} = 0$ defines lack of instabilities and hence characterising noise level may not be a concern if such a goal could be reached in optimisation.

Evaluation of C_{s} can be computationally expensive, but with the aid of model reduction and parallel computing, it can be made to be efficient. In the following, we give the general frame-work for evaluating C_{s}. The reduced stiffness matrices of the multi-patch disc can be defined with C&B method as

[2]In the scope of uncertainty, we do not consider random perturbation of μ with in a contact surface

$$\hat{\mathbf{K}}^{(\mathrm{d})} = \begin{bmatrix} \hat{\mathcal{I}}^{(\mathrm{d})} & 0 \\ 0 & \hat{\mathbf{K}}^{(\mathrm{d})}_{\mathrm{vv}} \end{bmatrix} \tag{2.56}$$

where the matrix is defined by the coordinates $\boldsymbol{Z}^{(\mathrm{d})} = \begin{bmatrix} \mathscr{M}^{(\mathrm{d})} \\ \boldsymbol{U}^{(\mathrm{d})}_{\mathrm{v}} \end{bmatrix}$, with $\boldsymbol{U}^{(\mathrm{d})}_{\mathrm{v}}$ defining the degrees of freedom on $\Gamma^{(\mathrm{d})}_{C}$ [3]. The matrix is essentially the same in optimisation where we consider optimisation only on Ω^{p}. Hence, for a given definition of shape, the following matrix is computed

$$\hat{\mathbf{K}}^{(\mathrm{p})} = \begin{bmatrix} \hat{\mathcal{I}}^{(\mathrm{p})} & 0 \\ 0 & \hat{\mathbf{K}}^{(\mathrm{p})}_{\mathrm{vv}} \end{bmatrix} \tag{2.57}$$

The evaluation of C_{s} demands the definition of $\hat{\mathbf{K}}^{(\mathrm{d-p})}$ for several values of μ. Since μ is the property of interface, the characteristics at the interface can be decoupled as interface degrees of freedom $\boldsymbol{U}_{\mathrm{v}}$ in C&B reduced coordinates. For the definition of $\hat{\mathbf{K}}^{(\mathrm{d-p})}_{F}$ (refer §2.4), μ can be factored out as $\mu\hat{\mathbf{K}}^{(\mathrm{d-p})}_{F}|_{\mu=1}$ [4]. The idea is that for the evaluation of C_{s}, with numerical integration defined over μ, the matrix $\hat{\mathbf{K}}^{(\mathrm{d-p})}_{F}|_{\mu}$ does not need to be evaluated for discrete values of μ, but instead $\hat{\mathbf{K}}^{(\mathrm{d-p})}_{F}|_{\mu}$ can be computed as $\mu\hat{\mathbf{K}}^{(\mathrm{d-p})}_{F}|_{\mu=1}$, where $\hat{\mathbf{K}}^{(\mathrm{d-p})}_{F}$ in this case is computed only once with $\mu = 1$.

The computational cost of evaluating C_{s} with numerical integration for discrete values of μ can be reduced through parallel computation. The only varying parameter for parallelisation is μ for the definition of $\hat{\mathbf{K}}^{(\mathrm{d-p})}_{F}$, hence the computation of the matrices $\hat{\mathbf{M}}^{(\mathrm{p})}$, $\hat{\mathbf{K}}^{(\mathrm{p})}$, $\hat{\mathbf{K}}^{(\mathrm{d-p})}_{C}$ and $\hat{\mathbf{K}}^{(\mathrm{d-p})}_{F}|_{\mu=1}$ are achieved on single core. Further with $\hat{\mathbf{M}}^{(\mathrm{d})}$ and $\hat{\mathbf{K}}^{(\mathrm{d})}$ already computed, the reduced matrices of $\hat{\mathbf{M}}^{(\mathrm{d-p})}$ and $\hat{\mathbf{K}}^{(\mathrm{d-p})}$ can also be defined on single core as

$$\hat{\mathbf{M}}^{(\mathrm{d-p})} = \begin{bmatrix} \hat{\mathbf{M}}^{(\mathrm{d})} & 0 \\ 0 & \hat{\mathbf{M}}^{(\mathrm{p})} \end{bmatrix} \tag{2.58}$$

$$\hat{\mathbf{K}}^{(\mathrm{d-p})}_{\uplus C} = \begin{bmatrix} \hat{\mathcal{I}}^{(\mathrm{a})} & 0 & 0 & 0 \\ 0 & \hat{\mathbf{K}}^{(\mathrm{d})}_{\mathrm{vv}} + \hat{\mathbf{K}}^{(\mathrm{d})}_{C} & 0 & \hat{\mathbf{K}}^{(\mathrm{d,p})}_{C} \\ 0 & 0 & \hat{\mathcal{I}}^{(\mathrm{p})} & 0 \\ 0 & \hat{\mathbf{K}}^{(\mathrm{p,d})}_{C} & 0 & \hat{\mathbf{K}}^{(\mathrm{p})}_{\mathrm{vv}} + \hat{\mathbf{K}}^{(\mathrm{p})}_{C} \end{bmatrix} \tag{2.59}$$

where the matrices are expressed in coordinates $\mathbf{Z}^{(\mathrm{d-p})}$. Similarly, the matrix $\hat{\mathbf{K}}^{(\mathrm{d-p})}_{F}|_{\mu=1}$ can be expressed in $\mathbf{Z}^{(\mathrm{d-p})}$ coordinates as

[3] It should be noted that in the context of multi-patch parameterisation, detailed in §,$\Gamma^{(\mathrm{d})}_{C}$ corresponds to $\Gamma^{(\mathrm{d}_1)}_{C}$, where the contact interface is defined to be on $\Omega^{(\mathrm{d}_1)}$.

[4] $\hat{\mathbf{K}}^{(\mathrm{d-p})}_{F}|_{\mu=1}$ can be interpreted as $\hat{\mathbf{K}}^{(\mathrm{d-p})}_{F}$ computed with $\mu = 1$

$$\hat{\mathbf{K}}^{(\mathrm{d-p})}_{\cup F}|_{\mu=1} = \begin{bmatrix} 0 & 0 & 0 & 0 \\ 0 & \hat{\mathbf{K}}^{(\mathrm{d})}_{F} & 0 & \hat{\mathbf{K}}^{(\mathrm{d,p})}_{F} \\ 0 & 0 & 0 & 0 \\ 0 & \hat{\mathbf{K}}^{(\mathrm{p,d})}_{F} & 0 & \hat{\mathbf{K}}^{(\mathrm{p})}_{F} \end{bmatrix}_{\mu=1} \tag{2.60}$$

The evaluation of C_{s} with numerical integration can be expressed as

$$\int_{\mu} max\{\Re(\mathbf{\Lambda}_{\mu}(\boldsymbol{X}))\}\, d\mu \approx \sum_{\mu_{\mathsf{i}}\in[0,1]} max\{\Re(\mathbf{\Lambda}_{\mu_{\mathsf{i}}}(\boldsymbol{X}))\}\, w_{\mathsf{i}} \tag{2.61}$$

where μ_{i} can be spaced evenly in the interval $[0, 1]$. Hence, on each parallel core, the matrix $\hat{\mathbf{K}}^{(\mathrm{d-p})}_{\uplus CF}$ can be computed as

$$\hat{\mathbf{K}}^{(\mathrm{d-p})}_{\uplus CF} = \hat{\mathbf{K}}^{(\mathrm{d-p})}_{\uplus C} + \mu_{\mathsf{i}}\, \hat{\mathbf{K}}^{(\mathrm{d-p})}_{\cup F}|_{\mu=1} \tag{2.62}$$

Along with the definition of $\hat{\mathbf{K}}^{(\mathrm{d-p})}_{\uplus CF}$, the computation in parallel cores is defined for Eq. (2.54) in reduced coordinates, where in each core, the computation of the characteristics eigenvalue problem in reduced coordinates can be expressed as

$$(\lambda^2\hat{\mathbf{M}}^{(\mathrm{d-p})} + \hat{\mathbf{K}}^{(\mathrm{d-p})}_{\uplus C} + \mu_{\mathsf{i}}\, \hat{\mathbf{K}}^{(\mathrm{d-p})}_{\cup F}|_{\mu=1})\Theta = 0 \tag{2.63}$$

This eventually leads to the evaluation of $max\{\Re(\mathbf{\Lambda}_{\mu_{\mathsf{i}}}(\boldsymbol{X}))\}$ in each parallel core and hence with the evaluation of $max\{\Re(\mathbf{\Lambda}_{\mu_{\mathsf{i}}}(\boldsymbol{X}))\}$ on all parallel cores, C_{s} can be computed from $\sum_{\mu_{\mathsf{i}}\in[0,1]} max\{\Re(\mathbf{\Lambda}_{\mu_{\mathsf{i}}}(\boldsymbol{X}))\}\, w_{\mathsf{i}}$.

3 Numerical modelling of contact and friction

Contact and friction phenomena are highly discontinuous in nature at least in the essence of mathematical elegance (2.8)(2.11). It can be mathematically challenging to handle such discontinuities and hence through regularisation of such discontinuities, the model for contact and friction should be able to describe the desired characteristics. Taking in to account such considerations for numerical modelling is also important for applications sensitive to contact and friction characteristics. We focus on approximation of contact and friction definitions in (2.29) with finite element approach. We give a short introduction for the definition of finite-dimensional approximation space ${}_h\boldsymbol{V}$ in the context of both classical FEM and Isogeometric approach. We primarily focus on view from Isogeometric approach for defining contact and friction formulations, though parallels could be drawn between the two. We also discuss the widely used node-to-node contact formulation of classical finite element methods to extend the intuition of collocation approach in Isogeometric approach.

3.1 Finite-dimensional function space

3.1.1 Classical finite element approach

In classical finite element method, typically a domain Ω is discretised as

$$\Omega \approx {}_h\Omega = \bigcup {}_{el}\Omega \tag{3.1}$$

${}_h\Omega$ is the discretisation of Ω by union of elements, with ${}_{el}\Omega$ being the domain of an element. ${}_{el}\Omega$ is typically parameterised by polynomials like Lagrange or Hermitian polynomials, where the parameterisation in $\mathbb{R}^3$can be expressed as

$${}_{el}\boldsymbol{X}(x,y,z) = \sum_{i=1}^{n} {}_{el}N_i(x,y,z)\,{}_{el}\boldsymbol{P}_i \tag{3.2}$$

where ${}_{el}\boldsymbol{P}_i$ defines the coordinates of the node i, with ${}_{el}N_i(\boldsymbol{\Xi})$ being the interpolating function of the node i. With Isoparametric approach, ${}_{el}\Omega$ is expressed as mapping from a parametric space ${}_{el}\hat{\Omega}$, where ${}_{el}\hat{\Omega} \in \mathbb{R}^3$ is typically defined by cube: $[-1,1] \times [-1,1] \times [-1,1]$. This approach avoids the problem of explicitly referring to each element with generalised coordinates, which is also convenient for defining

numerical quadrature with in elements. ${}_{el}\Omega$ can be expressed directly in parametric coordinates $\boldsymbol{\Xi} := [\xi, \eta, \zeta]$ that parameterises ${}_{el}\hat{\Omega}$ as

$$ {}_{el}\boldsymbol{X}(\boldsymbol{\Xi}) = \sum_{i=1}^{n} {}_{el}N_i(\boldsymbol{\Xi}) {}_{el}\boldsymbol{P}_i \tag{3.3} $$

With this notion, the approximation of a solution $\boldsymbol{u}$ at element level can be expressed as

$$ {}_{el}\boldsymbol{u}(\boldsymbol{\Xi}) = \sum_{i=1}^{n} {}_{el}N_i(\boldsymbol{\Xi}) {}_{el}\boldsymbol{u}_i \tag{3.4} $$

The approximation of solution $\boldsymbol{u}$ over ${}_{h}\Omega$ can be roughly expressed as

$$ {}_{h}\boldsymbol{u} = \sum_{el} {}_{el}\boldsymbol{u} \tag{3.5} $$

We provide a short description of parameterising ${}_{el}\Omega$ with Lagrange polynomials, where such elements are known as Lagrange elements. In 1-dimension, Lagrange polynomial of order $n-1$ can be expressed in parametric coordinates as

$$ N_i(\xi) = \prod_{i=1, j\neq i}^{n} \frac{\xi_j - \xi}{\xi_j - \xi_i} \tag{3.6} $$

For higher dimensions, the interpolation functions are defined by tensor product, where in $\mathbb{R}^3$, the interpolation function can be expressed as

$$ N_i(\xi, \eta, \zeta) = N_j(\xi) N_k(\eta) N_l(\zeta) \tag{3.7} $$

In classical FEM, the main idea is that the space ${}_{h}\boldsymbol{V}$ is defined by N_i that defines ${}_{h}\Omega$ as basis functions. The solution continuity over ${}_{h}\Omega$, which is known as compatibility condition is preserved by defining $\bigcup {}_{el}\Omega$ such that common nodes and edges are defined between elements. This means that common interpolation function is defined for common nodes between elements. This implicitly defines C_0 continuity of solution between adjacent elements, unless explicitly constraints are defined for solution continuity between elements.

3.1.2 Isogeometric approach

With the isoparametric approach of classical FEM, the parametrisation ${}_{el}\boldsymbol{X}$ is local to ${}_{el}\Omega$, where the parametrisation ${}_{h}\boldsymbol{X}$ over ${}_{h}\Omega$ is explicitly achieved by $\bigcup {}_{el}\Omega$. Typically, ${}_{h}\Omega$ is defined from CAD definition of Ω which is parametrised by NURBS. Even though ${}_{h}\Omega$ is defined over Ω, there is no innate relation between the two which makes it harder to achieve a robust definition of ${}_{h}\Omega$ from Ω. This brings the idea of Isogeometric approach where the parameterisation of ${}_{h}\Omega$ from Ω is defined with in same

parametric space, typically through NURBS. Isogeometric approach was developed to merge design and analysis descriptions of a geometry through same class of basis functions [69, 70], where the basis functions used for defining a geometry are also used for approximation of solutions in the context of finite element approach. The parameterisation of a geometry defined with mapping from a parametric space is achieved through NURBS with a set of basis functions, where its subsequent analysis-suitable parameterisation which is usually more refined with a new set of increased number of basis functions is defined with in the same parametric space. This means that ${}_h\Omega$ can be achieved robustly from Ω by defining refinement with in the parametric space that defines Ω. Since ${}_h\Omega$ defines the geometry also as CAD parameterisation, no distinguish can be made between Ω and ${}_h\Omega$, hence $\Omega = {}_h\Omega$. But distinguish is certainly made in the sense of parameterisations, where initial parameterisation $\check{\boldsymbol{X}}$ of Ω is purely defined as design description in the perspective of CAD, while the analysis-suitable parameterisation $\boldsymbol{X}$ of Ω is defined by refinement over $\check{\boldsymbol{X}}$ considering accuracy for approximation of solution.

We start with the definition of B-spline functions with extension to B-spline curves, from which NURBS curves are introduced with the definition of a weighing parameter and a non-uniform knot vector. This is followed by description of higher dimensional geometries through extension by tensor product definition.

The B-spline basis functions can be defined by Cox de Boor's formula as follows,

$$N_{i,0}\left(\xi\right) = \begin{cases} 1 & \xi_i \leq \xi < \xi_{i+1} \\ 0 & otherwise \end{cases} \tag{3.8}$$

$$N_{i,p}\left(\xi\right) = \frac{\xi - \xi_i}{\xi_{i+p} - \xi_i} N_{i,p-1}\left(\xi\right) + \frac{\xi_{i+p+1} - \xi}{\xi_{i+p+1} - \xi_{i+1}} N_{i+1,p-1}\left(\xi\right) \tag{3.9}$$

where p is defined recursively for $p > 0$ to obtain a curve of degree p, which starts with a piecewise constant at $p = 0$. Naturally, a uniform knot vector can be defined as $\boldsymbol{\xi} = \{\xi_1, \xi_2, \cdots, \xi_{n+p+1}\}$, where any $\xi_i - \xi_{i+1}$ is uniformly spaced. For a uniform knot vector, the bases span with continuity C^{p-1} between the knots, where it satisfies partition of unity $\sum_{i=1}^{n} N_{i,p}\left(\xi\right) = 1$ for $[\xi_p, \xi_{n+1}]$, with n being the number of control points. Further, the span of any $N_{i,p}\left(\xi\right)$ is defined in $[\xi_i, \xi_{i+p+1}]$, and $N_{i,p}\left(\xi\right) \geq 0$, $\forall \xi$.

The knot vector need not be equidistant and the multiplicity of a knot ξ_i by $\mathcal{M}$ in the knot vector decreases the continuity by $C^{p-\mathcal{M}}$ across the knot ξ_i, which defines a non-uniform knot vector. The multiplicity $\mathcal{M} = p$ for the first knot and the last knot defines a open knot vector, where the basis functions model interpolation between the first and the last knots. The basis functions defined with an open knot vector satisfies partition of unity $\forall \xi$. Through B-spline basis functions and a knot vector $\boldsymbol{\xi} = \{\xi_1, \cdots, \xi_{n+p+1}\}$, a B-spline curve can be defined with coefficients of the basis functions as follows

$$\boldsymbol{X}_c(\xi) = \sum_{i=1}^{n} N_{i,p}(\xi)\boldsymbol{P}_i \tag{3.10}$$

where with a open knot vector for a curve, the ends of the curve are C^0. The coefficients $\boldsymbol{P}_i \in \mathbb{R}^d$ are the control points, with d being the dimension of the space. The definition of a weighing parameter $w_i > 0$ associated with a re spective basis function N_i, normalized defines rational B-splines where it respects the partition of unity, given as follows

$$\boldsymbol{X}_c(\xi) = \sum_{i=1}^{n} \underbrace{\frac{w_i N_{i,p}(\xi)}{\sum_{i=0}^{n} w_i N_{i,p}(\xi)}}_{R_{i,p}} \boldsymbol{P}_i \tag{3.11}$$

The parameter w_i provides a new dimension for controlling the geometry through projective transformation, while the affine transformation is achieved by $\boldsymbol{P}_i$. Hence, the combination of non-uniform knot vectors and rational basis functions define NURBS. Further, if all weights are the same, NURBS is simply a B-spline with non-uniform knot vector.

The higher dimensional NURBS are a natural extension of its 1-dimensional precursor through tensor product definition where the order of the tensor is the same as the dimension of the geometry. For a 2-dimensional geometry, the tensor product NURBS surface is defined as follows

$$\boldsymbol{X}_s(\xi,\eta) = \sum_{i=1}^{n}\sum_{j=1}^{m} R_{i,p}(\xi)R_{j,q}(\eta)\boldsymbol{P}_{i,j} \tag{3.12}$$

which is supported by knot vectors $\boldsymbol{\xi} = \{\xi_1, \cdots, \xi_{n+p+1}\}$ and $\boldsymbol{\eta} = \{\eta_1, \cdots, \eta_{m+q+1}\}$, for the domain $[\xi_1, \xi_{m+q+1}] \times [\eta_1, \eta_{m+q+1}]$, with $n \times m$ net of control points $\boldsymbol{P}_{i,j}$. Similarly, to define volume, the tensor product NURBS volume is defined as follows

$$\boldsymbol{X}_v(\xi,\eta,\zeta) = \sum_{i=1}^{n}\sum_{j=1}^{m}\sum_{k=1}^{l} \underbrace{R_{i,p}(\xi)R_{j,q}(\eta)R_{k,r}(\zeta)}_{R_{i,j,k}(\boldsymbol{\Xi})} \boldsymbol{P}_{i,j,k} \tag{3.13}$$

where the knot vectors are given as $\boldsymbol{\xi} = \{\xi_1, \cdots, \xi_{n+p+1}\}, \boldsymbol{\eta} = \{\eta_1, \cdots, \eta_{m+q+1}\}$ and $\boldsymbol{\zeta} = \{\zeta_1, \cdots, \zeta_{l+r+1}\}$. The above expression can be simply expressed in matrix form as $\boldsymbol{X}_v(\boldsymbol{\Xi}) = \mathbf{R}(\boldsymbol{\Xi})\mathbf{P}$.

The main idea with Isogeometric approach is to define the space ${}_h\boldsymbol{V}$ with NURBS basis functions which parameterises the geometry. The parameterisation of a domain $\Omega \in \mathbb{R}^3$ as an initial geometric description through NURBS can be expressed as $\check{\boldsymbol{X}}_v^{(\mathrm{k})}(\check{\boldsymbol{\Xi}}^{(\mathrm{k})}) = \check{\mathbf{R}}^{(\mathrm{k})}(\check{\boldsymbol{\Xi}}^{(\mathrm{k})})\check{\mathbf{P}}^{(\mathrm{k})}$, $\boldsymbol{X} : \hat{\Omega} \to \Omega$, where $\boldsymbol{X}$ defines the mapping from the parametric domain $\hat{\Omega}$ to the physical domain Ω – for simplicity, we consider

the parameterisation of the domain Ω_{k} through a single patch: $[\xi_1, \cdots, \xi_{n+p+1}] \times [\eta_1, \cdots, \eta_{m+q+1}] \times [\zeta_1, \cdots, \zeta_{l+r+1}]$. The analysis-suitable parameterization $\boldsymbol{X}$ [1] can be achieved through the refinement of $\check{\boldsymbol{X}} \rightarrow \boldsymbol{X}$ with one or several of the refinement methods (h, p and k), where $\boldsymbol{X}$ can be defined as $\boldsymbol{X}_v(\boldsymbol{\Xi}) = \mathbf{R}(\boldsymbol{\Xi})\mathbf{P}$ to take in to account of the modified knot vectors and control points – more on parameterisation and refinement for our applicative example of disc-pad system is discussed in. It should be noted that the mapping for parameterisation is for the whole domain, i.e., $\boldsymbol{X} : \hat{\Omega} \rightarrow \Omega$ contrary to mapping ${}_{el}\boldsymbol{X}$ of Isoparametric approach which is only local to an element ${}_{el}\Omega$.

3.2 Contact and friction discretization

It should be noted that the following definition of contact and friction approximations are specific for modelling flutter-type dynamic instability with CEA, detailed in §2.5. This can also be seen as analogous to the classic mesh-tying problem.

3.2.1 Idea of collocation method from classical finite element method (Node-to-Node contact)

We discuss the classical collocation method of Node-to-Node contact in classical FEM [71], mainly to provide intuition for extending collocation method to Isogeometric approach. The Lagrange interpolating polynomials define unity at nodes, which is typical of interpolating polynomials in classical FEM –In the sense of interpolation, nodes can be thought as coefficients in generalised or natural coordinates which are essentially interpolated. This property means that nodes lie on the surface discretised by Lagrange elements, which brings the intuition of Node-to-Node contact where the contact is defined between nodes of conforming meshes at the contact interface. Node-to-Node contact can be essentially considered as the collocation method where the strong form of contact or friction definition is satisfied at the nodes in Γ_C. Considering Eq. (2.38), for classical FEM with Lagrange elements, the space ${}_h\boldsymbol{V}$ is defined by the bases ${}_h\boldsymbol{v}_i$ of Lagrange polynomials.

The contact definition of the initial-boundary value problem Eq. (2.29) can be defined in finite element context as

$$ {}_h\sigma_n^{(\mathrm{k})}({}_h\widetilde{\boldsymbol{u}}^{(\mathrm{k})})\hat{\mathbf{v}}_n = -p\,{}_h\widetilde{u}_n{}^{(\mathrm{k})}\hat{\mathbf{v}}_n \quad \text{on} \quad \Gamma_C^{(\mathrm{k})} \tag{3.14} $$

where for a system with two domains $\Omega^{(a)}$ and $\Omega^{(b)}$ in contact, with confirming mesh at $\Gamma_C^{(a)}$ and $\Gamma_C^{(b)}$, it can be said that for any node $i \in \Gamma_C^{(\mathrm{a})}$, there exists a unique

[1] For simplicity of the notation, we define $\boldsymbol{X}$ to be the default notation for analysis-suitable parameterization of a domain $\Omega \in \mathbb{R}^3$

node $j \in \Gamma_C^{(\mathrm{b})}$ that forms contact. Hence, the contact force for a given node $i \in \Gamma_C^{(a)}$ in contact with a node $j \in \Gamma_C^{(b)}$ can simply be expressed with Node-to-Node contact as

$$p[({}_h\widetilde{\boldsymbol{u}}^{(\mathrm{a})} - {}_h\widetilde{\boldsymbol{u}}^{(\mathrm{b})}).\hat{\mathbf{v}}_n]\hat{\mathbf{v}}_n\Big|_{{}_hv_i^{(\mathrm{a})}={}_hv_j^{(\mathrm{b})}=1} = p[(\widetilde{\boldsymbol{u}}_i^{(\mathrm{a})} - \widetilde{\boldsymbol{u}}_j^{(\mathrm{b})}).\hat{\mathbf{v}}_n]\hat{\mathbf{v}}_n \tag{3.15}$$

where ${}_h\widetilde{\boldsymbol{u}}^{(\mathrm{a})} = \sum_{\forall i\in\Omega^{(\mathrm{a})}} {}_hv_i^{(\mathrm{a})}\widetilde{\boldsymbol{u}}_i^{(\mathrm{a})}$ and ${}_h\widetilde{\boldsymbol{u}}^{(\mathrm{b})} = \sum_{\forall j\in\Omega^{(\mathrm{b})}} {}_hv_j^{(\mathrm{b})}\widetilde{\boldsymbol{u}}_j^{(\mathrm{b})}$. Since the collocation is defined at the nodes itself, the bases ${}_hv_i^{(\mathrm{a})} = {}_hv_j^{(\mathrm{b})} = 1$ for Lagrange elements or typically for elements in classical FEM. The above equation is stated specifically for linear case, where normal compliance terms are expressed to be linear.

As an alternative interpretation, the collocation method can also be defined from the weak form of contact (3.19) as

$$\langle {}_h\boldsymbol{\sigma}_n^{(\mathrm{a})}, {}_h\boldsymbol{v}_i^{(\mathrm{a})}\rangle_{\Gamma_C^{(\mathrm{a})}} = \int_{\Gamma_C^{(a)}} p[({}_h\widetilde{\boldsymbol{u}}^{(\mathrm{a})} - {}_h\widetilde{\boldsymbol{u}}^{(\mathrm{b})}).\hat{\mathbf{v}}_n]{}_h\boldsymbol{v}_i^{(\mathrm{a})}.\hat{\mathbf{v}}_n \; d\Gamma_C^{(\mathrm{a})} \rightarrow$$
$$p[(\widetilde{\boldsymbol{u}}_i^{(\mathrm{a})} - \widetilde{\boldsymbol{u}}_j^{(\mathrm{b})}).\hat{\mathbf{v}}_n]\hat{\mathbf{v}}_n \tag{3.16}$$

if the weighting function ${}_h\boldsymbol{v}_i^{(\mathrm{a})}$ of the weak form is defined to be the Dirac-delta function ($\delta_D(.)$) as ${}_h\boldsymbol{v}_i^{(\mathrm{a})} = \delta_D(\widetilde{\boldsymbol{u}}_i^{(\mathrm{a})} - \widetilde{\boldsymbol{u}}^{(\mathrm{a})})$ [2].

Similarly, the friction definition of the initial-boundary value problem Eq. (2.29) can be defined in finite element context as

$${}_h\sigma_t^{(\mathrm{k})}({}_h\widetilde{\boldsymbol{u}}^{(\mathrm{k})})\hat{\mathbf{v}}_k = \mu p_h {}_h\widetilde{u}_n^{(\mathrm{k})}\hat{\mathbf{v}}_k \quad \text{on} \quad \Gamma_C^{(\mathrm{k})} \tag{3.17}$$

Similar to the definition of contact force, the tangential force of friction can be defined with Node-to-Node collocation as

$$\mu[p({}_h\widetilde{\boldsymbol{u}}^{(\mathrm{a})} - {}_h\widetilde{\boldsymbol{u}}^{(\mathrm{b})}).\hat{\mathbf{v}}_n]\hat{\mathbf{v}}_k\Big|_{{}_hv_i^{(\mathrm{a})}={}_hv_j^{(\mathrm{b})}=1} = \mu[p(\widetilde{\boldsymbol{u}}_i^{(\mathrm{a})} - \widetilde{\boldsymbol{u}}_j^{(\mathrm{b})}).\hat{\mathbf{v}}_n]\hat{\mathbf{v}}_k \tag{3.18}$$

The interpretation of collocation from weak form can also be defined with friction, similar to Eq. (3.16). For the d − p system, the friction force can be resolved in to tangential and radial components relative to the disc axis. Since, the relative sliding velocity is negligible in the radial direction, the frictional force component of the radial direction is also negligible and hence often ignored.

While physically, Node-to-Node formulation is more intuitive, there is no restriction for collocation to be achieved elsewhere rather than exclusively at nodes where ${}_hv_i^{(\mathrm{a})} = {}_hv_j^{(\mathrm{b})} = 1$. This already gives intuition for collocation with Isogeometric

[2] $\delta_D(\widetilde{\boldsymbol{u}}_i^{(\mathrm{a})} - \widetilde{\boldsymbol{u}}^{(\mathrm{a})}) : {}_h\boldsymbol{v}_i^{(\mathrm{a})} = 0,\ \forall \widetilde{\boldsymbol{u}}_i^{(\mathrm{a})} \neq \widetilde{\boldsymbol{u}}^{(\mathrm{a})}$ and ${}_h\boldsymbol{v}_i^{(\mathrm{a})} = 1$ if $\widetilde{\boldsymbol{u}}_i^{(\mathrm{a})} = \widetilde{\boldsymbol{u}}^{(\mathrm{a})}$

approach where the control points need not be physically on the surface to achieve an equivalent collocation formulation. A very similar interpretation of nodes can be defined by taking average over knots in NURBS, known as Greville abscissae which are physically on the surface and hence can be defined for collocation [72, 73]. Nevertheless, we expand the weak form of contact and friction ((3.19) & (3.20)) with Isogeometric approach from which collocation can be achieved explicitly in place of quadrature schemes. This approach also aids in considering area which can be more effective for approximation of contact pressure, though not very precise as expensive mortor based approaches .

Some of the limitations of Node-to-Node contact formulation can be owed to meshing. Given that we focus on shape optimisation, Node-to-Node formulation places severe constraints in meshing, where structured meshing must be preferred to define confirming meshes at the contact interface. Depending on the design space in shape optimisation, this may not be a very robust strategy, since structured meshing can severely restrict mesh adaptation to avoid distorted elements that can effect the Isoparametric definition of integrals. On the other hand, it is well known that unstructured mesh definition may not also lead to robust meshing with classical FEM. Due to such complications with meshing, Isogeometric approach can be considered by choosing a robust parameterization strategy which would be rather difficult with classical FEM. We also remind that defining an initial Parametrisation may also be cumbersome with Isogeomtric approach but given a well-defined initial parameterisation, Isogeometric approach can achieve robust refinement. Although the complications with meshing for classical FEM can be avoided with contact formulations that do not demand confirming meshes at the interface, empirically, we find that developing such formulations with Isogeometric approach can be more advantageous in shape optimisation. The effect of contact formulation to the prediction of instabilities with CEA has not been largely studied, where the interest is on the contact characteristics pertaining to the dynamics of the perturbation $\widetilde{\boldsymbol{u}}$ rather than $\boldsymbol{u}_{eq}$ (2.23). This also comes as limitation to choosing the right contact and friction formulations considering computational cost and developing more advanced models.

3.2.2 Expansion of contact and friction weak forms with Isogeometric approach

A detailed review of contact definitions with Isogeometric approach can be found in [74]. The Isogeometric approach for approximation of the solution $\boldsymbol{u}$ 2.29 is achieved through the same NURBS bases $R_{i,j,k}$. For a vector-valued function space ${}_h\boldsymbol{V}$, the vectorial definition of the bases $\boldsymbol{R}_{i,j,k} \in \mathbb{R}^3$ can be defined as

$$\left\{\begin{bmatrix} R_{i,j,k} \\ 0 \\ 0 \end{bmatrix}\right\} \bigcup \left\{\begin{bmatrix} 0 \\ R_{i,j,k} \\ 0 \end{bmatrix}\right\} \bigcup \left\{\begin{bmatrix} 0 \\ 0 \\ R_{i,j,k} \end{bmatrix}\right\}$$

where in matrix form, $\boldsymbol{R}_{i,j,k}(\boldsymbol{\Xi}) := \begin{bmatrix} R_{i,j,k}(\boldsymbol{\Xi}) & 0 & 0 \\ 0 & R_{i,j,k}(\boldsymbol{\Xi}) & 0 \\ 0 & 0 & R_{i,j,k}(\boldsymbol{\Xi}) \end{bmatrix}$

which is taken in to account through the definition of the matrix $\mathbf{R}(\boldsymbol{\Xi})$ and the vector $\mathbf{P}$ as

$$\mathbf{R}(\boldsymbol{\Xi}) = \begin{bmatrix} \boldsymbol{R}_{1,1,1}(\boldsymbol{\Xi}) & \cdots & \boldsymbol{R}_{n,m,l}(\boldsymbol{\Xi}) \end{bmatrix}$$

$$\mathbf{P} = \begin{bmatrix} \boldsymbol{P}_{1,1,1} & \cdots & \boldsymbol{P}_{n,m,l} \end{bmatrix}^T, \quad \boldsymbol{P}_{i,j,k} = \begin{bmatrix} P^x_{i,j,k} & P^y_{i,j,k} & P^z_{i,j,k} \end{bmatrix}$$

In a abstract sense, the bases $\boldsymbol{R}_{i,j,k}(\boldsymbol{\Xi})$ in parametric space is transformed to the bases $\boldsymbol{\phi}_{i,j,k}(x,y,z)$ in physical space using the push-forward operator $\circ$, where the bases $\boldsymbol{\phi}_{\mathrm{i}}$ is defined with the property $\boldsymbol{\phi}_{\mathrm{i}} = \boldsymbol{\phi}_{i,j,k}(\boldsymbol{X}) = \boldsymbol{R}_{i,j,k}(\boldsymbol{\Xi}) \circ \boldsymbol{X}^{-1}$. Hence, the approximation of a field variable on Ω is defined through all the bases $\boldsymbol{\phi}_{\mathrm{i}}$ spanning the finite-dimensional function space $\boldsymbol{\Phi}$. For Isogeometric approach, we express the finite-dimensional space ${}_h\boldsymbol{V}$ as $\boldsymbol{\Phi}$, and its associated bases ${}_h\boldsymbol{v}_{\mathrm{i}}$ as $\boldsymbol{\phi}_{\mathrm{i}}$. The approximation of $\widetilde{\boldsymbol{u}} \in \boldsymbol{\Phi}$ can be defined as ${}_h\widetilde{\boldsymbol{u}} = \sum_{\forall \mathrm{i} \in \Omega} \phi_{\mathrm{i}} \widetilde{\boldsymbol{u}}_{\mathrm{i}}$, expressed in matrix form as ${}_h\widetilde{\boldsymbol{u}} = \boldsymbol{N}(\boldsymbol{X})\widetilde{\boldsymbol{U}}$, where

$$\boldsymbol{N}(\boldsymbol{X}) = \begin{bmatrix} \boldsymbol{\phi}_{\mathrm{i}}(\boldsymbol{X}) & \cdots & \boldsymbol{\phi}_{n\times m\times l}(\boldsymbol{X}) \end{bmatrix}$$

$$\widetilde{\boldsymbol{U}} = \begin{bmatrix} \widetilde{\mathbf{U}}_1 & \cdots & \widetilde{\mathbf{U}}_{n\times m\times l} \end{bmatrix}^T, \quad \widetilde{\mathbf{U}}_{\mathrm{i}} = \begin{bmatrix} \widetilde{U}^x_{\mathrm{i}} & \widetilde{U}^y_{\mathrm{i}} & \widetilde{U}^z_{\mathrm{i}} \end{bmatrix}$$

Hence, the approximation of $\langle \boldsymbol{\sigma}^{(\mathrm{a})}_n, \delta\boldsymbol{u}^{(\mathrm{a})} \rangle_{\Gamma^{(\mathrm{a})}_C}$ (3.19) and $\langle \boldsymbol{\sigma}^{(\mathrm{a})}_t, \delta\boldsymbol{u}^{(\mathrm{a})} \rangle_{\Gamma^{(\mathrm{a})}_C}$ (3.20) in the function space $\boldsymbol{\Phi}$ can be defined as

$$\langle {}_h\boldsymbol{\sigma}^{(\mathrm{a})}_n, \boldsymbol{\phi}^{(\mathrm{a})}_{\mathrm{i}} \rangle_{\Gamma^{(\mathrm{a})}_C} = \int_{\Gamma^{(\mathrm{a})}_C} p[(\widetilde{\boldsymbol{u}}^{(\mathrm{a})} - \widetilde{\boldsymbol{u}}^{(\mathrm{b})}).\hat{\mathbf{v}}_n]\boldsymbol{\phi}^{(\mathrm{a})}_{\mathrm{i}}.\hat{\mathbf{v}}_n \; d\Gamma^{(\mathrm{a})}_C \qquad \forall \boldsymbol{\phi}^{(\mathrm{a})}_{\mathrm{i}\in\Gamma^{(\mathrm{a})}_C} \in \boldsymbol{\Phi}^{(\mathrm{a})} \tag{3.19}$$

$$\langle {}_h\boldsymbol{\sigma}^{(\mathrm{a})}_t, \boldsymbol{\phi}^{(\mathrm{a})}_{\mathrm{i}} \rangle_{\Gamma^{(\mathrm{a})}_C} = \int_{\Gamma^{(\mathrm{a})}_C} \mu p[(\widetilde{\boldsymbol{u}}^{(\mathrm{a})} - \widetilde{\boldsymbol{u}}^{(\mathrm{b})}).\hat{\mathbf{v}}_n]\boldsymbol{\phi}^{(\mathrm{a})}_{\mathrm{i}}.\hat{\mathbf{v}}_k \; d\Gamma^{(\mathrm{a})}_C \qquad \forall \boldsymbol{\phi}^{(\mathrm{a})}_{\mathrm{i}\in\Gamma^{(\mathrm{a})}_C} \in \boldsymbol{\Phi}^{(\mathrm{a})} \tag{3.20}$$

The parameterization of the domains $\Omega^{(\mathrm{a})}$ and $\Omega^{(\mathrm{b})}$ defined through NURBS can be expressed as $\boldsymbol{X}^{(\mathrm{a})} = \mathbf{R}^{(\mathrm{a})}(\boldsymbol{\Xi}^{(\mathrm{a})})$ and $\boldsymbol{X}^{(\mathrm{b})} = \mathbf{R}^{(\mathrm{b})}(\boldsymbol{\Xi}^{(\mathrm{b})})$. For the perturbed displacement field $\widetilde{\boldsymbol{u}}$ around a equilibrium $\boldsymbol{u}_{eq}$ (§2.3.3), Γ_C was hypothesized to be stationary, where the effect of $\widetilde{\boldsymbol{u}}$ for a stationary Γ_C was modelled through the normal compliance approach. Hence, Γ_C is known a prior from the solution $\boldsymbol{u}_{eq}$ in solving for an equilibrium configuration. Further, $\Gamma_C : g_n = 0$, i.e., $\boldsymbol{X}^{(\mathrm{a})}.\hat{\mathbf{v}}_{\boldsymbol{n}} = \overleftarrow{\boldsymbol{X}}^{(\mathrm{b})}.\hat{\mathbf{v}}_{\boldsymbol{n}}$, where $\hat{\mathbf{v}}_{\boldsymbol{n}}$ in this case is taken to be the outward normal projection from the slave side $\Gamma^{(\mathrm{a})}_C$ to the master side $\Gamma^{(\mathrm{b})}_C$. This means that $\overleftarrow{\boldsymbol{X}}^{(\mathrm{b})} : \overleftarrow{\boldsymbol{X}}^{(\mathrm{b})}(\boldsymbol{X}^{(\mathrm{a})})$, hence for $\boldsymbol{X}^{(\mathrm{a})}$ that

parametrizes $\Gamma_C^{(\mathrm{a})}$, a projection exists that maps $\boldsymbol{X}^{(\mathrm{a})}$ on $\Gamma_C^{(\mathrm{b})}$ as $\overleftarrow{\boldsymbol{X}}^{(\mathrm{b})}$. For the following explanations, we detail the derivation of traction forces on $\Gamma_C^{(\mathrm{a})}$ which can be extended to $\Gamma_C^{(\mathrm{b})}$ depending on the considered contact formulation.

$$\langle {}_h\boldsymbol{\sigma}_n^{(\mathrm{a})}, \boldsymbol{\phi}_{\mathrm{i}}^{(\mathrm{a})} \rangle_{\Gamma_C^{(\mathrm{a})}} = \int_{\Gamma_C^{(\mathrm{a})}} p[(\boldsymbol{N}^{(\mathrm{a})}(\boldsymbol{X}^{(\mathrm{a})})\widetilde{\boldsymbol{U}}^{(\mathrm{a})} - \boldsymbol{N}^{(\mathrm{b})}(\overleftarrow{\boldsymbol{X}}^{(\mathrm{b})})\widetilde{\boldsymbol{U}}^{(\mathrm{b})}).\hat{\mathbf{v}}_n]\boldsymbol{\phi}_{\mathrm{i}}^{(\mathrm{a})}.\hat{\mathbf{v}}_n \; d\Gamma_C^{(\mathrm{a})} \qquad \forall \boldsymbol{\phi}^{(\mathrm{a})}_{\mathrm{i}\in\Gamma_C^{(\mathrm{a})}} \in \boldsymbol{\Phi}^{(\mathrm{a})} \tag{3.21}$$

$$\langle {}_h\boldsymbol{\sigma}_t^{(\mathrm{a})}, \boldsymbol{\phi}_{\mathrm{i}}^{(\mathrm{a})} \rangle_{\Gamma_C^{(\mathrm{a})}} = \int_{\Gamma_C^{(\mathrm{a})}} \mu p[(\boldsymbol{N}^{(\mathrm{a})}(\boldsymbol{X}^{(\mathrm{a})})\widetilde{\boldsymbol{U}}^{(\mathrm{a})} - \boldsymbol{N}^{(\mathrm{b})}(\overleftarrow{\boldsymbol{X}}^{(\mathrm{b})})\widetilde{\boldsymbol{U}}^{(\mathrm{b})}).\hat{\mathbf{v}}_n]\boldsymbol{\phi}_{\mathrm{i}}^{(\mathrm{a})}.\hat{\mathbf{v}}_t \; d\Gamma_C^{(\mathrm{a})} \qquad \forall \boldsymbol{\phi}^{(\mathrm{a})}_{\mathrm{i}\in\Gamma_C^{(\mathrm{a})}} \in \boldsymbol{\Phi}^{(\mathrm{a})} \tag{3.22}$$

where in matrix form,

$$\boldsymbol{\phi}_{\mathrm{i}}.\hat{\mathbf{v}} := \begin{bmatrix} \phi_{i,j,k}(\boldsymbol{X})\hat{\mathrm{v}}^x & 0 & 0 \\ 0 & \phi_{i,j,k}(\boldsymbol{X})\hat{\mathrm{v}}^y & 0 \\ 0 & 0 & \phi_{i,j,k}(\boldsymbol{X})\hat{\mathrm{v}}^z \end{bmatrix}$$

The expression for $\langle {}_h\boldsymbol{\sigma}_n^{(\mathrm{a})}, \boldsymbol{\phi}_{\mathrm{i}}^{(\mathrm{a})} \rangle_{\Gamma_C^{(\mathrm{a})}}$ and $\langle {}_h\boldsymbol{\sigma}_t^{(\mathrm{a})}, \boldsymbol{\phi}_{\mathrm{i}}^{(\mathrm{a})} \rangle_{\Gamma_C^{(\mathrm{a})}}$ can be further expanded as

$$\langle {}_h\boldsymbol{\sigma}_n^{(\mathrm{a})}, \boldsymbol{\phi}_{\mathrm{i}}^{(\mathrm{a})} \rangle_{\Gamma_C^{(\mathrm{a})}} = \int_{\Gamma_C^{(\mathrm{a})}} p[(\boldsymbol{\phi}_{\mathrm{i}}^{(\mathrm{a})}.\hat{\mathbf{v}}_n)(\boldsymbol{N}^{(\mathrm{a})}.\hat{\mathbf{v}}_n) \quad (\boldsymbol{\phi}_{\mathrm{i}}^{(\mathrm{a})}.\hat{\mathbf{v}}_n)(-\boldsymbol{N}^{(\mathrm{b})}.\hat{\mathbf{v}}_n)]\widetilde{\boldsymbol{U}}^{(\mathrm{a-b})} \; d\Gamma_C^{(\mathrm{a})} \qquad \forall \boldsymbol{\phi}^{(\mathrm{a})}_{\mathrm{i}\in\Gamma_C^{(\mathrm{a})}} \in \boldsymbol{\Phi}^{(\mathrm{a})} \tag{3.23}$$

$$\langle {}_h\boldsymbol{\sigma}_t^{(\mathrm{a})}, \boldsymbol{\phi}_{\mathrm{i}}^{(\mathrm{a})} \rangle_{\Gamma_C^{(\mathrm{a})}} = \int_{\Gamma_C^{(\mathrm{a})}} \mu p[(\boldsymbol{\phi}_{\mathrm{i}}^{(\mathrm{a})}.\hat{\mathbf{v}}_t)(\boldsymbol{N}^{(\mathrm{a})}.\hat{\mathbf{v}}_n) \quad (\boldsymbol{\phi}_{\mathrm{i}}^{(\mathrm{a})}.\hat{\mathbf{v}}_t)(-\boldsymbol{N}^{(\mathrm{b})}.\hat{\mathbf{v}}_n)]\widetilde{\boldsymbol{U}}^{(\mathrm{a-b})} \; d\Gamma_C^{(\mathrm{a})} \qquad \forall \boldsymbol{\phi}^{(\mathrm{a})}_{\mathrm{i}\in\Gamma_C^{(\mathrm{a})}} \in \boldsymbol{\Phi}^{(\mathrm{a})} \tag{3.24}$$

where

$$\boldsymbol{N}.\hat{\mathbf{v}} := \begin{bmatrix} \boldsymbol{\phi}_1(\boldsymbol{X}).\hat{\mathbf{v}} & \cdots & \boldsymbol{\phi}_{n\times m\times l}(\boldsymbol{X}).\hat{\mathbf{v}} \end{bmatrix}$$

$$\widetilde{\boldsymbol{U}}^{(\mathrm{a-b})} = \begin{bmatrix} \widetilde{\boldsymbol{U}}^{(\mathrm{a})} \\ \widetilde{\boldsymbol{U}}^{(\mathrm{b})} \end{bmatrix}$$

We expand the terms of the form $\int_{\Gamma_C^{(\mathrm{a})}} \boldsymbol{\phi}_{\mathrm{i}}^{(\mathrm{a})} \boldsymbol{N}^{(\mathrm{b})}(\boldsymbol{X}^{(\mathrm{b})})\, d\Gamma_C^{(\mathrm{a})}$ [3] in Eq. (3.23) and Eq. (3.24), given as

$$\int_{\Gamma_C^{(\mathrm{a})}} \boldsymbol{\phi}_{\mathrm{i}}^{(\mathrm{a})} \boldsymbol{N}^{(\mathrm{b})}(\boldsymbol{X}^{(\mathrm{b})}) d\Gamma_C^{(\mathrm{a})} = \Big[\int_{\Gamma_C^{(\mathrm{a})}} \boldsymbol{\phi}_{\mathrm{i}}^{(\mathrm{a})}(\boldsymbol{X}^{(\mathrm{a})}).\boldsymbol{\phi}_{1}^{(\mathrm{b})}(\overleftarrow{\boldsymbol{X}}^{(\mathrm{b})}(\boldsymbol{X}^{(\mathrm{a})}))\, d\Gamma_C^{(\mathrm{a})} \quad \cdots \int_{\Gamma_C^{(\mathrm{a})}} \boldsymbol{\phi}_{\mathrm{i}}^{(\mathrm{a})}(\boldsymbol{X}^{(\mathrm{a})}).\boldsymbol{\phi}_{\mathrm{n\times m\times l}}^{(\mathrm{b})}(\overleftarrow{\boldsymbol{X}}^{(\mathrm{b})}(\boldsymbol{X}^{(\mathrm{a})}))\, d\Gamma_C^{(\mathrm{a})} \Big] \quad (3.25)$$

where the integral is simultaneously defined over the bases of the two contact domains, since $\boldsymbol{\phi}^{(\mathrm{a})} \in H^{-1/2}(\Gamma^{(\mathrm{a})})_C$ and $\boldsymbol{\phi}^{(\mathrm{b})} \in H^{-1/2}(\Gamma_C^{(\mathrm{b})})$. Even though the definition of integral is possible for $\boldsymbol{\phi}_{1}^{(\mathrm{b})}(\overleftarrow{\boldsymbol{X}}^{(\mathrm{b})}(\boldsymbol{X}^{(\mathrm{a})}))$ on $\Gamma_C^{(\mathrm{a})}$, for dissimilar meshes at the contact interface, the definition of numerical quadrature scheme for the integral demands domain decomposition to find the common span: $\boldsymbol{\phi}^{(\mathrm{a})}_{\mathrm{i}\in\Gamma_C^{(\mathrm{a})}} \cap \boldsymbol{\phi}^{(\mathrm{b})}_{\mathrm{j}\in\Gamma_C^{(\mathrm{b})}}$ [75, 76]. This means that the integral can only be defined through a quadrature scheme specific on the span of $\boldsymbol{\phi}^{(\mathrm{a})}_{\mathrm{i}\in\Gamma_C^{(\mathrm{a})}}$ or $\boldsymbol{\phi}^{(\mathrm{b})}_{\mathrm{j}\in\Gamma_C^{(\mathrm{b})}}$ for which the projection $\boldsymbol{\phi}^{(\mathrm{a})}_{\mathrm{i}\in\Gamma_C^{(\mathrm{a})}} \boldsymbol{\phi}^{(\mathrm{b})}_{\mathrm{j}\in\Gamma_C^{(\mathrm{b})}} \neq 0$. Alternatively, this can be viewed as the projection of $\boldsymbol{\phi}^{(\mathrm{a})}_{\mathrm{i}\in\Gamma_C^{(\mathrm{a})}}$ on $\boldsymbol{\phi}^{(\mathrm{b})}_{\mathrm{j}\in\Gamma_C^{(\mathrm{b})}}$ for which the relation of weak sense should hold, given as

$$\int_{\Gamma_C^{(\mathrm{a})}} [\boldsymbol{\phi}_{\mathrm{i}}^{(\mathrm{a})}.\boldsymbol{\phi}_{1}^{(\mathrm{a})} + \quad \cdots \quad + \boldsymbol{\phi}_{\mathrm{i}}^{(\mathrm{a})}.\boldsymbol{\phi}_{\mathrm{n\times m\times l}}^{(\mathrm{a})}]\, d\Gamma_C^{(\mathrm{a})} = \int_{\Gamma_C^{(\mathrm{a})}} [\boldsymbol{\phi}_{\mathrm{i}}^{(\mathrm{a})}.\boldsymbol{\phi}_{1}^{(\mathrm{b})} + \quad \cdots \quad + \boldsymbol{\phi}_{\mathrm{i}}^{(\mathrm{a})}.\boldsymbol{\phi}_{\mathrm{n\times m\times l}}^{(\mathrm{b})}]\, d\Gamma_C^{(\mathrm{a})} \quad (3.26)$$

where it verifies the conservation of momentum at the contact interface. We satisfy the relation in an approximate sense, where we consider the integral $\int_{\Gamma_C} \boldsymbol{\phi}_{\mathrm{i}}\, d\Gamma_C$ on one of the domains – in this case $\Gamma^{(\mathrm{a})}$ – through collocation as $\int_{\Gamma_C^{(\mathrm{a})}} \boldsymbol{\phi}_{\mathrm{i}}^{(\mathrm{a})} d\Gamma_C^{(\mathrm{a})} \rightarrow \sum_{\forall \boldsymbol{i}\in\boldsymbol{I}^{(\mathrm{a})}} {}^{\boldsymbol{i}}\boldsymbol{\phi}_{\mathrm{i}}^{(\mathrm{a})}$ where $\boldsymbol{I}^{(\mathrm{a})}$ is the set of points on $\Gamma_C^{(\mathrm{a})}$ which depends on the collocation scheme [73, 77]. Hence, for Eq. (3.26), the integral for the projection of $\boldsymbol{\phi}_{\mathrm{i}}^{(\mathrm{a})}$ on the bases in $H^{-1/2}(\Gamma_C^{(\mathrm{a})})$ and $H^{-1/2}(\Gamma_C^{(\mathrm{b})})$ can be given through collocation as

[3] For simplicity of the expansion, we ignore the unit vectors $\hat{\mathbf{v}}_n$ and $\hat{\mathbf{v}}_t$

$$\sum_{\forall \boldsymbol{i} \in \boldsymbol{I}^{(\mathrm{a})}} [{}^{\boldsymbol{i}}\boldsymbol{\phi}_{\mathrm{i}}^{(\mathrm{a})}.{}^{\boldsymbol{i}}\boldsymbol{\phi}_{1}^{(\mathrm{a})} + \quad \cdots \quad + {}^{\boldsymbol{i}}\boldsymbol{\phi}_{\mathrm{i}}^{(\mathrm{a})}.{}^{\boldsymbol{i}}\boldsymbol{\phi}_{\mathrm{n}\times\mathrm{m}\times\mathrm{l}}^{(\mathrm{a})}] =$$
$$\sum_{\forall \boldsymbol{i} \in \boldsymbol{I}^{(\mathrm{a})}} [{}^{\boldsymbol{i}}\boldsymbol{\phi}_{\mathrm{i}}^{(\mathrm{a})}.{}^{\boldsymbol{i}}\boldsymbol{\phi}_{1}^{(\mathrm{b})} + \quad \cdots \quad + {}^{\boldsymbol{i}}\boldsymbol{\phi}_{\mathrm{i}}^{(\mathrm{a})}.{}^{\boldsymbol{i}}\boldsymbol{\phi}_{\mathrm{n}\times\mathrm{m}\times\mathrm{l}}^{(\mathrm{b})}] \quad (3.27)$$

where ${}^{\boldsymbol{i}}\boldsymbol{\phi}^{(\mathrm{a})} := \boldsymbol{\phi}^{(\mathrm{a})}({}^{\boldsymbol{i}}\boldsymbol{X}^{(\mathrm{a})})$ and ${}^{\boldsymbol{i}}\boldsymbol{\phi}^{(\mathrm{b})} := \boldsymbol{\phi}^{(\mathrm{b})}(\overleftarrow{\boldsymbol{X}}^{(\mathrm{b})}({}^{\boldsymbol{i}}\boldsymbol{X}^{(\mathrm{a})}))$. This implicitly satisfies the conditions for conservation of momentum even though the integral $\int_{\Gamma_C^{(\mathrm{a})}} (\boldsymbol{\phi}_{\mathrm{i}}^{(\mathrm{a})})(\boldsymbol{\phi}_{1}^{(\mathrm{b})})\, d\Gamma_C^{(\mathrm{a})}$ may not be defined accurately. But this can effect the continuity of the solution, which is typically verified through Patch-test. For any $\boldsymbol{i}$, the following relation also holds

$$[{}^{\boldsymbol{i}}\boldsymbol{\phi}_{\mathrm{i}}^{(\mathrm{a})}.{}^{\boldsymbol{i}}\boldsymbol{\phi}_{1}^{(\mathrm{a})} + \quad \cdots \quad + {}^{\boldsymbol{i}}\boldsymbol{\phi}_{\mathrm{i}}^{(\mathrm{a})}.{}^{\boldsymbol{i}}\boldsymbol{\phi}_{\mathrm{n}\times\mathrm{m}\times\mathrm{l}}^{(\mathrm{a})}] =$$
$$[{}^{\boldsymbol{i}}\boldsymbol{\phi}_{\mathrm{i}}^{(\mathrm{a})}.{}^{\boldsymbol{i}}\boldsymbol{\phi}_{1}^{(\mathrm{b})} + \quad \cdots \quad + {}^{\boldsymbol{i}}\boldsymbol{\phi}_{\mathrm{i}}^{(\mathrm{a})}.{}^{\boldsymbol{i}}\boldsymbol{\phi}_{\mathrm{n}\times\mathrm{m}\times\mathrm{l}}^{(\mathrm{b})}] = {}^{\boldsymbol{i}}\boldsymbol{\phi}_{\mathrm{i}}^{(\mathrm{a})} \quad (3.28)$$

This means that any quantity defined through collocation at $\boldsymbol{i}$ over ${}^{\boldsymbol{i}}\boldsymbol{\phi}_{\mathrm{i}}^{(\mathrm{a})}$ is projected equally over the bases in $H^{-1/2}(\Gamma_C^{(\mathrm{a})})$ and $H^{-1/2}(\Gamma_C^{(\mathrm{b})})$. It should be noted that the collocation strategy can be replaced by a numerical quadrature scheme as $\int_{\Gamma_C^{(\mathrm{a})}} \boldsymbol{\phi}_{\mathrm{i}}^{(\mathrm{a})} d\Gamma_C^{(\mathrm{a})} \approx \sum_{\forall \boldsymbol{i} \in \boldsymbol{I}^{(\mathrm{a})}} {}^{\boldsymbol{i}}w\, {}^{\boldsymbol{i}}\boldsymbol{\phi}_{\mathrm{i}}^{(\mathrm{a})}$ where $\boldsymbol{I}^{(\mathrm{a})}$ in this case corresponds to the quadrature points with ${}^{\boldsymbol{i}}w$ being the quadrature weights. But the notion of ${}^{\boldsymbol{i}}w$ on $\boldsymbol{\phi}^{(\mathrm{b})} \in H^{-1/2}(\Gamma_C^{(\mathrm{b})})$ may not be realistic when ${}^{\boldsymbol{i}}w$ is defined for $\boldsymbol{\phi}^{(\mathrm{a})} \in H^{-1/2}(\Gamma_C^{(\mathrm{a})})$.

The Eqs. (3.23) and (3.24) defined through collocation can be expressed as

$$\langle {}_h\boldsymbol{\sigma}_n^{(\mathrm{a})}, \boldsymbol{\phi}_{\mathrm{i}}^{(\mathrm{a})} \rangle_{\boldsymbol{I}^{(\mathrm{a})}} =$$
$$\sum_{\forall \boldsymbol{i} \in \boldsymbol{I}^{(\mathrm{a})}} p[({}^{\boldsymbol{i}}\boldsymbol{\phi}_{\mathrm{i}}^{(\mathrm{a})}.\hat{\mathbf{v}}_n)({}^{\boldsymbol{i}}\boldsymbol{N}^{(\mathrm{a})}.\hat{\mathbf{v}}_n) \quad ({}^{\boldsymbol{i}}\boldsymbol{\phi}_{\mathrm{i}}^{(\mathrm{a})}.\hat{\mathbf{v}}_n)(-{}^{\boldsymbol{i}}\boldsymbol{N}^{(\mathrm{b})}.\hat{\mathbf{v}}_n)]\widetilde{\boldsymbol{U}}^{(\mathrm{a-b})}\, d\Gamma_C^{(\mathrm{a})}$$
$$\forall \boldsymbol{\phi}_{\mathrm{i}\in\Gamma_C^{(\mathrm{a})}}^{(\mathrm{a})} \in \boldsymbol{\Phi}^{(\mathrm{a})} \quad (3.29)$$

$$\langle {}_h\boldsymbol{\sigma}_t^{(\mathrm{a})}, \boldsymbol{\phi}_{\mathrm{i}}^{(\mathrm{a})} \rangle_{\boldsymbol{I}^{(\mathrm{a})}} =$$
$$\sum_{\forall \boldsymbol{i} \in \boldsymbol{I}^{(\mathrm{a})}} \mu p[({}^{\boldsymbol{i}}\boldsymbol{\phi}_{\mathrm{i}}^{(\mathrm{a})}.\hat{\mathbf{v}}_t)({}^{\boldsymbol{i}}\boldsymbol{N}^{(\mathrm{a})}.\hat{\mathbf{v}}_n) \quad ({}^{\boldsymbol{i}}\boldsymbol{\phi}_{\mathrm{i}}^{(\mathrm{a})}.\hat{\mathbf{v}}_t)(-{}^{\boldsymbol{i}}\boldsymbol{N}^{(\mathrm{b})}.\hat{\mathbf{v}}_n)]\widetilde{\boldsymbol{U}}^{(\mathrm{a-b})}\, d\Gamma_C^{(\mathrm{a})}$$
$$\forall \boldsymbol{\phi}_{\mathrm{i}\in\Gamma_C^{(\mathrm{a})}}^{(\mathrm{a})} \in \boldsymbol{\Phi}^{(\mathrm{a})} \quad (3.30)$$

or alternalively can be expressed as

$$[\mathbf{K}_C^{(\mathrm{a})} \quad \mathbf{K}_C^{(\mathrm{a,b})}] = \sum_{\forall \boldsymbol{i} \in \boldsymbol{I}^{(\mathrm{a})}} p[({}^{\boldsymbol{i}}\boldsymbol{N}^{(\mathrm{a})}.\hat{\mathbf{v}}_n)^T({}^{\boldsymbol{i}}\boldsymbol{N}^{(\mathrm{a})}.\hat{\mathbf{v}}_n) \quad ({}^{\boldsymbol{i}}\boldsymbol{N}^{(\mathrm{a})}.\hat{\mathbf{v}}_n)^T(-{}^{\boldsymbol{i}}\boldsymbol{N}^{(\mathrm{b})}.\hat{\mathbf{v}}_n)]\widetilde{\boldsymbol{U}}^{(\mathrm{a-b})} \tag{3.31}$$

$$[\mathbf{K}_F^{(\mathrm{a})} \quad \mathbf{K}_F^{(\mathrm{a,b})}] = \sum_{\forall \boldsymbol{i} \in \boldsymbol{I}^{(\mathrm{a})}} \mu p[({}^{\boldsymbol{i}}\boldsymbol{N}^{(\mathrm{a})}.\hat{\mathbf{v}}_t)^T({}^{\boldsymbol{i}}\boldsymbol{N}^{(\mathrm{a})}.\hat{\mathbf{v}}_n) \quad ({}^{\boldsymbol{i}}\boldsymbol{N}^{(\mathrm{a})}.\hat{\mathbf{v}}_t)^T(-{}^{\boldsymbol{i}}\boldsymbol{N}^{(\mathrm{b})}.\hat{\mathbf{v}}_n)]\widetilde{\boldsymbol{U}}^{(\mathrm{a-b})} \tag{3.32}$$

where ${}^{\boldsymbol{i}}\boldsymbol{N} := \begin{bmatrix} {}^{\boldsymbol{i}}\boldsymbol{\phi}_1 & \cdots & {}^{\boldsymbol{i}}\boldsymbol{\phi}_{n\times m\times l} \end{bmatrix}$

Similar to the Isoparametric approach in the classical FEM, the integral is defined over the parametric domain $\hat{\Omega}$, where the above expression takes the form

$$[\mathbf{K}_C^{(\mathrm{a})} \quad \mathbf{K}_C^{(\mathrm{a,b})}] = \sum_{\forall \boldsymbol{i} \in \boldsymbol{I}^{(\mathrm{a})}} \left[p[({}^{\boldsymbol{i}}\mathbf{R}^{(\mathrm{a})}.\hat{\mathbf{v}}_n)^T({}^{\boldsymbol{i}}\mathbf{R}^{(\mathrm{a})}.\hat{\mathbf{v}}_n) \quad ({}^{\boldsymbol{i}}\mathbf{R}^{(\mathrm{a})}.\hat{\mathbf{v}}_n)^T(-{}^{\boldsymbol{i}}\mathbf{R}^{(\mathrm{b})}.\hat{\mathbf{v}}_n)]|{}^{\boldsymbol{i}}\boldsymbol{J}^{(\mathrm{a})}|\right]\widetilde{\boldsymbol{U}}^{(\mathrm{a-b})} \tag{3.33}$$

$$[\mathbf{K}_F^{(\mathrm{a})} \quad \mathbf{K}_F^{(\mathrm{a,b})}] = \sum_{\forall \boldsymbol{i} \in \boldsymbol{I}^{(\mathrm{a})}} \left[\mu p[({}^{\boldsymbol{i}}\mathbf{R}^{(\mathrm{a})}.\hat{\mathbf{v}}_t)^T({}^{\boldsymbol{i}}\mathbf{R}^{(\mathrm{a})}.\hat{\mathbf{v}}_n) \quad ({}^{\boldsymbol{i}}\mathbf{R}^{(\mathrm{a})}.\hat{\mathbf{v}}_t)^T(-{}^{\boldsymbol{i}}\mathbf{R}^{(\mathrm{b})}.\hat{\mathbf{v}}_n)]|{}^{\boldsymbol{i}}\boldsymbol{J}^{(\mathrm{a})}|\right]\widetilde{\boldsymbol{U}}^{(\mathrm{a-b})} \tag{3.34}$$

where ${}^{\boldsymbol{i}}\mathbf{R} := \mathbf{R}({}^{\boldsymbol{i}}\boldsymbol{\Xi})$, with ${}^{\boldsymbol{i}}\boldsymbol{\Xi}$ being the collocation point in the parametric space. ${}^{\boldsymbol{i}}\boldsymbol{\Xi}^{(\mathrm{b})}$ is the corresponding map of $\overleftarrow{\boldsymbol{X}}^{(\mathrm{b})}$ in the parametric space, which can determined through Newton-Rhapson method in solving for $\boldsymbol{X}^{(\mathrm{b})}({}^{\boldsymbol{i}}\boldsymbol{\Xi}^{(\mathrm{b})}) = \overleftarrow{\boldsymbol{X}}^{(\mathrm{b})}(\boldsymbol{X}^{(\mathrm{a})}({}^{\boldsymbol{i}}\boldsymbol{\Xi}^{(\mathrm{a})}))$. Hence, there exists a mapping ${}^{\boldsymbol{i}}\boldsymbol{\Xi}^{(\mathrm{a})} \rightarrow {}^{\boldsymbol{i}}\boldsymbol{\Xi}^{(\mathrm{b})}$ for which $\boldsymbol{X}^{(\mathrm{a})}({}^{\boldsymbol{i}}\boldsymbol{\Xi}^{(\mathrm{a})}) = \boldsymbol{X}^{(\mathrm{b})}({}^{\boldsymbol{i}}\boldsymbol{\Xi}^{(\mathrm{b})})$.

From the conservation of momentum at the interface, the following relation holds $\boldsymbol{\sigma}_n^{(\mathrm{a})} = -\boldsymbol{\sigma}_n^{(\mathrm{b})}$ and $\boldsymbol{\sigma}_t^{(\mathrm{a})} = -\boldsymbol{\sigma}_t^{(\mathrm{b})}$. Hence, the traction stresses on $\Gamma_C^{(\mathrm{b})}$ can be similarly defined as

$$[\mathbf{K}_C^{(\mathrm{b,a})} \quad \mathbf{K}_C^{(\mathrm{b})}] = \sum_{\forall \boldsymbol{i} \in \boldsymbol{I}^{(\mathrm{a})}} \left[p[({}^{\boldsymbol{i}}\mathbf{R}^{(\mathrm{b})}.\hat{\mathbf{v}}_n)^T(-{}^{\boldsymbol{i}}\mathbf{R}^{(\mathrm{a})}.\hat{\mathbf{v}}_n) \quad ({}^{\boldsymbol{i}}\mathbf{R}^{(\mathrm{b})}.\hat{\mathbf{v}}_n)^T({}^{\boldsymbol{i}}\mathbf{R}^{(\mathrm{b})}.\hat{\mathbf{v}}_n)]|{}^{\boldsymbol{i}}\boldsymbol{J}^{(\mathrm{a})}| \right] \widetilde{\boldsymbol{U}}^{(\mathrm{a-b})} \tag{3.35}$$

$$[\mathbf{K}_F^{(\mathrm{b,a})} \quad \mathbf{K}_F^{(\mathrm{b})}] = \sum_{\forall \boldsymbol{i} \in \boldsymbol{I}^{(\mathrm{a})}} \left[p[({}^{\boldsymbol{i}}\mathbf{R}^{(\mathrm{b})}.\hat{\mathbf{v}}_t)^T(-{}^{\boldsymbol{i}}\mathbf{R}^{(\mathrm{a})}.\hat{\mathbf{v}}_n) \quad ({}^{\boldsymbol{i}}\mathbf{R}^{(\mathrm{b})}.\hat{\mathbf{v}}_t)^T({}^{\boldsymbol{i}}\mathbf{R}^{(\mathrm{b})}.\hat{\mathbf{v}}_n)]|{}^{\boldsymbol{i}}\boldsymbol{J}^{(\mathrm{a})}| \right] \widetilde{\boldsymbol{U}}^{(\mathrm{a-b})} \tag{3.36}$$

With the above definitions, the matrices $\mathbf{K}_C^{(\mathrm{a-b})}$ and $\mathbf{K}_F^{(\mathrm{a-b})}$ for the system can be given as

$$\mathbf{K}_C^{(\mathrm{a-b})} = \begin{bmatrix} \mathbf{K}_C^{(\mathrm{a})} & \mathbf{K}_C^{(\mathrm{a,b})} \\ \mathbf{K}_C^{(\mathrm{b,a})} & \mathbf{K}_C^{(\mathrm{b})} \end{bmatrix} \text{ and } \mathbf{K}_F^{(\mathrm{a-b})} = \begin{bmatrix} \mathbf{K}_F^{(\mathrm{a})} & \mathbf{K}_F^{(\mathrm{a,b})} \\ \mathbf{K}_F^{(\mathrm{b,a})} & \mathbf{K}_F^{(\mathrm{b})} \end{bmatrix}$$

It should be noted that, for the Eqs. (3.35) and (3.36) even though the integral should be defined over $\Gamma^{(\mathrm{b})}$ as $\langle {}_h\boldsymbol{\sigma}^{(\mathrm{b})}, \boldsymbol{\phi}_{\mathrm{i}}^{(\mathrm{b})} \rangle_{\Gamma^{(\mathrm{b})}}$, the collocation points $\boldsymbol{I}^{(\mathrm{a})}$ are determined only on $\Gamma^{(\mathrm{a})}$, where its corresponding projection on $\Gamma^{(\mathrm{b})}$ is defined through the projection $\overleftarrow{\boldsymbol{X}}^{(\mathrm{b})}$. This is commonly also known as one-pass. The Eqs. (3.35) and (3.36) can be further simplified based on the relation (3.28), where the following could be stated

$${}^{\boldsymbol{i}}\boldsymbol{\phi}_{\mathrm{i}}^{(\mathrm{a})}.{}^{\boldsymbol{i}}\boldsymbol{\phi}_{\mathrm{i}}^{(\mathrm{a})} = \sum_{\substack{\forall \boldsymbol{\phi}_{\mathrm{i}}^{(\mathrm{a})} \\ \mathrm{i} \in \Gamma_C^{(\mathrm{a})}}} {}^{\boldsymbol{i}}\boldsymbol{\phi}_{\mathrm{i}}^{(\mathrm{a})}.{}^{\boldsymbol{i}}\boldsymbol{\phi}_{\mathrm{j}}^{(\mathrm{a})} = {}^{\boldsymbol{i}}\boldsymbol{\phi}_{\mathrm{i}}^{(\mathrm{a})} \tag{3.37}$$

$${}^{\boldsymbol{i}}\boldsymbol{\phi}_{\mathrm{i}}^{(\mathrm{b})}.{}^{\boldsymbol{i}}\boldsymbol{\phi}_{\mathrm{i}}^{(\mathrm{b})} = \sum_{\substack{\forall \boldsymbol{\phi}_{\mathrm{i}}^{(\mathrm{b})} \\ \mathrm{i} \in \Gamma_C^{(\mathrm{b})}}} {}^{\boldsymbol{i}}\boldsymbol{\phi}_{\mathrm{i}}^{(\mathrm{b})}.{}^{\boldsymbol{i}}\boldsymbol{\phi}_{\mathrm{j}}^{(\mathrm{b})} = {}^{\boldsymbol{i}}\boldsymbol{\phi}_{\mathrm{i}}^{(\mathrm{b})} \tag{3.38}$$

This is similar to the lumping approach where the off-diagonal terms of a row on a given domain is summed to the diagonal. It should be noted that, also the following relation holds

$$\sum_{\substack{\forall \boldsymbol{\phi}_{\mathrm{i}}^{(\mathrm{a})} \\ \mathrm{i} \in \Gamma_C^{(\mathrm{a})}}} {}^{\boldsymbol{i}}\boldsymbol{\phi}_{\mathrm{i}}^{(\mathrm{a})}.{}^{\boldsymbol{i}}\boldsymbol{\phi}_{\mathrm{j}}^{(\mathrm{b})} = {}^{\boldsymbol{i}}\boldsymbol{\phi}_{\mathrm{i}}^{(\mathrm{a})} \tag{3.39}$$

$$\sum_{\substack{\forall \boldsymbol{\phi}_{\mathrm{i}}^{(\mathrm{b})} \\ \mathrm{i} \in \Gamma_C^{(\mathrm{b})}}} {}^{\boldsymbol{i}}\boldsymbol{\phi}_{\mathrm{i}}^{(\mathrm{b})}.{}^{\boldsymbol{i}}\boldsymbol{\phi}_{\mathrm{j}}^{(\mathrm{a})} = {}^{\boldsymbol{i}}\boldsymbol{\phi}_{\mathrm{i}}^{(\mathrm{b})} \tag{3.40}$$

which preserves conservation of momentum at the interface 3.27.

As a side note, It is well known that the choice of master and slave can lead to bias with one pass. The bias can be eliminated by the so called two-pass formulation where after one pass, the role of the master and the slave is switched, and the average of the projections is taken in to account, given for $\Gamma_C^{(\mathrm{a})}$ as

$$\langle {}_h\boldsymbol{\sigma}_n^{(\mathrm{a})}, \boldsymbol{\phi}_{\mathrm{i}}^{(\mathrm{a})} \rangle_{\boldsymbol{I}^{(\mathrm{a,b})}} = \frac{1}{2} \langle {}_h\boldsymbol{\sigma}_n^{(\mathrm{a})}, \boldsymbol{\phi}_{\mathrm{i}}^{(\mathrm{a})} \rangle_{\boldsymbol{I}^{(\mathrm{a})}} + \frac{1}{2} \langle {}_h\boldsymbol{\sigma}_n^{(\mathrm{b})}, \boldsymbol{\phi}_{\mathrm{i}}^{(\mathrm{b})} \rangle_{\boldsymbol{I}^{(\mathrm{b})}} \tag{3.41}$$

$$\langle {}_h\boldsymbol{\sigma}_t^{(\mathrm{a})}, \boldsymbol{\phi}_{\mathrm{i}}^{(\mathrm{a})} \rangle_{\boldsymbol{I}^{(\mathrm{a,b})}} = \frac{1}{2} \langle {}_h\boldsymbol{\sigma}_t^{(\mathrm{a})}, \boldsymbol{\phi}_{\mathrm{i}}^{(\mathrm{a})} \rangle_{\boldsymbol{I}^{(\mathrm{a})}} + \frac{1}{2} \langle {}_h\boldsymbol{\sigma}_t^{(\mathrm{b})}, \boldsymbol{\phi}_{\mathrm{i}}^{(\mathrm{b})} \rangle_{\boldsymbol{I}^{(\mathrm{b})}} \tag{3.42}$$

4 Sensitivity analysis

Sensitivity analysis essentially defines analysis of sensitivity of a function with respect to change in parameters. Global sensitivity analysis for the involved shape parameters was performed using the Variance-based method which comes from Hoeffding-Sobol decomposition [78]. This method is based on decomposing the variance of a function to its variance associated with the parameters and the interaction between the parameters. Hence, higher the variance in output of a function induced by a parameter infers higher sensitivity. The method is applied through Monte-Carlo based estimation defined by latin hypercube sampling for efficiency. In effect, to evaluate the global behaviour and to increase the accuracy for the given Monte-Carlo based estimation on the presumed asymptotic case demands a large computation of design points, which is simply impossible to converge with a reasonable time given the computational cost to evaluate the stability criteria C_{s}. Hence, a metamodel based on Gaussian process regression was used, detailed in §6.1. The stability criteria given by the metamodel can hence be expressed as $\hat{C}_{\mathsf{s}} \approx C_{\mathsf{s}}$.

To understand the effect of the shape parameters on the stability criteria, the first-order and the total-order sensitivity indices are computed. The first-order indices define the contribution of a given parameter to the change in unconditional variance $V(\hat{C}_{\mathsf{s}})$, while the total-order indices add to it the contribution of all the higher-order interactions on the given parameter. The general expression of the first-order index S_i and the total-order index S_{ti} can be defined as

$$S_i = \frac{V_{X_i}(\mathrm{E}_{X_{\sim i}}(\hat{C}_{\mathsf{s}}|X_i))}{V(\hat{C}_{\mathsf{s}})} \tag{4.1}$$

$$S_{ti} = 1 - \frac{V_{X_{\sim i}}(\mathrm{E}_{X_i}(\hat{C}_{\mathsf{s}}|X_{\sim i}))}{V(\hat{C}_{\mathsf{s}})} \tag{4.2}$$

where $V_{X_i}(\mathrm{E}_{X_{\sim i}}(\hat{C}_{\mathsf{s}}|X_i))$ is the variance of the conditional expectation on the function of the stability criteria $\hat{C}_{\mathsf{s}}$ evaluated by conditioning the parameter X_i for several values across the bounded design space and similarly, $V_{X_{\sim i}}(\mathrm{E}_{X_i}(\hat{C}_{\mathsf{s}}|X_{\sim i}))$ is the variance of the conditional expectation obtained by conditioning all the parameters except for X_i.

The described probability measures are estimated based on the estimators proposed in [79]. The Monte-Carlo based estimation for the given estimators require two matrices $\boldsymbol{Y}^A$ and $\boldsymbol{Y}^B$ of equal size with rows and columns representing the design points and the parameters respectively. To evaluate the first order index of the

ith parameter, all the parameters of $\boldsymbol{Y}^B$ are unchanged except for the ith parameter (ith column of the matrix) which is replaced by the ith parameter of $\boldsymbol{Y}^A$ to obtain the matrix $\boldsymbol{Y}_i^B$. Similarly, to evaluate the total-order index of the ith parameter, all the parameters of $\boldsymbol{Y}^B$ are changed with the parameters of $\boldsymbol{Y}^A$ except for the ith parameter to obtain the matrix $\boldsymbol{Y}_{ti}^B$. Hence, the matrices $\boldsymbol{Y}_i^B$ and $\boldsymbol{Y}_{ti}^B$ represent the conditioning of the parameters with respect to the matrix $\boldsymbol{Y}^A$, which in a sense is used to evaluate the conditional probability terms and also to describe the effective unconditional variance, as given by the estimators. For n parameters and p design points, it requires evaluation of $(n+1)p$ design points to evaluate S_i or S_{ti} for all the n parameters.

We consider sensitivity analysis of the disc-pad system with classical shapes (given in table 4.1) for the setting of constant force at the interface 2.3.4. The contact formulation was achieved through Node-to-Node contact and the convergence test for the contact formulation is given in 9.1.

	Disc			Pad			
	Thickness	External radius	Internal radius	Thickness	Internal radius	External radius	Angle (degree)
min	125.e-4	15.e-2	25.e-3	11.e-3	8.e-2	11.e-2	26
max	2.e-2	16.e-2	4.e-2	15.e-3	9.e-2	12.e-2	50

Table 4.1: Parameter range in meters

The value of p was chosen to be 1500 and hence evaluating a total of 24000 design points with metamodel to define first-order and total-order indices. The evaluation was repeated for different sample sets to check for convergence which was observed to be not difficult with the chosen p value, given an estimated standard error for the indices of no more than 0.02.

As it can be observed, the first-order indices show relatively high values for the thickness of the disc and the pad. The total-order indices also increase relatively for the two parameters. Further, the global variance of $\hat{C}_{\mathsf{s}}$ can be largely attributed to independent effect of the parameters rather than interaction between them.

The results are also shown with closed second-order indices, combining independent effects and interaction between any two parameters.

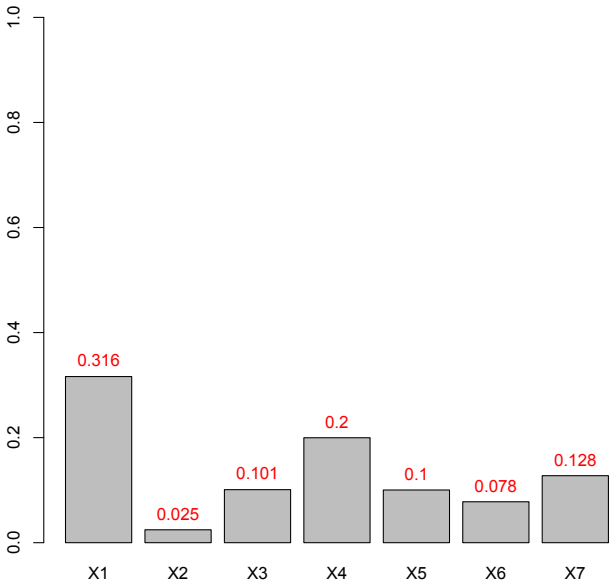

Figure 4.1: First-order Sobol indices

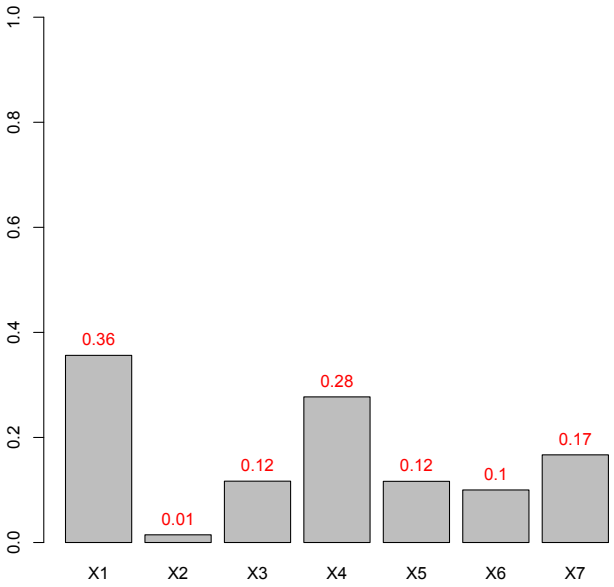

Figure 4.2: Total-order Sobol indices

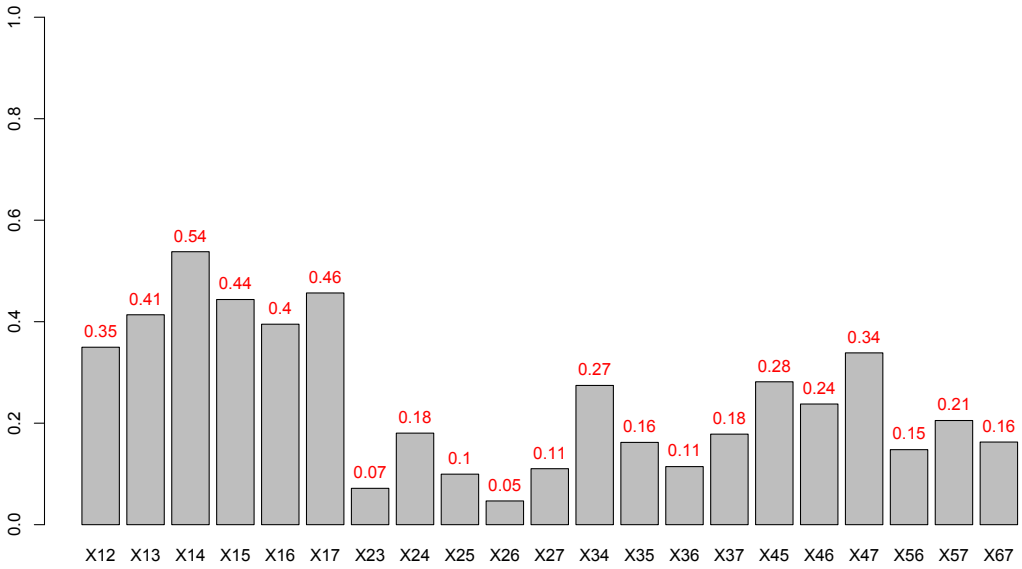

Figure 4.3: Closed second-order Sobol indices

5 Shape optimisation setting

In this section, we detail shape optimization defined through NURBS parameterization of shapes for the pad, with its associated constraints and objectives for optimization. We also provide a short description of parameterization and refinement strategy for the disc-pad system domain $\Omega^{(\mathrm{d-p})}$.

5.1 NURBS parameterisation of shape for optimisation

The optimization is defined for the boundary $\partial\Gamma_C^{(\mathrm{p})}$ of the planar surface $\Gamma_C^{(\mathrm{p})}$ of the pad which is in contact with the disc, where the thickness of the pad and the design parameters of the disc are set to be constant. The geometry of $\Gamma_C^{(\mathrm{p})}$ can be parameterized through NURBS as

$$\check{\boldsymbol{X}}_s^{(\mathrm{p})}(\xi,\eta) = \sum_{i=0}^{n}\sum_{j=0}^{m} R_{i,p}(\xi)R_{j,q}(\eta)\boldsymbol{P}_{i,j} \tag{5.1}$$

Hence, in this setting, the shape optimization is defined for the shape of the NURBS curves $\check{\boldsymbol{X}}_c^{(1)}(s), \check{\boldsymbol{X}}_c^{(2)}(t), \check{\boldsymbol{X}}_c^{(3)}(u)$and $\check{\boldsymbol{X}}_c^{(4)}(v)$ which parameterizes $\partial\Gamma_C^{(\mathrm{p})}$ that encloses the surface $\check{\boldsymbol{X}}_s^{(\mathrm{p})}(\xi,\eta)$, as shown in Figure 5.1, where the curves can be expressed as

$$\begin{aligned}
\check{\boldsymbol{X}}_s^{(\mathrm{p})}(\xi,\eta|\xi=0) &= \check{\boldsymbol{X}}_c^{(1)}(s)\\
\check{\boldsymbol{X}}_s^{(\mathrm{p})}(\xi,\eta|\eta=0) &= \check{\boldsymbol{X}}_c^{(2)}(t)\\
\check{\boldsymbol{X}}_s^{(\mathrm{p})}(\xi,\eta|\xi=1) &= \check{\boldsymbol{X}}_c^{(3)}(u)\\
\check{\boldsymbol{X}}_s^{(\mathrm{p})}(\xi,\eta|\eta=1) &= \check{\boldsymbol{X}}_c^{(4)}(v)
\end{aligned} \tag{5.2}$$

This leads to the problem of defining the parameterisation $\check{\boldsymbol{X}}_s^{(\mathrm{p})}(\xi,\eta)$ given the four parametric curves $\check{\boldsymbol{X}}_c^{(1)}(s), \check{\boldsymbol{X}}_c^{(2)}(t), \check{\boldsymbol{X}}_c^{(3)}(u)$ and $\check{\boldsymbol{X}}_c^{(4)}(v)$. The parameterisation should be characterized by injective mapping which is ensured if the Jacobian does not vanish. For $\boldsymbol{X} : \hat{\Omega} \to \Omega$, verifying Jacobian on $\hat{\Omega}$ in transfinite sense would be impossible, for which it can be verified in a finite sense with the property of determinant-Jacobian function for a NURBS parameterisation. The definition of determinant of Jacobian for a NURBS parameterisation can be expressed as a function of higher-order NURBS to the NURBS parameterisation, given as

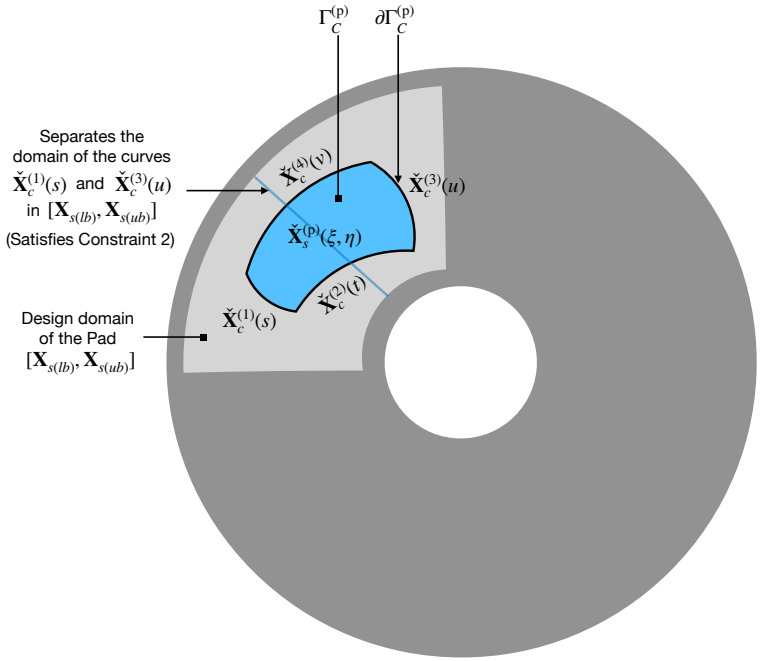

Figure 5.1: An illustration describing the parameterisation of $\Gamma_C^{(\mathrm{p})}$ and $\partial\Gamma_C^{(\mathrm{p})}$ relative to $\Omega^{(\mathrm{d})}$

$$|\boldsymbol{J}(\check{\boldsymbol{X}}_s(\xi,\eta))| = \left|\begin{bmatrix}\frac{\partial \boldsymbol{X}_s}{\partial \xi} & \frac{\partial \boldsymbol{X}_s}{\partial \eta}\end{bmatrix}\right| = \sum_{i=1}^{2n-1}\sum_{j=1}^{2m-1} R_{i,2p-1}(\xi) R_{j,2q-1}(\eta) \boldsymbol{O}_{i,j} \tag{5.3}$$

The condition for injective mapping $|\boldsymbol{J}(\check{\boldsymbol{X}}_s(\xi,\eta))| > 0$ for $(\xi,\eta) \in [0,1]^2$ can be said to be satisfied if $\boldsymbol{O}_{i,j} > 0$, which is a sufficient condition but not a necessary one. This is because, if $|\boldsymbol{J}(\check{\boldsymbol{X}}_s(\xi,\eta))| = 0$ for any point on boundary, even though $|\boldsymbol{J}(\check{\boldsymbol{X}}_s(\xi,\eta))| > 0$ on $(0,1)^2$, $\boldsymbol{O}_{i,j} < 0$. To obtain a more restrictive convex hull for tighter Jacobian bound, B-splines can be reduced to Bezier patches by internal knot refinement. Nevertheless, $\boldsymbol{O}_{i,j}$ is often considered to check the validity of a parameterisation for injectivity, especially in the scope of defining optimisation to achieve an injective parameterisation.

The general idea behind Isogeometric approach is that given an initial parameterisation $\check{\boldsymbol{X}}$ of a domain Ω with NURBS, analysis-suitable parameterisation $\boldsymbol{X}$ can be achieved with in the same parametric space, through addition or manipulation of knots and control points. But achieving initial parameterisation with injective mapping can be a difficult challenge especially for arbitrary definition of shapes in an optimisation, where to achieve a quality parameterisation with injective mapping can be even more challenging. The problem of defining $\check{\boldsymbol{X}}$ is more related to

computer-aided design (CAD), where the role of CAD is typically not focused on defining $\boldsymbol{X}$. This is because, for the illustration of CAD, there can be multiple ways to parametrise a domain, that may not necessarily be suited for defining an approximation space ${}_h\boldsymbol{V}$ in the context of isogeometric analysis as $\boldsymbol{\Phi}$ [1]. A typical approach in CAD is that a complicated domain being defined as a trimmed domain[2] (Fig. 5.2) or union of several trimmed domains.

For the definition of a trimmed domain, since only essential part of the mapping that defines the domain from the parametric space to the physical space is considered, it does not place severe restriction over the complete parametric space to be mapped to the domain, illustrated in. This can be better in the context of designing where a surface can be loosely defined to contain a closed curve, but may not be suitable for defining $\boldsymbol{\Phi}$. One could say that for $\Omega \subset \Omega_{\uplus}$, with $\Omega_{\uplus}$ parameterised by $\boldsymbol{X}$, and given the bases $\boldsymbol{\phi}_{\mathrm{i}} := \boldsymbol{R}_{i,j,k}(\boldsymbol{\Xi}) \circ \boldsymbol{X}^{-1}$, only the bases $\boldsymbol{\phi}_{\mathrm{i}}$ defining Ω can be considered for approximation. This is essentially the approach of the immersed methods, where typically the bases $\boldsymbol{\phi}_{\mathrm{i}}$ defining Ω is distinguished with material properties at the quadrature points, along with local refinement at the boundary of $\Omega \subset \Omega_{\uplus}$ through hierarchical refinement. Though immersed methods can have more flexibility in defining ${}_h\boldsymbol{V}$, we do not focus on such approaches owing to its novelty which can require immense time to develop. We purely focus on defining $\boldsymbol{X} : \hat{\Omega} \to \Omega$ which can be called body-fitted parameterisation. The point is that to achieve body-fitted injective parameterisation for any shape as initial parameterisation can be too demanding from purely the perspective of CAD (Fig. 5.2).

For complex shapes, it is typically preferred to define analysis-suitable parameterisation directly, rather from a prior definition of initial parameterisation, where analysis-suitable parameterisation with sufficient refinement can be well suited to define injective parameterisation. From the perspective of CAD, this makes no difference as along as body-fitted injective parameterisation is achieved and hence, sometimes, no distinguish can necessarily be made between initial and analysis-suitable parameterisations (Fig. 5.2). Nevertheless, given the complexity of defining initial or analysis-suitable parameterisation, it is seen as a more robust strategy to define ${}_h\boldsymbol{V}$ compared to classical FEM. It should also be reminded that a complex domain can also be defined through multiple patches, where each patch corresponds to body-fitted parameterisation. But this also requires a more robust strategy to split a complex domain in to patches for any arbitrary definition of shape, at least for a fixed topology. Nevertheless, we adapt multi-patch parameterisation as a strategy for local refinement and sub-structuring in optimisation.

For the scope of this thesis, we consider discrete Coon's patch method as a preliminary approach for the parameterisation part of the Bayesian shape optimisation

[1] To distinguish the space ${}_h\boldsymbol{V}$ in the context of isogeometric approach, we define $\boldsymbol{\Phi}$ to be ${}_h\boldsymbol{V}$

[2] The definition of Ω as a trimmed domain can be defined as $\Omega \subset \Omega_{\uplus}$, where $\hat{\Omega} \to \Omega_{\uplus}$

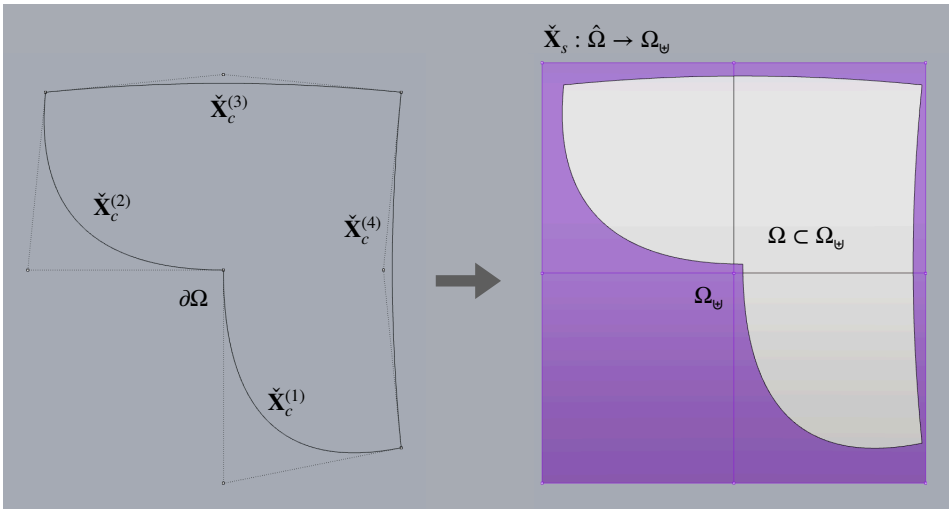

(a) Parameterisation with trimmed domain

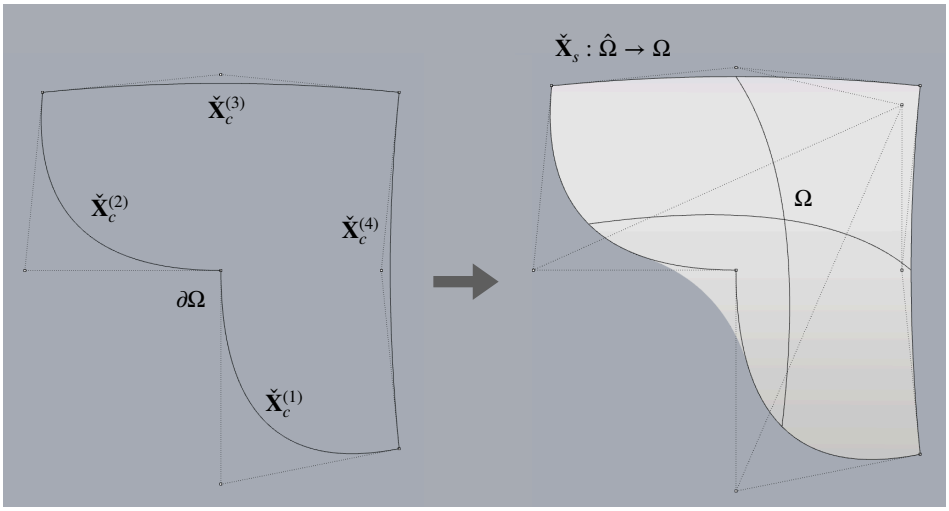

(b) Body-fitted non-injective parameterisation

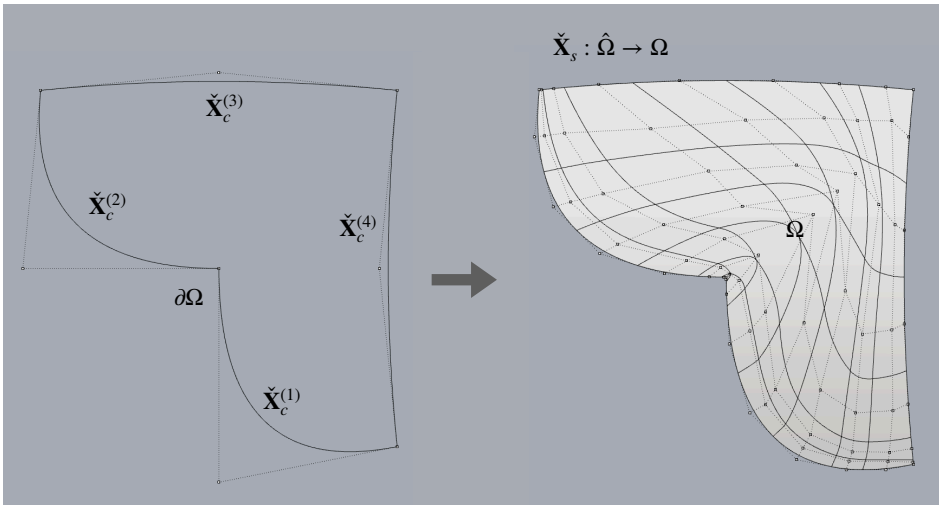

(c) Body-fitted injective parameterisation

Figure 5.2: Examples of parameterisation with NURBS

framework. The idea is to adapt a more advanced parameterisation strategy for future evolution of the framework.

The parameterization of$\check{\boldsymbol{X}}_s^{(\mathrm{p})}(\xi,\eta)$ with the above four curves (5.2) by discrete Coon's patch method can be given as

$$\begin{aligned}\check{\boldsymbol{X}}_s^{(\mathrm{p})}(\xi,\eta) = \check{\boldsymbol{X}}_c^{(1)}(s)(1-\xi) + \check{\boldsymbol{X}}_c^{(3)}(u)(\xi) + \check{\boldsymbol{X}}_c^{(2)}(t)(1-\eta) + \check{\boldsymbol{X}}_c^{(4)}(v)(\eta) \\ - \check{\boldsymbol{X}}_c^{(1)}(0)(1-\xi)(1-\eta) - \check{\boldsymbol{X}}_c^{(1)}(1)(1-\xi)(\eta) \\ - \check{\boldsymbol{X}}_c^{(3)}(0)(\xi)(1-\eta) - \check{\boldsymbol{X}}_c^{(3)}(1)(\xi)(\eta) \quad (5.4)\end{aligned}$$

where the Coon's patch method is an explicit linear method and hence computationally efficient in realising parameterisation, but the method doesn't guarantee injective mapping. In our experience, the shapes realised through Coon's patch method that doesn't satisfy injective mapping are largely too conceptual for pad shapes and hence, given the complexity of realising parameterisation for such shapes, we only stick with the shapes realised through Coon's patch method for which injective property is satisfied.

In the scope of shape optimisation,$\check{\boldsymbol{X}}_s^{(\mathrm{p})}(\xi,\eta)$ can be defined as the function to be optimised, on which constraints can be imposed. We define *Constraint set 1*, which contains constraints intrinsic of the boundary curves (5.2). For simplicity owing to the preliminary definition of framework, in order to limit the parameters in optimization, we restricted the degree of each curve to 2 and hence, this leads to the surface$\check{\boldsymbol{X}}_s^{(\mathrm{p})}(\xi,\eta)$ with the property $p = q = 2$, and each curve is defined only through three control points which are just enough to define a curve of degree 2. Furthermore, the optimisation is defined only for the position of the control points $\boldsymbol{P}_{i,j}$ for $w_{i,j} = 1$ (3.11), i.e, we considered the optimization of the NURBS geometry only through affine transformation without considering projective transformation.

While the end control points will be constrained relative to the disc domain, given in *Constraint set 3*, we impose constraint on the mid-control point of each curve segment. The control points for any curve segment can be expressed as $\boldsymbol{P}_1$, $\boldsymbol{P}_2$ and $\boldsymbol{P}_3$, where $\boldsymbol{P}_1$ and $\boldsymbol{P}_3$ define the end control points. If the initial configuration of the curve can be expressed as a line segment $\overline{\boldsymbol{P}_1\boldsymbol{P}_3}$ with $\boldsymbol{P}_2 = \frac{\boldsymbol{P}_1+\boldsymbol{P}_3}{2}$, then the constraint on $\boldsymbol{P}_2$ can be expressed relative to the initial configuration as $\boldsymbol{P}_2 \perp \overline{\boldsymbol{P}_1\boldsymbol{P}_3}$.

Constraints between curve segments are given as *Constraint set 2* which contains constraints to confirm injective mapping, which also implicitly preserves topology. Injective parameterisation can be said to be achieved if $|\boldsymbol{J}(\check{\boldsymbol{X}}_s(\xi,\eta))|$ does not vanish on all $\hat{\Omega}$. With the mid-control points constrained, the set of constraints for testing this condition was realised geometrically, given as

Constraint set 2:

$$\{\check{\boldsymbol{X}}_c^{(1)}(s) \cap \check{\boldsymbol{X}}_c^{(2)}(t)\} \cup \{\check{\boldsymbol{X}}_c^{(3)}(u) \cap \check{\boldsymbol{X}}_c^{(4)}(v)\} \cup \{\check{\boldsymbol{X}}_c^{(1)}(s) \cap \check{\boldsymbol{X}}_c^{(3)}(u)\} \cup \{\check{\boldsymbol{X}}_c^{(1)}(s) \cap \check{\boldsymbol{X}}_c^{(4)}(v)\} \cup \{\check{\boldsymbol{X}}_c^{(2)}(t) \cap \check{\boldsymbol{X}}_c^{(3)}(u)\} \cup \{\check{\boldsymbol{X}}_c^{(2)}(t) \cap \check{\boldsymbol{X}}_c^{(4)}(v)\} = \emptyset \quad s,t,u,v \in (0,1)$$

$$\begin{aligned}
&\{\check{\boldsymbol{X}}_c^{(1)}(0)(1-\xi) + \check{\boldsymbol{X}}_c^{(3)}(0)(\xi)\} \cap \{\check{\boldsymbol{X}}_c^{(1)}(0+\Delta s)(1-\xi) + \check{\boldsymbol{X}}_c^{(3)}(0+\Delta u)(\xi)\} = \emptyset \\
&\{\check{\boldsymbol{X}}_c^{(1)}(1)(1-\xi) + \check{\boldsymbol{X}}_c^{(3)}(1)(\xi)\} \cap \{\check{\boldsymbol{X}}_c^{(1)}(1-\Delta s)(1-\xi) + \check{\boldsymbol{X}}_c^{(3)}(1-\Delta u)(\xi)\} = \emptyset \\
&\{\check{\boldsymbol{X}}_c^{(2)}(0)(1-\eta) + \check{\boldsymbol{X}}_c^{(4)}(0)(\eta)\} \cap \{\check{\boldsymbol{X}}_c^{(2)}(0+\Delta t)(1-\eta) + \check{\boldsymbol{X}}_c^{(4)}(0+\Delta v)(\eta)\} = \emptyset \\
&\{\check{\boldsymbol{X}}_c^{(2)}(1)(1-\eta) + \check{\boldsymbol{X}}_c^{(4)}(1)(\eta)\} \cap \{\check{\boldsymbol{X}}_c^{(2)}(1-\Delta t)(1-\eta) + \check{\boldsymbol{X}}_c^{(4)}(1-\Delta v)(\eta)\} = \emptyset \\
&\qquad\qquad \xi,\eta \in [0,1] \quad (5.5)
\end{aligned}$$

where Δ represents an arbitrary small variation. The first constraint avoids intersection between the curves except for the end points. Satisfying the first constraint which guarantees a fixed topology does not assure injective parameterisation through Coon's patch method, for which the last set of four constraints are necessary. The last set of four constraints implicitly avoid concave intersection between the curves. Given that the curves do not intersect except for convex intersection at the end points, and with constraints on the mid-control points, injective parameterisation can be achieved with Coon's patch method.

Further, the definition of the pad surface to be with in the bounds of the disc surface is given through a box constraint as follows

Constraint set 3:

$$(\boldsymbol{X}_{s(lb)} \leq \check{\boldsymbol{X}}_s^{(\mathrm{p})}(\xi,\eta) \leq \boldsymbol{X}_{s(ub)}) : \{[\boldsymbol{X}_{c(lb)}^{(i)}, \boldsymbol{X}_{c(ub)}^{(i)}]\} \cap \{[\boldsymbol{X}_{c(lb)}^{(j)}, \boldsymbol{X}_{c(ub)}^{(j)}]\} = \emptyset \qquad (5.6)$$

where the choice of $\boldsymbol{X}_{s(lb)}$ and $\boldsymbol{X}_{s(ub)}$ depends on the design choice for the domain of the disc to be in contact with the pad. Further, the box constraint is adapted to limit the redundancies in geometric description i.e, to limit the scope for a given shape to be defined in more than one way with in the same design space. To avoid this type of redundancy, we restricted the domain through box constraints for at least two curves $\check{\boldsymbol{X}}_c^{(i)}(.)$ and $\check{\boldsymbol{X}}_c^{(j)}(.)$ of the four curves, such that the intersection of their domains is a null set. This leads to restriction of the design space with compromise on reducing the redundancies. Hence, we avoided some of the redundancies on empirical notion, such that the restricted design space has lesser meaningful designs. This maybe an interesting anomaly to investigate, since the redundancies may lead to larger design space with more severe multi-modality.

We further impose an inequality constraint in order to avoid designs with smaller contact surface, given as

Constraint 4:

$$Area(\check{\boldsymbol{X}}_s^{(\mathrm{p})}(\xi,\eta)) \geq A_{min} \tag{5.7}$$

where $Area(\check{\boldsymbol{X}}_s^{(\mathrm{p})}(\xi,\eta)) : \int_\xi \int_\eta |\frac{\partial \check{\boldsymbol{X}}_s^{(\mathrm{p})}}{\partial \xi} \times \frac{\partial \check{\boldsymbol{X}}_s^{(\mathrm{p})}}{\partial \eta}| d\xi d\eta$ and the choice of A_{min} depends on the minimum contact surface area that is required on the Pareto-front, since maximization of $Area(\check{\boldsymbol{X}}_s^{(\mathrm{p})}(\xi,\eta))$ is defined to be one of the objectives.

The definition of the shape of$\check{\boldsymbol{X}}_s^{(\mathrm{p})}(\xi,\eta)$ through this strategy means that there is no requisite for a reference configuration to define optimization, but instead the pad shapes are defined through random generation of curves with C^0 continuity between them. We assume that this restricts bias to any specific shape and hence encouraging more randomness in defining a meaningful geometry. This highly restricts the use of gradient-based approaches for optimization, since the constraints are also black-box and may have discontinuities. Some of the limitations can also be attributed to lack of exploring classical shapes such as the annulus sector pad shapes in our application even though such shapes are already a subset of the the design space defined. The randomness in the definition of shapes can lead to higher probability of failure for the constraints, and hence more constraint evaluation in optimisation.

Finally, the objectives for the Multi-objective optimization can be posed as optimization of the following functionals:

- *Objective 1*: $min\, C_{\mathsf{s}}(\check{\boldsymbol{X}}_s^{(\mathrm{p})}(\xi,\eta) \,|\, \Im(\boldsymbol{\Lambda}(\boldsymbol{X}^{(\mathrm{d-p})}) \in [10KHz, 13KHz])$
- *Objective 2*: $max\, Area(\check{\boldsymbol{X}}_s^{(\mathrm{p})}(\xi,\eta))$

where the optimisation of the functionals are defined over the space of NURBS functions. Since we fixed the order and the number of control points of the NURBS surface$\check{\boldsymbol{X}}_s^{(\mathrm{p})}(\xi,\eta)$, the optimisation is restricted to a fixed number of control points. Further, the shape optimisation is considered for the setting of constant pressure at the interface2.3.4 for varying contact area.

5.2 Isogeometric parameterization and refinement strategies for the disc-pad system domain with contact considerations

For the following, we do not focus on the mesh sensitivity for CEA or the stability criterion C_{s}, but instead the below refinement strategies can be seen as to realise the classical mesh refinement considerations for a contact problem, where more elements are typically defined on Γ_C and at the vicinity of $\partial\Gamma_C$ to capture more accurately the contact characteristics and the strong solution gradient. This is especially more

challenging with local refinement for NURBS parameterization, hence we expose here some strategies to achieve local refinement. Empirically, the refinement at Γ_C and around $\partial\Gamma_C$ seems to effect the results of CEA and converges with sufficient refinement, but a more qualitative assessment of the sensitivity has not been developed here, since it requires a detailed study of not only the refinement but also the contact formulation and the nature of modelling contact stiffness.

The planar parameterization$\check{\boldsymbol{X}}_s^{(\mathrm{p})}$ can be easily extended to define $\Omega^{(\mathrm{p})}$ as $\check{\boldsymbol{X}}_v^{(\mathrm{p})}$ considering the thickness of the pad through the tensor product definition (3.13), given a NURBS line along the thickness. The disc domain $\Omega^{(\mathrm{d})}$ was realised by multi-patch parameterization $\check{\boldsymbol{X}}_v^{(\mathrm{d})} := \check{\boldsymbol{X}}_v^{(\mathrm{d}_1)} \cup \check{\boldsymbol{X}}_v^{(\mathrm{d}_2)}$ to achieve local refinement on $\Gamma_C^{(\mathrm{d}_2)}$. The surface parameterization for the disc patches$\check{\boldsymbol{X}}_s^{(\mathrm{d}_1)}$ and$\check{\boldsymbol{X}}_s^{(\mathrm{d}_1)}$ can be achieved through the concept of revolved surface, detailed in [17], which assures robust injective parameterisation since the curve to be revolved is a straight line perpendicular to the disc axis, given that the straight line does not pass through the axis. The planar parameterizations$\check{\boldsymbol{X}}_s^{(\mathrm{d}_1)}$ and$\check{\boldsymbol{X}}_s^{(\mathrm{d}_2)}$ can be extended to $\check{\boldsymbol{X}}_v^{(\mathrm{d}_1)}$ and $\check{\boldsymbol{X}}_v^{(\mathrm{d}_2)}$ respectively, similar to achieving $\check{\boldsymbol{X}}_v^{(\mathrm{p})}$.

For any refinement, the space for parameterisation remains the same i.e, $(\xi, \eta, \zeta) \in [0, 1]^3$ and the refinement is defined only through manipulation or addition of knots and control point to achieve an analysis-suitable parameterisation. After an analysis-suitable parameterisation, to take in to account of the additional control points and the manipulated knot vectors, $\check{\boldsymbol{X}}_v^{(\mathrm{p})}$ and $\check{\boldsymbol{X}}_v^{(\mathrm{d})}$ can be expressed as $\boldsymbol{X}_v^{(\mathrm{p})}$ and $\boldsymbol{X}_v^{(\mathrm{d})}$. Hence, the NURBS bases associated with $\boldsymbol{X}_v^{(\mathrm{p})}$ and $\boldsymbol{X}_v^{(\mathrm{d})}$ are used to define the space for approximation in isogeometric approach. It should be noted that often analysis-suitable parameterisation is achieved directly in the scope of defining an injective parameterisation, since for complex shapes, analysis-suitable parameterisation with sufficient refinement can be well suited to define injective parameterisation. Hence, often no distinguish can be made between initial and analysis-suitable parameterisations, since the definition of body-fitted initial parameterisation in the context of CAD may already demand sufficient refinement to achieve even an elementary injective parameterisation. Since we only choose designs for which injective parameterisation exists with Coon's patch method, it is safe to say that for any analysis-suitable injective parameterisation achieved through Coon's patch method, initial injective parameterisation can also be achieved by Coon's patch method. Hence, we talk in the context that initial parameterisation of CAD does not have sufficient refinement to define the space ${}_h\boldsymbol{V}$ and hence we explicitly define analysis-suitable parameterisation through refinement.

Normally across the boundary $\partial\Gamma_C$ of a contact domain Γ_C, there is drastic change in the solution gradient and hence, the parameterization needs special attention owing to the continuity of the NURBS bases. The tensor product property of the NURBS gives further challenge for local refinement which is usually desired on Γ_C. These chal-

lenges can be largely overcome by adaptation of NURBS bases to T-splines [69] or THB-splines [80], but requires extensive adaptation. Hence, we defined a multi-patch parameterization strategy through collocation and projection of properties defined on control points between two merging surfaces, which was simple and efficient for our application with fewer adaptation. Even though the considered multi-patch approach only considers C^0 solution continuity between the patches, the post-processing of the mode shapes show sufficient smoothness in displacement field across the patches, shown in Figure 5.3.

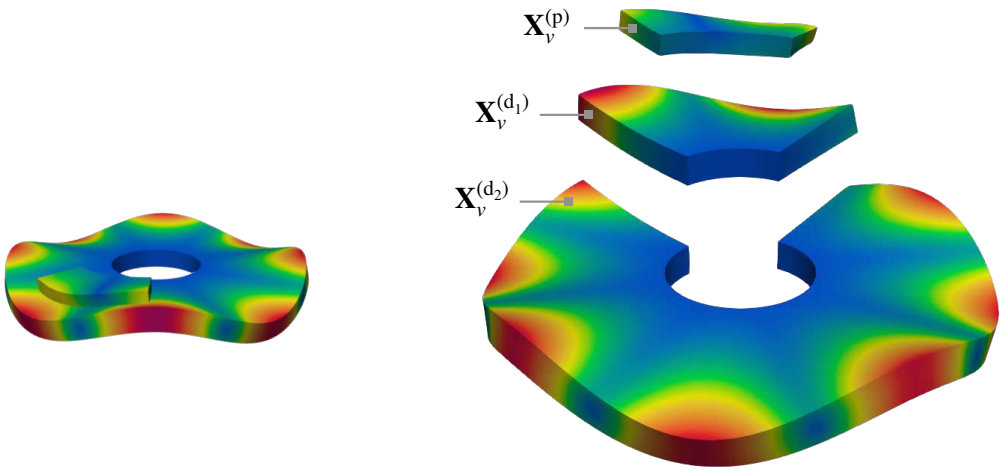

Figure 5.3: Anatomy of parameterization for the disc-pad system, shown here for Mode 9, Frequency: 3630 Hz

The multi-patch parameterization of $\Omega^{(d)}$ to break the NURBS tensor product definition is shown in Figure 5.4, where one patch $\boldsymbol{X}_v^{(d_1)}$ contains the contact domain $\Gamma_C^{(d_1)}$ defined through a fine mesh by h-refinement and the other patch $\boldsymbol{X}_v^{(d_2)}$ with a relatively coarse mesh sufficient to capture the required dynamic properties. And different strategies were used to reduce the solution smoothness induced by the continuity of the NURBS approximation across the boundary $\partial\Gamma_C^{(d_2)}$ where typically strong solution gradient exists. For pad shapes where the knot lines on $\boldsymbol{X}_v^{(d_1)}$ can be aligned with $\partial\Gamma_C^{(d_1)}$, h-refinement can be used with finer refinement around $\partial\Gamma_C^{(d_1)}$, while the contact domain $\Gamma_C^{(d_1)}$ itself is discretized by h-refinement through a relatively coarse mesh compared to the refinement around $\partial\Gamma_C^{(d_1)}$, but finer than the rest of the domain. For pad shapes where the knot lines on $\boldsymbol{X}_v^{(d_1)}$ cannot be aligned with the boundary $\partial\Gamma_C^{(d_1)}$, we purely relied on h-refinement with much finer refinement. For the shape optimization, we used the later strategy due to random definition of shapes.

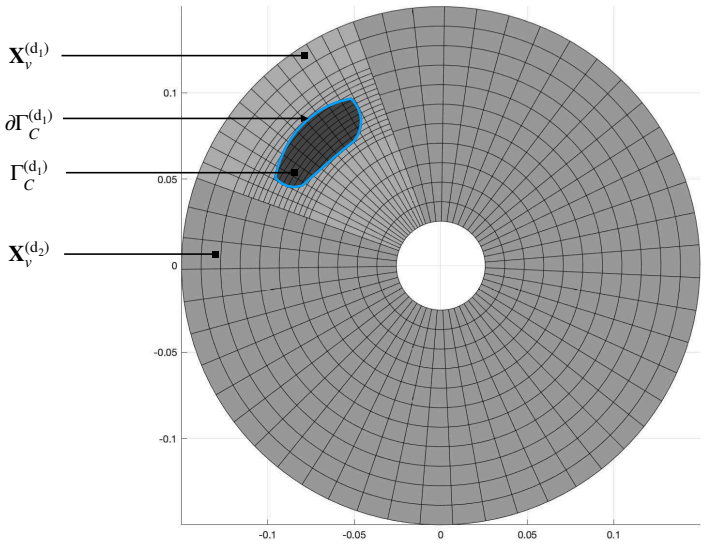

Figure 5.4: Multi-patch parameterization of $\Omega^{(\mathrm{d})}$ as $\boldsymbol{X}_v^{(\mathrm{d})} := \boldsymbol{X}_v^{(\mathrm{d}_1)} \cup \boldsymbol{X}_v^{(\mathrm{d}_2)}$, with h-refinement at the contact region $\Gamma_C^{(\mathrm{d}_1)}$.

6 Bayesian optimization

Bayesian optimization is an effective strategy for optimising computationally expensive objective functions [10] [81]. We begin the following explanations without defining the specifics of modelling the probability $\mathcal{P}$ which is given as knowledge and considering the optimisation of a single function $f(\boldsymbol{x})$ for $\underset{\boldsymbol{x}\in\mathcal{X}}{min}\, f(\boldsymbol{x})$. The idea is based on Bayes rule where the prior knowledge $\mathcal{P}(\mathcal{H})$ of the hypothesis $\mathcal{H}$ and the likelihood of the evidence $\mathcal{E}$ given the hypothesis, $\mathcal{P}(\mathcal{E}|\mathcal{H})$, are used to infer the posterior knowledge of the hypothesis given the evidence, $\mathcal{P}(\mathcal{H}|\mathcal{E})$, where the proportionality can be expressed as

$$\mathcal{P}(\mathcal{H}|\mathcal{E}) \propto \mathcal{P}(\mathcal{E}|\mathcal{H})\mathcal{P}(\mathcal{H}) \tag{6.1}$$

Hence, $\mathcal{P}(\mathcal{H}|\mathcal{E})$ defines Bayesian inference. In our setting, the hypothesis $\mathcal{H}$ corresponds to the function $f(\boldsymbol{x})$ and the evidence $\mathcal{E}$ to $\mathcal{F}_{1:\mathfrak{n}} : \{f(\boldsymbol{x}_1), f(\boldsymbol{x}_2), \ldots, f(\boldsymbol{x}_\mathfrak{n})\}$ where $f(\boldsymbol{x})$ is sampled on $\mathcal{X}_{1:\mathfrak{n}} : \{\boldsymbol{x}_1, \boldsymbol{x}_2, \ldots, \boldsymbol{x}_\mathfrak{n}\}$, with $\mathcal{D}_{1:\mathfrak{n}} : \{\mathcal{X}_{1:\mathfrak{n}}, \mathcal{F}_{1:\mathfrak{n}}\}$. This is typically known as function-space view, since the probability is defined on the space of functions. It can be hard to conceptualise such view with functions, but it is possible if one can imagine the existence of a function in a mere probabilistic sense such that a random draw from the probability distribution is a function. The relation (6.2) can be expressed in this case as

$$\mathcal{P}(f(\boldsymbol{x})|\mathcal{D}_{1:\mathfrak{n}}) \propto \mathcal{P}(\mathcal{D}_{1:\mathfrak{n}}|f(\boldsymbol{x}))\mathcal{P}(f(\boldsymbol{x})) \tag{6.2}$$

The prior over a function, $\mathcal{P}(f(\boldsymbol{x}))$, is typically modelled through spatial correlation which is assumed to be known a priori, where the hypothesis is that a given function exhibits certain characteristics of spatial correlation which can be generalized globally. In other words, a prior belief is defined over the space of functions, such that the functions in the space largely exhibit certain characteristics of spatial correlation. With the prior $\mathcal{P}(f(\boldsymbol{x}))$ defined, and given the likelihood of the points sampled on the function, $\mathcal{P}(\mathcal{D}_{1:\mathfrak{n}}|f(\boldsymbol{x}))$, the posterior knowledge of the function, $\mathcal{P}(f(\boldsymbol{x})|\mathcal{D}_{1:\mathfrak{n}})$, can be inferred from the relation (6.2). The posterior knowledge $\mathcal{P}(f(\boldsymbol{x})|\mathcal{D}_{1:\mathfrak{n}})$ is then used to infer the next point $\boldsymbol{x}_{\mathfrak{n}+1}$ to be sampled, depending on the strategy set for sampling in optimization. The sampled point $\boldsymbol{x}_{\mathfrak{n}+1}$ is then used to update the belief of the prior $\mathcal{P}(f(\boldsymbol{x}))$ in the light of $\mathcal{D}_{1:\mathfrak{n}+1}$, and with the likelihood $\mathcal{P}(\mathcal{D}_{1:\mathfrak{n}+1}|f(\boldsymbol{x}))$ to infer a new posterior $\mathcal{P}(f(\boldsymbol{x})|\mathcal{D}_{1:\mathfrak{n}+1})$, which characterizes active learning. The process is run subsequently with the prospect of finding the global optimum for the function through active learning, models Bayesian optimization.

6.1 Gaussian process regression/Kriging

With the general idea of Bayesian optimisation for a function, we can now define the notion of modelling $\mathcal{P}$ which is typically defined through Gaussian process ($\mathcal{GP}$) [34]. While a Gaussian distribution defines distribution over a random variable or in the case of a multi-variate Gaussian distribution over random variables, a $\mathcal{GP}$ defines distribution over a function, such that each draw from a $\mathcal{GP}$ is a function. For some intuition of the following explanations, this can be thought in a discrete sense as all the points, of a function drawn from a $\mathcal{GP}$ as being related through a dependent multi-variate Gaussian distribution such that each point is a univariate Gaussian distribution over a value of the function.

The prior over a function can hence be defined as $\mathcal{GP}$ prior, where the advantage of modelling the prior as Gaussian means that it preserves the conditioning of the Gaussian prior given the likelihood to infer the posterior as Gaussian as well. This is advantageous for Bayesian optimisation, since inferring the posterior as Gaussian presents the prediction as mean and the uncertainty of the prediction as variance, which provides a decisive knowledge to construct an acquisition function to sample more efficiently. The $\mathcal{GP}$ posterior defined through Bayesian inference from conditioning a $\mathcal{GP}$ prior given the likelihood of the sampled points over the function, characterizes a regression model, known as $\mathcal{GP}$ regression. Hence, the meta-modelisation of the function $f(\boldsymbol{x})$ can be defined through $\mathcal{GP}$ regression.

The $\mathcal{GP}$ prior $\mathcal{P}(f(\boldsymbol{x}))$ over $f(\boldsymbol{x})$ can be expressed as

$$f(\boldsymbol{x}) \approx \mathcal{P}(f(\boldsymbol{x})) = \mathcal{GP}(\mu(\boldsymbol{x}), k(\boldsymbol{x}, \boldsymbol{x}^{'})),$$
$$\mu(\boldsymbol{x}) = \mathrm{E}[f(\boldsymbol{x})], \quad k(\boldsymbol{x}, \boldsymbol{x}^{'}) = \mathrm{E}[(f(\boldsymbol{x}) - \mu(\boldsymbol{x}))(f(\boldsymbol{x}') - \mu(\boldsymbol{x}'))] \quad (6.3)$$

where the distribution constitutes a mean function $\mu(\boldsymbol{x})$ and a covariance function $k(\boldsymbol{x}, \boldsymbol{x}^{'})$. The function $\mu(\boldsymbol{x})$ can be seen as the deterministic part which captures the general trend of $f(\boldsymbol{x})$, while the covariance function $k(\boldsymbol{x}, \boldsymbol{x}^{'})$ models the stochastic trend which is the spatial correlation between any $f(\boldsymbol{x}) - \mu(\boldsymbol{x})$ and $f(\boldsymbol{x}') - \mu(\boldsymbol{x}')$. The deterministic part $\mu(\boldsymbol{x})$ is largely modelled as a constant or through polynomials, which is demanding to estimate a priori and also higher degree polynomial trend functions can lead to overfitting over the sampled points. Hence, care should be taken in defining the general trend such that some spatial correlation exists with respect to the trend. Recently, focus has also been in defining $\mu(\boldsymbol{x})$ with Polynomial chaos expansion approach.

The spatial correlation is modelled by hyperparameters $\boldsymbol{\theta}$ which are the constants known a priori in a covariance function $cov(f(\boldsymbol{x}) - \mu(\boldsymbol{x}), f(\boldsymbol{x}') - \mu(\boldsymbol{x}'))$, where the choice of the covariance function depends on the application. Even though the prior knowledge is defined to be known, it is often determined from the light of the sampled

points. Hence, to define the prior over $k(\boldsymbol{x}, \boldsymbol{x}^{'})$, the hyperparameters are estimated a priori from the sampled points, which is usually achieved by optimising the likelihood function for $arg\,max_{\boldsymbol{\theta}}\ L(\mathcal{F}|\boldsymbol{\theta})$. More on optimising for hyperparameters will be detailed in the upcoming explanations, where $\boldsymbol{\theta}$ often contains parameters to model $\mu(\boldsymbol{x})$ in addition to the hyperparameters.

With $\boldsymbol{\theta}$ determined, the $\mathcal{GP}$ prior $\mathcal{P}(f(\boldsymbol{x}))$ can now be defined. The conditioning of $\mathcal{P}(f(\boldsymbol{x}))$ with the likelihood of the sampled points $\mathcal{D}_{1:\mathfrak{n}}$ results in a $\mathcal{GP}$ posterior $\mathcal{P}(f(\boldsymbol{x})|\mathcal{D}_{1:\mathfrak{n}}, \boldsymbol{\theta})$ which can be viewed in a finite-dimensional sense as the posterior joint Gaussian distribution of $\mathcal{P}(f(\boldsymbol{x}_1^*)), \mathcal{P}(f(\boldsymbol{x}_2^*)), \ldots, \mathcal{P}(f(\boldsymbol{x}_{\cdot}^*))$ across rest of the function where its arguments $\boldsymbol{x}_{\mathfrak{i}}^*$ has not been sampled, i.e. $\boldsymbol{x}_{\mathfrak{i}}^* \notin \mathcal{X}_{1:\mathfrak{n}}$.

To move on from the abstractness of $\mathcal{GP}$ to a practical finite-dimensional Gaussian distribution useful for making inference at an arbitrary point $\boldsymbol{x}^* \in \mathcal{X}$, given the sampled points $\mathcal{X}_{1:\mathfrak{n}}$, the properties of multi-variate Gaussian distribution allow to isolate a part of the $\mathcal{GP}$ prior $\mathcal{P}(f(\boldsymbol{x}))$ to define a joint Gaussian distribution of only the sampled points $\mathcal{X}_{1:\mathfrak{n}}$ and an argument $\boldsymbol{x}^*$ where the inference is to be made, where the joint distribution can be expressed as

$$\begin{bmatrix} \mathcal{P}(f(\boldsymbol{x}_1)) \\ \vdots \\ \mathcal{P}(f(\boldsymbol{x}_n)) \\ \mathcal{P}(f(\boldsymbol{x}^*)) \end{bmatrix} = \mathcal{N}\left(\begin{bmatrix} \mu(\boldsymbol{x}_1) \\ \vdots \\ \mu(\boldsymbol{x}_{\mathfrak{n}}) \\ \mu(\boldsymbol{x}^*) \end{bmatrix}, \begin{bmatrix} k(\boldsymbol{x}_1, \boldsymbol{x}_1) & \ldots & k(\boldsymbol{x}_1, \boldsymbol{x}_{\mathfrak{n}}) & k(\boldsymbol{x}_1, \boldsymbol{x}^*) \\ \vdots & \ddots & \vdots & \vdots \\ k(\boldsymbol{x}_{\mathfrak{n}}, \boldsymbol{x}_1) & \ldots & k(\boldsymbol{x}_{\mathfrak{n}}, \boldsymbol{x}_{\mathfrak{n}}) & k(\boldsymbol{x}_{\mathfrak{n}}, \boldsymbol{x}^*) \\ k(\boldsymbol{x}^*, \boldsymbol{x}_1) & \ldots & k(\boldsymbol{x}^*, \boldsymbol{x}_{\mathfrak{n}}) & k(\boldsymbol{x}^*, \boldsymbol{x}^*) \end{bmatrix} \right) \tag{6.4}$$

The above joint distribution can be partitioned to define the mean and the covariance for the sampled points and the point to be inferred as

$$\boldsymbol{\Sigma} = \begin{bmatrix} k(\boldsymbol{x}_1, \boldsymbol{x}_1) & \ldots & k(\boldsymbol{x}_1, \boldsymbol{x}_{\mathfrak{n}}) \\ \vdots & \ddots & \vdots \\ k(\boldsymbol{x}_{\mathfrak{n}}, \boldsymbol{x}_1) & \ldots & k(\boldsymbol{x}_{\mathfrak{n}}, \boldsymbol{x}_{\mathfrak{n}}) \end{bmatrix}, \boldsymbol{\Sigma}^* = \begin{bmatrix} k(\boldsymbol{x}_1, \boldsymbol{x}^*) \\ \vdots \\ k(\boldsymbol{x}_{\mathfrak{n}}, \boldsymbol{x}^*) \end{bmatrix}, \boldsymbol{\mu}(\mathcal{X}) = \begin{bmatrix} \mu(\boldsymbol{x}_1) \\ \vdots \\ \mu(\boldsymbol{x}_{\mathfrak{n}}) \end{bmatrix} \tag{6.5}$$

The conditioning of the joint distribution Eq.(6.4) defined by the prior knowledge of $\boldsymbol{\theta}$ with the sampled data $\mathcal{D}$ gives the prediction for $\boldsymbol{x}^*$ as follows

$$\mathcal{P}(f(\boldsymbol{x}_i^*)|\mathcal{D}, \boldsymbol{\theta}) = \mathcal{N}(\underbrace{\mu(\boldsymbol{x}_i^*) + \boldsymbol{\Sigma}^{-1}\boldsymbol{\Sigma}^*(\mathcal{F} - \boldsymbol{\mu}(\mathcal{X}))}_{\hat{\mu}(\boldsymbol{x}^*)}, \underbrace{k(\boldsymbol{x}^*, \boldsymbol{x}^*) - \boldsymbol{\Sigma}^*\boldsymbol{\Sigma}^{-1}\boldsymbol{\Sigma}^{*T}}_{\hat{\sigma}^2(\boldsymbol{x}^*)}) \tag{6.6}$$

where the function $f(\boldsymbol{x})$ approximated by the Gaussian process regression model can be defined as $\hat{f}(\boldsymbol{x}) := \mathcal{N}(\hat{\mu}(\boldsymbol{x}), \hat{\sigma}(\boldsymbol{x}))$.

6.1.1 Covariance function and Hyperparameters

The choice of the covariance function and the estimation of the hyperparameters in defining spatial correlation are important since they are the determining factors that distinguish the above distribution for a given observation. The hyperparameters parameterizes spatial correlation through smoothness or correlation length or sometimes both [1], for which a large class of covariance functions exist to choose from depending on the application. The most commonly used in engineering optimisation are the Gaussian and the Matérn class of covariance functions, where for isotropic correlation, the Gaussian covariance function can be defined as

$$k(\boldsymbol{x}, \boldsymbol{x}^{'}) = exp\bigg(-\frac{1}{2\theta^2}||\boldsymbol{h}||^2 \bigg) \tag{6.7}$$

where $\boldsymbol{h} := [h_1, h_2, \cdots, h_{\mathsf{l}}]$, $h = (f(x) - \mu(x)) - (f(x') - \mu(x'))$ and $\boldsymbol{x}$ is considered to be in $\mathbb{R}^{\mathsf{l}}$. This is defined with only a single hyperparameter θ since it assumes the spatial correlation to be isotropic. The anisotropic consideration of spatial correlation can be defined as

$$k(\boldsymbol{x}, \boldsymbol{x}^{'}) = exp\bigg(-\sum_{\mathsf{k}=1}^{\mathsf{l}} \frac{1}{2\theta_{\mathsf{k}}^2}|h|^2 \bigg) \tag{6.8}$$

where it leads to determining l no. of θ. The Gaussian covariance function models spatial correlation only with correlation length defined through the factor $\frac{1}{2\theta^2}$, while the smoothness for the variation of h is defined for a fixed power 2. The Matérn class of covariance functions provide flexibility in modelling smoothness through a predefined parameter υ, where the function can be expressed for anisotropic variation as

$$k(\boldsymbol{x}, \boldsymbol{x}^{'}) = \sum_{\mathsf{k}=1}^{\mathsf{l}} \sigma^2 \frac{2^{(1-\upsilon)}}{\mathsf{G}(\upsilon)} \bigg(\frac{\sqrt{2\upsilon}|h_{\mathsf{k}}|}{\theta_{\mathsf{k}}} \bigg)^{\upsilon} \mathsf{B} \bigg(\frac{\sqrt{2\upsilon}|h_{\mathsf{k}}|}{\theta_{\mathsf{k}}} \bigg) \tag{6.9}$$

where G and B are the Gamma function and the Bessel function of order υ respectively. The value of υ is typically defined to be $5/2$ or $3/2$, where as $\upsilon \to \infty$, it converges to squared exponential function and for $\upsilon = 1/2$, it simply characterizes an exponential function. The Gaussian covariance makes strong smoothness assumption with the infinite differentiability of the function which can be unreal and hence, Matérn class of functions are typically preferred which are $\upsilon - 1$ times differentiable. We used Matérn with $\upsilon = 5/2$, expressed as

[1] It should be noted that the parameters modelling smoothness and correlation length are not independent, but rather interdependent such that parameters modelling smoothness has influence on correlation length and vice-versa. But largely, smoothness parameters can be said to quantify the gradient factor for the variation of h, while correlation length parameters can be said to quantify the influence of the points on each other for the variation of h

$$k(\boldsymbol{x}, \boldsymbol{x}^{'}) = \sum_{\mathsf{k}=1}^{\mathsf{l}} \sigma^2 \bigg(1 + \frac{\sqrt{5}|h_{\mathsf{k}}|}{\theta_{\mathsf{k}}} + \frac{5h^2}{3\theta_{\mathsf{k}}^2}\bigg) exp\bigg(- \frac{\sqrt{5}|h_{\mathsf{k}}|}{\theta_{\mathsf{k}}}\bigg) \tag{6.10}$$

With the definition of a covariance function, the optimisation of the hyperparameters to model the prior (6.4) is given by $arg\,max_{\boldsymbol{\theta}}\ L(\mathcal{F}|\boldsymbol{\theta})$, where $L(\mathcal{F}|\boldsymbol{\theta})$ defines the likelihood of the observed data given the hyperparameters, defined by the joint probability as

$$L(\mathcal{F}|\mu(\boldsymbol{\theta}), \sigma(\boldsymbol{\theta})) = \frac{1}{\sqrt{(2\pi\sigma^2)^n|\boldsymbol{\Sigma}|}} exp\bigg[- \frac{(\mathcal{F} - \boldsymbol{\mu}(\mathcal{X}))^T \boldsymbol{\Sigma}^{-1} (\mathcal{F} - \boldsymbol{\mu}(\mathcal{X})}{2\sigma^2}\bigg] \tag{6.11}$$

In optimising the above function for maximum likelihood, the function can be simplified by taking the natural logarithm while preserving the monotonicity of the function as

$$ln(L) = -\frac{n}{2} ln(2\pi) - \frac{n}{2} ln(\sigma^2) - \frac{1}{2} ln|\boldsymbol{\Sigma}| - \frac{(\mathcal{F} - \boldsymbol{\mu}(\mathcal{X}))^T \boldsymbol{\Sigma}^{-1} (\mathcal{F} - \boldsymbol{\mu}(\mathcal{X}))}{2\sigma^2} \tag{6.12}$$

The definition of the logarithm preserves the monotonicity of the function and hence also the optimum point of the function. Mean can be defined as $\boldsymbol{\mu} = \mathsf{X}\boldsymbol{\theta}_{\boldsymbol{\mu}}$ when modelled as regression with hyperparameters $\boldsymbol{\theta}_{\boldsymbol{\mu}}$ [2], where X defines a matrix of size $\mathfrak{n} \times \mathsf{p}$, with p being the number of linear combination of functions defined for regression. The maximum likelihood estimate of $\boldsymbol{\mu}$ in this case is simply the maximum likelihood estimate of $\boldsymbol{\theta}_{\boldsymbol{\mu}}$ which can be deduced from $\frac{\partial ln(L)}{\partial \boldsymbol{\theta}_{\boldsymbol{\mu}}} = 0$ as

$$\check{\boldsymbol{\theta}}_{\boldsymbol{\mu}} = (\mathsf{X}^T \boldsymbol{\Sigma}^{-1} \mathsf{X})^{-1} \mathsf{X}^T \boldsymbol{\Sigma}^{-1} \mathcal{F} \tag{6.13}$$

which is simply the minimiser for generalized least-squares. This is apparent, since the minimiser of $\boldsymbol{\theta}_{\boldsymbol{\mu}}$ can be viewed as the minimisation of the generalised least-squares problem given as

$$\check{\boldsymbol{\theta}}_{\boldsymbol{\mu}} = arg\,min_{\boldsymbol{\theta}_{\boldsymbol{\mu}}} \frac{(\mathcal{F} - \boldsymbol{\mu}(\mathcal{X}, \boldsymbol{\theta}_{\boldsymbol{\mu}}))^T \boldsymbol{\Sigma}^{-1} (\mathcal{F} - \boldsymbol{\mu}(\mathcal{X}, \boldsymbol{\theta}_{\boldsymbol{\mu}}))}{2\sigma^2} \tag{6.14}$$

Similarly, the maximum likelihood estimate for σ can be defined from $\frac{\partial ln(L)}{\partial \sigma} = 0$ as

$$\check{\sigma} = (\mathcal{F} - \mathsf{X}\boldsymbol{\theta}_{\boldsymbol{\mu}})^T \boldsymbol{\Sigma}^{-1} (\mathcal{F} - \mathsf{X}\boldsymbol{\theta}_{\boldsymbol{\mu}}) \tag{6.15}$$

Substituting the maximum likelihood estimates of $\check{\boldsymbol{\theta}}_{\boldsymbol{\mu}}$ and $\check{\sigma}$ in to Eq.(6.12), and with the constants removed as affine terms, one obtains

$$ln(L(\boldsymbol{\theta})) \approx -\frac{n}{2} ln(\check{\sigma}^2(\boldsymbol{\theta})) - \frac{1}{2} ln|\boldsymbol{\Sigma}(\boldsymbol{\theta}_{\boldsymbol{\Sigma}})| \tag{6.16}$$

[2] $\boldsymbol{\theta} := \{\boldsymbol{\theta}_{\boldsymbol{\mu}}\} \cup \{\boldsymbol{\theta}_{\boldsymbol{\Sigma}}\}$, where $\boldsymbol{\theta}_{\boldsymbol{\mu}}$ and $\boldsymbol{\theta}_{\boldsymbol{\Sigma}}$ correspond to the hyperparameters of $\boldsymbol{\mu}$ and $\boldsymbol{\Sigma}$

The above function can be typically expected to be multimodal and hence the optimisation is typically achieved with Genetic algorithm (GA) for global convergence, followed by the best individuals from the GA as seeds for the quasi-newton algorithms like BFGS for local convergence. As a variation, quasi-newton schemes are also applied with in GA for the best individuals in each generation to define the parent population of the next generation.

6.2 Acquistion function

The Bayesian inference $\mathcal{P}(f(\boldsymbol{x}_i^*)|\mathcal{D}_{1:\mathrm{n}}, \boldsymbol{\theta})$ can be used in sampling for optimisation from the inference of the prediction $\hat{\mu}(\boldsymbol{x}^*)$ and the uncertainty $\hat{\sigma}^2(\boldsymbol{x}^*)$ of the prediction. Naturally, question arises for the goal of sampling in balance between exploration and exploitation. Exploration can viewed as the means to gain more knowledge about the function especially where high uncertainty is reflected by the $\mathcal{GP}$ posterior. But with pure exploration, it diverts the goal in search for a global optimum with the consequence of reducing the uncertainty over the knowledge of the function, unless reducing the uncertainty also exposes the global optimum as a repercussion which happens rarely. In contrast, exploitation focuses on parts of the function which is inferred to define optimum through the prediction from the $\mathcal{GP}$ posterior. Pure exploitation in optimisation can be viewed as more optimistic with the predictions and hence can underestimate the uncertain parts reflected by the $\mathcal{GP}$ posterior.

This is where sampling through an acquisition function plays an important role in guiding the search for optimisation where the construction of the acquisition function can be adapted to set the balance between exploration and exploitation depending on the objective, for which a wide range of acquisition functions exist. In general, acquisition functions define improvement with respect to a reference value $f(\boldsymbol{x}^+)$ through a probabilistic metric, where $f(\boldsymbol{x}^+)$ typically corresponds to the utopian value [3] of the function, at least in the context of single objective optimisation. While in multi-objective optimisation the definition of utopian value corresponds to empirical Pareto front which will be discussed later. We will introduce some of the acquisition functions for single-objective optimisation which will be referred for the upcoming explanations. As defined before, we consider the case of optimising $f(\boldsymbol{x})$ for $\min_{\mathcal{X}} f(\boldsymbol{x})$ for the following explanations and hence the utopian value $f(\boldsymbol{x}^{++})$[4] is defined by $\boldsymbol{x}^{++} = arg\,min_{\boldsymbol{x}_\mathrm{i} \in \mathcal{X}_{1:\mathrm{n}}} f(\boldsymbol{x}_\mathrm{i})$.

Probability of Improvement (PI) for any $\mathcal{GP}$ outcome $\hat{f}(\boldsymbol{x})$ is given as

$$PI(\boldsymbol{x}) = \mathcal{P}(f(\boldsymbol{x}) \leq f(\boldsymbol{x}^{++})) \tag{6.17}$$

[3] Utopian value is the observed optimum value of the function

[4] We use the notation $f(\boldsymbol{x}^{++})$ to define the Utopian value as reference value and $f(\boldsymbol{x}^+)$ to define an arbitrary reference value

where,

$$\mathcal{P}(f(\boldsymbol{x}) \leq f(\boldsymbol{x}^{+})) = CDF\left(\frac{\hat{\mu}(\boldsymbol{x}) - f(\boldsymbol{x}^{++})}{\hat{\sigma}(\boldsymbol{x})}\right) \tag{6.18}$$

PI gives more weight on exploitation than exploration in optimisation. This can be seen with the following case, where for a point with low variance for $\hat{\mu} < f(\boldsymbol{x}^{++})$ reflects more scope for improvement than for a point with the same $\hat{\mu}$ but larger variance, where PI reflects more focus on exploitation which leads to highly exhaustive search locally. PI is the same when both points have $\hat{\mu} = f(\boldsymbol{x}^{++})$ and when $\hat{\mu} > f(\boldsymbol{x}^{++})$, the point with larger variance has larger PI, where PI reflects focus on exploration. This means that PI focuses on exploration unless there is no possibility for exploitation, where in real world, this leads to exhaustive search locally around the best points before moving on to the next exploration search. To overcome this effect, a trade-off parameter $\mathscr{E} \geq 0$ is introduced, given as

$$PI(\boldsymbol{x}) = \mathcal{P}(f(\boldsymbol{x}) \leq f(\boldsymbol{x}^{++}) + \mathscr{E}) \tag{6.19}$$

where typically $\mathscr{E}$ is set to be higher initially in an optimisation to drive exploration, and decreases to zero by the end of the optimisation to drive exploitation. PI clearly lacks a good balance between exploration and exploitation for which Expected Improvement EI is typically deemed to be effective.

EI is the expectation of the improvement, $E(I(\boldsymbol{x}))$, where the improvement is typically defined with respect to the utopian value $f(\boldsymbol{x}^{++})$ as $I(\boldsymbol{x}) = f(\boldsymbol{x}^{++}) - \hat{f}(\boldsymbol{x})$. The expectation of the improvement, $EI(\boldsymbol{x}|f(\boldsymbol{x}^{++}))$ [5] can hence be expressed as

$$EI(\boldsymbol{x}) = E(I(\boldsymbol{x})) = \int_{-\infty}^{f(\boldsymbol{x}^{++})} I(\boldsymbol{x}) PDF\left(\frac{f(\boldsymbol{x}) - \hat{\mu}(\boldsymbol{x}))}{\hat{\sigma}(\boldsymbol{x})}\right) df(\boldsymbol{x}) \tag{6.20}$$

For intuition, the above expression can be given as

$$EI(\boldsymbol{x}) = \left(f(\boldsymbol{x}^{++}) - \underbrace{\frac{\int_{-\infty}^{f(\boldsymbol{x}^{++})} f(\boldsymbol{x}) PDF\left(\frac{f(\boldsymbol{x}) - \hat{\mu}(\boldsymbol{x}))}{\hat{\sigma}(\boldsymbol{x})}\right) df(\boldsymbol{x})}{CDF\left(\frac{f(\boldsymbol{x}^{++}) - \hat{\mu}(\boldsymbol{x}))}{\hat{\sigma}(\boldsymbol{x})}\right)}}_{f_{cen}}\right) CDF\left(\frac{f(\boldsymbol{x}^{++}) - \hat{\mu}(\boldsymbol{x}))}{\hat{\sigma}(\boldsymbol{x})}\right) \tag{6.21}$$

where f_{cen} is the first moment of area/centroid of the $PDF\left(\frac{f(\boldsymbol{x}) - \hat{\mu}(\boldsymbol{x}))}{\hat{\sigma}(\boldsymbol{x})}\right) \in (-\infty, f(\boldsymbol{x}^{++})]$ on the axis of $f(\boldsymbol{x})$. Hence, EI can be understood as the measure of f_{cen} with

[5] For simplicity, we define $EI(\boldsymbol{x}|f(\boldsymbol{x}^{++}))$ as $EI(\boldsymbol{x})$ unless we want to emphasize the use of $f(\boldsymbol{x}^{++})$

respect to the reference value $f(\boldsymbol{x}^{++})$, given as $f(\boldsymbol{x}^{++}) - f_{cen}$, weighted by the $CDF\left(\frac{f(\boldsymbol{x}^{++})-\hat{\mu}(\boldsymbol{x}))}{\hat{\sigma}(\boldsymbol{x})}\right)$ which is simply $PI(\boldsymbol{x})$. The term $\int_{-\infty}^{f(\boldsymbol{x}^{++})} f(\boldsymbol{x})PDF\left(\frac{f(\boldsymbol{x})-\hat{\mu}(\boldsymbol{x}))}{\hat{\sigma}(\boldsymbol{x})}\right)df(\boldsymbol{x})$ can be seen as the measure of $E(\hat{f}(\boldsymbol{x}))$ in the interval $(-\infty, f(\boldsymbol{x}^{++})]$, where it defines the expected value rather than the expected improvement defined by EI with respect to a reference value. We elaborate these definitions since it will be useful for definitions to extend EI to MOO.

Overall, EI provides better trade-off between exploration and exploitation, unlike the greedy nature of PI which primarily focuses on exploitation. This is because the term $f(\boldsymbol{x}^{++}) - f_{cen}$ weighted by PI provides the additional factor in EI to balance the search for exploration. The above expression of EI can be simplified as

$$EI(\boldsymbol{x}) = (f(\boldsymbol{x}^{++}) - \hat{\mu}(\boldsymbol{x}))CDF\left(\frac{f(\boldsymbol{x}^{++}) - \hat{\mu}(\boldsymbol{x}))}{\hat{\sigma}(\boldsymbol{x})}\right) + \hat{\sigma}(\boldsymbol{x})PDF\left(\frac{f(\boldsymbol{x}^{++}) - \hat{\mu}(\boldsymbol{x}))}{\hat{\sigma}(\boldsymbol{x})}\right) \tag{6.22}$$

Similar to Eq. (6.19), it is possible to control the trade-off between exploration and exploitation by introducing $\mathscr{E} \geq 0$ to the above expression as follows

$$EI(\boldsymbol{x}) = (f(\boldsymbol{x}^{++}) - \hat{\mu}(\boldsymbol{x}) - \mathscr{E})CDF\left(\frac{f(\boldsymbol{x}^{++}) - \hat{\mu}(\boldsymbol{x}))}{\hat{\sigma}(\boldsymbol{x})}\right) + \hat{\sigma}(\boldsymbol{x})PDF\left(\frac{f(\boldsymbol{x}^{++}) - \hat{\mu}(\boldsymbol{x}))}{\hat{\sigma}(\boldsymbol{x})}\right) \tag{6.23}$$

The other common acquisition function is defined with the bound of $\hat{f}(\boldsymbol{x})$, where for a function to be minimised, the lower confidence bound can be defined as

$$LCB(\boldsymbol{x}) = \hat{\mu}(\boldsymbol{x}) - \epsilon\hat{\sigma}(\boldsymbol{x}) \tag{6.24}$$

where $\epsilon \geq 0$. It is quite intuitive to think that LCB favours exploration over exploitation. It is apparent that each acquisition function will give rise to distinct sampling behaviour and hence, the choice of the acquisition function depends on the goal for sampling. Similar to the approach of maximising Eq. (6.16), the optimisation of the acquisition functions can be achieved with the combination of GA and quasi-newton algorithms to determine the infill point $\boldsymbol{x}^{\iota}$.

6.3 Multi-objective optimisation

For MOO, the problem can be formulated as

$$\min_{\boldsymbol{x}\in\mathcal{X}} \boldsymbol{f}(\boldsymbol{x}) \tag{6.25}$$

where $\boldsymbol{f} = [f_1(\boldsymbol{x}), \cdots, f_{\mathsf{m}}(\boldsymbol{x})]$, $\boldsymbol{f} : \mathcal{X} \subset \mathbb{R}^{\mathsf{l}} \to \mathcal{S} \subset \mathbb{R}^{\mathsf{m}}$, with $\mathcal{S}$ being the objective space. The definition of optimality in single objective optimisation is defined with minimum or maximum of a function. While in MOO for a set of functions to be minimised, where typically the functions can not be minimised simultaneously without conflict between the objectives, where minimising one function can implicitly maximise the other. Hence, the definition of optimality in MOO is given by Pareto optimality which defines optimality considering the best compromise between the objectives.

Hence, any two vectors $\boldsymbol{x}_a, \boldsymbol{x}_b \in \mathcal{X}$, and $\boldsymbol{x}_a \neq \boldsymbol{x}_b$, the following conditions can be stated for Pareto-dominance to define Pareto-optimality on $\underset{\boldsymbol{x} \in \mathcal{X}}{min}\, \boldsymbol{f}(\boldsymbol{x})$, given as

- $\boldsymbol{x}_a \preceq \boldsymbol{x}_b$ ($\boldsymbol{x}_a$ weakly dominates $\boldsymbol{x}_b$) $i.f.f.$ $\forall \mathsf{i},\ f_{\mathsf{i}}(\boldsymbol{x}_a) \leq f_{\mathsf{i}}(\boldsymbol{x}_b)$
- $\boldsymbol{x}_a \prec \boldsymbol{x}_b$ ($\boldsymbol{x}_a$ dominates $\boldsymbol{x}_b$) $i.f.f.$ $\boldsymbol{x}_a \preceq \boldsymbol{x}_b$ & $\exists \mathsf{i}\ s.t\ f_{\mathsf{i}}(\boldsymbol{x}_a) < f_{\mathsf{i}}(\boldsymbol{x}_b)$
- $\boldsymbol{x}_a \sim \boldsymbol{x}_b$ (neither dominates the other) $i.f.f.$ $\boldsymbol{x}_a \not\prec \boldsymbol{x}_b$ and $\boldsymbol{x}_b \not\prec \boldsymbol{x}_a$

where $\mathsf{i} \in \{1, \cdots, \mathsf{m}\}$. Any $\boldsymbol{x}_a \in \mathcal{X}$ can be said as Pareto-optimal $i.f.f.$ $\nexists \boldsymbol{x}_b \in \mathcal{X}\ s.t.\ \boldsymbol{x}_a \prec \boldsymbol{x}_b$, given $\boldsymbol{x}_b \neq \boldsymbol{x}_a$. Hence, the Pareto-optimal set/Non-dominated solutions(NDS) $\mathscr{P}$ and Non-dominated points (NDS)/Pareto-front $\boldsymbol{f}(\mathscr{P})$ can be defined as follows

- $\mathscr{P} := \{\boldsymbol{x}_a \in \mathcal{X} : \boldsymbol{x}_a \neq \boldsymbol{x}_b, \nexists \boldsymbol{x}_b \in \mathcal{X}\ s.t.\ \forall \mathsf{i},\ f_{\mathsf{i}}(\boldsymbol{x}_a) \leq f_{\mathsf{i}}(\boldsymbol{x}_b)\ \&\ \exists \mathsf{i}\ s.t\ f_{\mathsf{i}}(\boldsymbol{x}_a) \leq f_{\mathsf{i}}(\boldsymbol{x}_b)\}$
- $\boldsymbol{f}(\mathscr{P}) := \{\boldsymbol{f}(\boldsymbol{x}), \boldsymbol{x} \in \mathscr{P}\}$

Hence, Pareto-front in the context of MOO corresponds to the optimal solution of a function. Often distinguish is made between the true Pareto-front which corresponds to the true optimal of a function in single objective case and the observed Pareto-front known as empirical Pareto-front which corresponds to the known optimal of a function in single objective case. For the following definitions, we define NDS as empirical Pareto-front unless otherwise specified. Similar to the Utopian point in Single objective optimisation, Utopian point in MOO corresponds to a vector of all the known optimal solutions in $\mathcal{S}$. While the Nadir point defines the opposite, if the optimal points are defined to be the minimum of functions in MOO, Nadir point defines the maximum of all the functions in the NDS.

Before moving on to the Multi-objective Bayesian optimisation (MOBO), we introduce some of the standard approaches in MOO, since most of the approaches in MOBO has influence of the standard approaches where in MOBO typically acquisition functions are replaced for expensive functions and optimised in the context

of MOO. Broadly MOO approaches can be classified in to two, where one approach typically converts MOO in to a set of single objective optimisations and optimise with classical single objective strategies. While the other approach works directly in the context of MOO, where Pareto-dominance measures are used directly in optimisation. The former approach is typically based on aggregation procedures, where a vector of objectives are scalarized by summation with assigning weights to each objective. Hence optimising the scalar function with different set of weights, one can obtain a set of Pareto-optimal points. The simplest of them can be given as $\sum_{\mathsf{i}}^{\mathsf{m}} \mathsf{w}_{\mathsf{i}} f_{\mathsf{i}}(\boldsymbol{x})$, where $\mathsf{w}_{\mathsf{i}} \geq 0$ and $\sum_{\mathsf{i}}^{\mathsf{m}} \mathsf{w}_{\mathsf{i}} = 1$. The major drawback is that due to linear scalarziation, only convex parts of the Pareto-front can be found. To over come this problem, the optimisation can be defined for any one function with other functions as constraints, or through modifying the scalarization as $\sum_{\mathsf{i}}^{\mathsf{m}} \mathsf{w}_{\mathsf{i}} (f_{\mathsf{i}}(\boldsymbol{x}))^{\mathsf{p}}$, where the parameter p should be defined a priori, which demands a priori knowledge of the Pareto-front. The other approach to generalize for non-convex type of Pareto-front is based on Tchebychev aggregartion which is simply the weighted norm in L_p metric as $p \to \infty$, given as

$$\underset{\mathsf{i}}{max}\ \mathsf{w}_{\mathsf{i}}(|f_{\mathsf{i}}(\boldsymbol{x}) - f_{\mathsf{i}}(\boldsymbol{x}^{\mathsf{i}++})|) \tag{6.26}$$

where $f_{\mathsf{i}}(\boldsymbol{x}^{\mathsf{i}++})$ is the Utopian value of f_{i}. Normally the above term is augmented to avoid weakly Pareto-optimal solutions as

$$\underset{\mathsf{i}}{max}\ \mathsf{w}_{\mathsf{i}}(f_{\mathsf{i}}(\boldsymbol{x}) - f_{\mathsf{i}}(\boldsymbol{x}^{\mathsf{i}++}))) + \beta \sum_{\mathsf{i}}^{\mathsf{m}} |f_{\mathsf{i}}(\boldsymbol{x}) - f_{\mathsf{i}}(\boldsymbol{x}^{\mathsf{i}++})| \tag{6.27}$$

where β can be any sufficiently small value. The main drawback with scalarization of the MOO problem is that it is hard to define a generic frame work considering flexibility, where it is highly sensitive to the parameters which need to be defined or actively learned with prior knowledge of the optimisation problem, where such prior knowledge are typically unknown. The other major drawback is also with enhancing diversity which cannot be often explicitly achieved with a priori definition of weight vectors. This is also a set back in applications to define a focused search on the Pareto-front. This can be overcome with penalty boundary insertion strategies which further require a good prior knowledge of parameters to initialize.

The other class of approaches in dealing with MOO are nature-inspired approaches which are meta-heuristic, where we focus on GA which belongs to the class of Evolutionary Algorithms. GAs are inspired from concepts based on evolution such as fitness, natural selection, cross-over and mutation to guide the search for optimisation. GAs are typically more robust, and can handle discontinuities well. Constraint definitions are also more easy and generic with GAs. GAs developed for MOO share the same advantages along with other major advantages well-suited for MOO, where it allows the possibility to utilise the optimality measure in MOO such as Pareto-dominance and diversity directly. There are several methods exist under the concept

multi-objective GAs, where typically the difference comes in defining the fitness measures and niching. We use NSGA-2 where the fitness measures are defined based on the ranking of the Pareto-front and the crowding distance. Some other typical variation of fitness measures are defined based on quality indicators of the Pareto-front such as Hypervolume (also known as $\mathcal{S}$-metric) and epsilon indicators.

6.4 Multi-objective Bayesian optimisation

Similar to the MOO problem, the Multi-objective Bayesian optimisation (MOBO) can be defined as through the scalarization approach of converting a multi-objective problem in to an aggregate set of single objective problems, where typically Augmented Tchebycheff aggregation is used. In [82], $\mathcal{GP}$ for the scalarized function is fitted and the subsequent definition of EI is optimised. [83] defined a variation of the approach, where the $\mathcal{GP}$ models are independently fitted to each objective function and the EI of the $\mathcal{GP}$ meta-models are scalarized, where the optimization of EI is defined in parallel for the aggregation. Further variations with scalarization approach typically involves the Penalty boundary insertion to maintain diversity of the NDS.

A more direct extension of the MOBO comes form the extension of the concept of EI to MOO in a direct or indirect sense. EI for a single objective optimization can be seen as the measure of improvement in lesbegue norm, and hence, a more direct extension of the EI for MOO leads to the defintion of improvement with lesbegue measure in higher dimensions, also known as S-metric or Hypervolume metric. This approach was introduced in [84] which can be seen as the extension of $SMS-EMOA$ [85]. Similar to the definition of improvement for a single objective case with respect to Utopian value, in MOO, the improvement is defined with respect to the empirical Pareto-front typically bounded by Nadir point. The hypervolume (HV) can be given as

$$HV(\boldsymbol{f}(\mathscr{P}_{\mathcal{S}})|\mathbf{R}) = \mathscr{L}\Bigg(\bigcup_{\boldsymbol{f}(\boldsymbol{p}_{\mathrm{i}})\in\boldsymbol{f}(\mathscr{P}_{\mathcal{S}})} \{\boldsymbol{f}(\boldsymbol{x}) : \boldsymbol{f}(\boldsymbol{p}_{\mathrm{i}}) \preceq \boldsymbol{f}(\boldsymbol{x}) \preceq \mathbf{R}\}\Bigg) \tag{6.28}$$

where $\mathscr{L}$ is the lesbegue measure in $\mathbb{R}^{\mathsf{m}}$ when $\boldsymbol{f}(\boldsymbol{x}) \in \mathbb{R}^{\mathsf{m}}$, bounded by the reference point $\mathbf{R} \in \mathbb{R}^{\mathsf{m}}$. The hypervolume improvement (HVI) can be defined as the hypervolume dominated by a point $\boldsymbol{f}_o$ with respect to the Pareto-front $\boldsymbol{f}(\mathscr{P}_{\mathcal{S}})$ bounded by $\mathbf{R}$, given as

$$HVI(\boldsymbol{f}_o|\boldsymbol{f}(\mathscr{P}_{\mathcal{S}}), \mathsf{R}) = HV(\boldsymbol{f}(\mathscr{P}_{\mathcal{S}}) \cap \boldsymbol{f}_o|\mathsf{R}) - HV(\boldsymbol{f}(\mathscr{P}_{\mathcal{S}})|\mathbf{R}) \tag{6.29}$$

Similar to defining the expectation of improvement $E(I(\boldsymbol{x}))$ in single-objective case, for the multi-objective case, the expectation is defined over HVI as $E(HVI(\boldsymbol{x}))$, given as

$$EHVI(\boldsymbol{x}|\boldsymbol{f}(\mathscr{P}_{\mathcal{S}}),\mathbf{R}) = \int_{\boldsymbol{f}(\boldsymbol{x})\prec\boldsymbol{f}(\mathscr{P}_{\mathcal{S}})|\mathbf{R}} HVI(\boldsymbol{f}(\boldsymbol{x})|\boldsymbol{f}(\mathscr{P}_{\mathcal{S}}),\mathbf{R}).PDF(\hat{\boldsymbol{f}}(\boldsymbol{x}))d\boldsymbol{f}(\boldsymbol{x}) \tag{6.30}$$

where $\hat{\boldsymbol{f}} : \mathcal{N}(\hat{\boldsymbol{\mu}}, \hat{\boldsymbol{\Sigma}})$ is the prediction defined by multivariate independent normal distribution [6]. Even though there exists some correlation between the predictions through which Pareto-optimal solutions are presumed to exist, the multi-variate Gaussian prediction is defined to be independent to avoid complexity, i.e., $\hat{\boldsymbol{\Sigma}}$ is diagonal. And hence for the joint distribution $\hat{\boldsymbol{f}}(\boldsymbol{x})$, $PDF(\hat{\boldsymbol{f}}(\boldsymbol{x})) := \prod_{\mathsf{i}=1}^{\mathsf{m}} PDF\left(\frac{f_{\mathsf{i}}-\mu_{\mathsf{i}}}{\sigma_{\mathsf{i}}}\right)$. The maximum of $EHVI$ can be chosen as the infill point for an iteration in MOBO where batch selection cannot be defined since the scalar value of $EHVI$ contains no metric to compare for diversity. Any target based improvement is defined through weights or truncation applied to the $EHVI$ [86, 87]. But the main disadvantage of this method is that it requires the computation of m dimensional hypervolume, where the integration is typically achieved by expensive Monte-Carlo methods. But recently, a formula has been proposed for any number of dimensions but the complexity still increases exponentially with number of objectives. Another approach similarly defined with $\mathcal{S}$-metric is based on LCB (6.24) but still requires the expensive evaluation of HVI for LCB prediction to optimise for the maximum of HVI to choose the infill points. Further if the LCB is dominated, penalty value is assigned to avoid plateaus of the criterion.

The other approach is given in [88] for two objective case, where this approach interprets the geometric nature of EI in single-objective case – detailed in (6.21) – and extends to multi-objective case to define an equivalent metric. The improvement $I(\boldsymbol{x})$ is modelled implicitly by the Euclidean distance (L_2 norm) between the centroid $\boldsymbol{f}_{cen}$ and the nearest point $\boldsymbol{f}_{near} \in \boldsymbol{f}(\mathscr{P}_{\mathcal{S}})$ to $\boldsymbol{f}_{cen}$. Hence, $E(I(\boldsymbol{x}))$ in this case is given as the product of $||\boldsymbol{f}_{cen} - \boldsymbol{f}_{near}||$ and the probability $\mathcal{P}(\boldsymbol{f}(\boldsymbol{x}) \prec \boldsymbol{f}(\mathscr{P}_{\mathcal{S}})|\mathbf{R})$ for the given prediction $\hat{\boldsymbol{f}}(\boldsymbol{x})$ that can dominate $\boldsymbol{f}(\mathscr{P}_{\mathcal{S}})$ bounded by $\mathbf{R}$. $\boldsymbol{f}_{cen}$ can be calculated from $\boldsymbol{f}_{cen} = \frac{E(\boldsymbol{f}(\boldsymbol{x})\prec\boldsymbol{f}(\mathscr{P}_{\mathcal{S}})|\mathbf{R})}{\mathcal{P}(\boldsymbol{f}(\boldsymbol{x})\prec\boldsymbol{f}(\mathscr{P}_{\mathcal{S}})|\mathbf{R})}$. For any prediction that does not dominate the Pareto-front, the improvement is given by so called augmented improvement. With the evaluation of the integral for higher dimensional $\hat{\boldsymbol{f}}(\boldsymbol{x})$, this method can become cumbersome.

EI has been extended to targeted MOO simply as the product of all the EIs of each objective, given as

$$mEI(x|\mathbf{R}) = \prod_{\mathsf{i}}^{\mathsf{m}} EI_{\mathsf{i}}(\boldsymbol{x}|\mathsf{R}_{\mathsf{i}}) \tag{6.31}$$

This approach is computationally efficient for a targeted search, since it only deals with univariate distributions and hence, analytical evaluation of the criteria and gra-

[6] The multi-variate Gaussian prediction is obtained through defining a joint distribution of independent univariate Gaussian predictions from $\mathcal{GP}$ meta-models

dient is possible for many objectives. One of the main concerns with this approach is choosing the reference vector $\mathbf{R}$ considering the target which is presumed to be part of the true Pareto-front, and hence, the main emphasis of this approach is defining a proper $\mathbf{R}$ for the target. In fact this approach is equivalent to $EHVI$ under some hypothesis when $\mathbf{R}$ is also a non-dominated point. As a default, the preference to the reference value is given to the centre of the Pareto-front, where the centre is identified by the closest point in Eucledian measure on the Utopian-Nadir line. With the user provided aspiration point $\mathbf{R}_o$, $\mathbf{R}$ is adapted dynamically by projecting the closest point of the empirical Pareto-front to the broken line joining $\mathbf{R}_o$ to the Utopian and the Nadir point.

Another approach was introduced in [40, 89] where EI functions are treated as objectives and optimised in multi-objective context typically with MOEA algorithms like NSGA-2. The main advantage of this approach is that it is generic, since it preserves the generic characteristics of NSGA-2 and also the analytical evaluation of EI criterion. Further, the optimisation of EI functions with NSGA-2 results in Pareto-optimal solutions where it expresses optimality explicitly in the context of MOO. This is unlike the previous approaches where optimality is expressed with scalar value which does not provide much information in multi-objective context. This is efficient since we are dealing with Pareto-optimal set of solutions from which infill points can be chosen for diversity or targeted search, or even it provides the choice to scalarize with quality indicators. Constraints can also be handled easily as part of NSGA-2 based on ranking for degree of constraint violation or even completely removing the individuals violating constraints from the population and hence discouraging such individuals for future generations.

6.4.1 Multiple reference points strategy

The main drawback with this approach is defining a reference value for EI in the context of MOO, where typically Utopian or Nadir value is chosen as reference. With single objective, the definition of improvement with EI can be expressed with respect to a reference value $f(\boldsymbol{x}^+)$ as $EI(\boldsymbol{x}|f(\boldsymbol{x}^+))$, where $f(\boldsymbol{x}^+)$ typically corresponds to the Utopian value $f(\boldsymbol{x}^{++})$. While in the context of MOO, the Utopian value of a function to seek improvement can be unrealistic on some parts of the objective space. With MOO of EI functions, it should be noted that the idea of choosing a reference value independently for each EI function implicitly defines a reference point in multi-objective context, where we do not explicitly focus on the choice of reference point. As well-known, $EI(\boldsymbol{x}|f(\boldsymbol{x}^+))$ can be extended to MOO through $EHVI(\boldsymbol{x}|\boldsymbol{f}(\mathscr{P}_{\mathcal{S}}), \mathbf{R})$ where improvement for a multi-variate gaussian prediction $\hat{\boldsymbol{f}}(\boldsymbol{x})$ is defined with respect to the empirical Pareto-front $\boldsymbol{f}(\mathscr{P}_{\mathcal{S}})$ bounded by $\mathbf{R}$, rather than a specific reference value $f(\boldsymbol{x}^+)$. But the evaluation of integration to define $EHVI$ for a multi-variate gaussian prediction can be cumbersome for large number of objectives, while also the measure of improvement is purely expressed in scalar

value. Hence, we extend the work of Jeong by defining multiple reference values in the MOO of EI functions to define infill points for MOBO, also while preserving the generic characteristics of the approach. This means that instead of a single reference value, a given prediction can have its own reference value which is realistic to define improvement. This requires a precise definition for realistic reference value to seek improvement, for which we define in a probabilistic sense with the following explanation.

The MOO of EIs for $\underset{\boldsymbol{x}\in\mathcal{X}}{min}\, \boldsymbol{f}(\boldsymbol{x})$ can be defined as

$$\underset{\boldsymbol{x}\in\mathcal{X}}{max}\Big[\underset{minf_1(\boldsymbol{x})}{EI}(\boldsymbol{x}|f_1(\boldsymbol{x}^{1+}))\cdots\underset{minf_{\mathsf{m}}(\boldsymbol{x})}{EI}(\boldsymbol{x}|f_{\mathsf{m}}(\boldsymbol{x}^{\mathsf{m}+}))\Big] \tag{6.32}$$

We consider the perspective from a single-objective $max\, EI(\boldsymbol{x}|f_{\mathsf{i}}(\boldsymbol{x}^{\mathsf{i}+})$ in the above MOO, so as to detail the independent effect of defining a reference value $f_{\mathsf{i}}(\boldsymbol{x}^{\mathsf{i}+})$ for $max\, EI(\boldsymbol{x}|f_{\mathsf{i}}(\boldsymbol{x}^{\mathsf{i}+})$ in characterising the Pareto-optimal solutions. While a Pareto-front could be achieved with a single reference value $f_{\mathsf{i}}(\boldsymbol{x}^{\mathsf{i}+})$ for $max\, EI(\boldsymbol{x}|f_{\mathsf{i}}(\boldsymbol{x}^{\mathsf{i}+})$, the resolution to define improvement is only efficient for a subset of the decision space depending on the $\mathcal{GP}$ prediction relative to $f_{\mathsf{i}}(\boldsymbol{x}^{\mathsf{i}+})$. This can be seen through the following cases for $\underset{minf_{\mathsf{i}}(\boldsymbol{x})}{EI}$ [7] as follows:

$$\begin{aligned}
&\textbf{Case 1}: For\ \hat{\mu}_{\mathsf{i}}(\boldsymbol{x})\pm\hat{\sigma}_{\mathsf{i}}(\boldsymbol{x}) \gg f_{\mathsf{i}}(\boldsymbol{x}^{\mathsf{i}+}),\ \underset{minf_{\mathsf{i}}(\boldsymbol{x})}{EI}(\boldsymbol{x}|f_{\mathsf{i}}(\boldsymbol{x}^{\mathsf{i}+}))\approx 0\\
&\textbf{Case 2}: For\ \hat{\mu}_{\mathsf{i}}(\boldsymbol{x})\pm\hat{\sigma}_{\mathsf{i}}(\boldsymbol{x}) \ll f_{\mathsf{i}}(\boldsymbol{x}^{\mathsf{i}+}),\ \underset{minf_{\mathsf{i}}(\boldsymbol{x})}{EI}(\boldsymbol{x}|f_{\mathsf{i}}(\boldsymbol{x}^{\mathsf{i}+}))\approx f_{\mathsf{i}}(\boldsymbol{x}^{\mathsf{i}+})-\hat{\mu}_{\mathsf{i}}(\boldsymbol{x})
\end{aligned} \tag{6.33}$$

Case 1 shows that the choice of the Utopian value $f_{\mathsf{i}}(\boldsymbol{x}^{\mathsf{i}+})$ to seek improvement for a subset of $\boldsymbol{x}$ in the objective space where $\hat{\mu}_{\mathsf{i}}(\boldsymbol{x})\pm\hat{\sigma}_{\mathsf{i}}(\boldsymbol{x}) \gg f_{\mathsf{i}}(\boldsymbol{x}^{\mathsf{i}+})$ can have no probabilistic chance for improvement and hence, to seek for improvement in this case can be said as being too greedy. While this is insignificant in the context of single-objective optimization where these measures can be ignored, zero or infinitesimal values provide less resolution for comparison to define NDS for MOO.

Case 2 shows that the measure of improvement is simply given by distance between the prediction $\hat{\mu}_{\mathsf{i}}(\boldsymbol{x})$ and the reference value $f_{\mathsf{i}}(\boldsymbol{x}^{\mathsf{i}+})$, which can only be acceptable in cases where there is no realistic reference value to seek improvement. This is possible when choosing Nadir value as reference, which can be said as being too pessimistic for improvement. The pessimistic sense of seeking improvement can be seen as lack of risk for exploration in the parts of the objective space where $\hat{\mu}_{\mathsf{i}}(\boldsymbol{x})\pm\hat{\sigma}_{\mathsf{i}}(\boldsymbol{x}) \ll f_{\mathsf{i}}(\boldsymbol{x}^{\mathsf{i}+})$ and hence the absence of the uncertainty term $\hat{\sigma}_{\mathsf{i}}(\boldsymbol{x})$ in evaluating $\underset{minf_{\mathsf{i}}(\boldsymbol{x})}{EI}$. The above two cases show the limitations of using a single reference value for EI and hence, it can be efficient to define improvements locally in the objective space. The above

[7] The following cases are shown specifically for the case of $min\, f_{\mathsf{i}}(\boldsymbol{x})$, while for $max\, f_{\mathsf{i}}(\boldsymbol{x})$, the relations are inversed

cases are graphically shown in Fig. 6.1

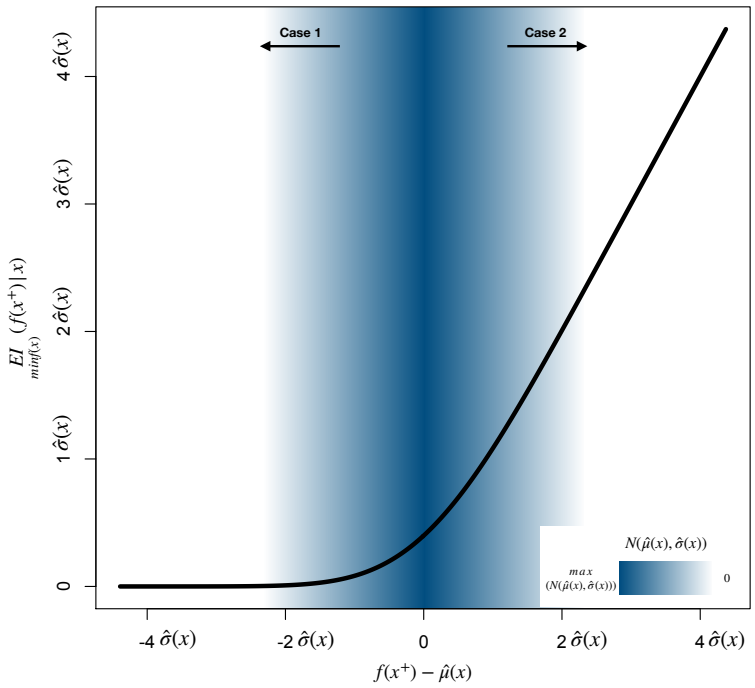

Figure 6.1: Variation of $\underset{minf(\boldsymbol{x})}{EI}(f(\boldsymbol{x}^+)|\boldsymbol{x})$ for change in reference value $f(\boldsymbol{x}^+)$

To avoid being too optimistic or pessimistic to define improvement, it can be said that for any two predictions $\hat{f}_\mathsf{i}$ and $\hat{f}_\mathsf{i}'$, with choosing a reference value for EI in the context of multi-objective optimisation, we can define the following properties,

- $\hat{\mu}_\mathsf{i} = \hat{\mu}_\mathsf{i}' \wedge \hat{\sigma}_\mathsf{i} > \hat{\sigma}_\mathsf{i}' \implies EI(\hat{f}_\mathsf{i}) > EI(\hat{f}_\mathsf{i}')$
- $\hat{\mu}_\mathsf{i} > \hat{\mu}_\mathsf{i}' \wedge \hat{\sigma}_\mathsf{i} = \hat{\sigma}_\mathsf{i}' \implies EI(\hat{f}_\mathsf{i}) > EI(\hat{f}_\mathsf{i}')$

We largely seek to achieve the above properties unless no suitable reference value can be defined. As a first thought, this can be overcome by choosing an appropriate reference value $f_\mathsf{i}(\boldsymbol{x}^{\mathsf{i}+})$ depending on the prediction $\hat{f}_\mathsf{i}(\boldsymbol{x})$. But choosing a reference value $f_\mathsf{i}(\boldsymbol{x}^{\mathsf{i}+})$ to define EI depending on where $\hat{f}_\mathsf{i}(\boldsymbol{x})$ lies in the objective space can make the improvements hard to be compared, since different predictions can have different definition of improvement depending on the choice of reference value. The comparison is also essential for defining NDS for optimization in the context of MOO. Hence, we augment the EI to have a common frame of reference for comparison, where we consider the axes of the objective space itself as the frame of reference for

comparison. The augmentation of EI with $f_{\mathsf{i}}(\boldsymbol{x}^{\mathsf{i}+})$ as reference value is given through the criterion expected value (EV)[8] as follows

$$\underset{minf_{\mathsf{i}}(\boldsymbol{x})}{EV}(\boldsymbol{x}|f_{\mathsf{i}}(\boldsymbol{x}^{\mathsf{i}+})) = f_{\mathsf{i}}(\boldsymbol{x}^{\mathsf{i}+}) - \underset{minf_{\mathsf{i}}(\boldsymbol{x})}{EI}(\boldsymbol{x}|f_{\mathsf{i}}(\boldsymbol{x}^{\mathsf{i}+})) \tag{6.34}$$

The definition of EV avoids the problem of comparing improvements with several reference values, but the above two cases take a different role for the EV criterion, given as

$$\begin{aligned} &\textbf{Case 1} : For\ \hat{\mu}_{\mathsf{i}}(\boldsymbol{x}) \pm \hat{\sigma}_{\mathsf{i}}(\boldsymbol{x}) \gg f_{\mathsf{i}}(\boldsymbol{x}^{\mathsf{i}+}),\ \underset{minf_{\mathsf{i}}(\boldsymbol{x})}{EV}(\boldsymbol{x}|f_{\mathsf{i}}(\boldsymbol{x}^{\mathsf{i}+})) \approx f_{\mathsf{i}}(\boldsymbol{x}^{\mathsf{i}+}) \\ &\textbf{Case 2} : For\ \hat{\mu}_{\mathsf{i}}(\boldsymbol{x}) \pm \hat{\sigma}_{\mathsf{i}}(\boldsymbol{x}) \ll f_{\mathsf{i}}(\boldsymbol{x}^{\mathsf{i}+}),\ \underset{minf_{\mathsf{i}}(\boldsymbol{x})}{EV}(\boldsymbol{x}|f_{\mathsf{i}}(\boldsymbol{x}^{\mathsf{i}+})) \approx \hat{\mu}_{\mathsf{i}}(\boldsymbol{x}) \end{aligned} \tag{6.35}$$

For **Case 1**, in the context of EI, the improvement becomes infinitesimal or zero for comparison. While in the context of EV, this leads to the problem of overestimation, where the value of EV becomes the reference value itself and hence, an unrealistic reference value can lead to overestimation of improvement. Similarly, the difference in context between EI and EV can be seen for **Case 2**, where EV simply converges to $\hat{\mu}(\boldsymbol{x})$. This means that two predictions with the same $\hat{\mu}(\boldsymbol{x})$ but different $\hat{\sigma}_{\mathsf{i}}(\boldsymbol{x})$ will have the same preference. The above cases are graphically shown in Fig. 6.2

We give the explanation in avoiding the above cases with EV criterion since it is much easier to work in the coordinates of the objective space. As defined before, **Case 1** can be avoided by seeking improvement with respect to a reference value which is more realistic for improvement rather than being too greedy. The realistic scope of improvement considering $f_{\mathsf{i}}(\boldsymbol{x}^{\mathsf{i}+})$ can be defined through the CDF : $\mathcal{P}(f_{\mathsf{i}}(\boldsymbol{x}) \leq f_{\mathsf{i}}(\boldsymbol{x}^{\mathsf{i}+}))$ for any $\mathcal{GP}$ outcome $\hat{f}_{\mathsf{i}}(\boldsymbol{x}) : \mathcal{N}(\hat{\mu}_{\mathsf{i}}(\boldsymbol{x}), \hat{\sigma}_{\mathsf{i}}(\boldsymbol{x}))$. We here remind that the given CDF is essentially the Probability of Improvement criterion (PI). Hence, the CDF constituting to zero for any reference value can be said as being too greedy for improvement, where there can be a limit set for the CDF measure to be considered with compromise on greed. The limit could be set in terms of $\hat{\mu}_{\mathsf{i}}(\boldsymbol{x}) - \epsilon\hat{\sigma}_{\mathsf{i}}(\boldsymbol{x})$[9] where we seek for $\mathcal{P}(f_{\mathsf{i}}(\boldsymbol{x}) \leq f_{\mathsf{i}}(\boldsymbol{x}^{\mathsf{i}+})) \geq \mathcal{P}(f_{\mathsf{i}}(\boldsymbol{x}) \leq \hat{\mu}_{\mathsf{i}}(\boldsymbol{x}) - \epsilon\hat{\sigma}_{\mathsf{i}}(\boldsymbol{x}))$, with ϵ being the parameter to be defined. A higher value of ϵ means higher the greed to seek improvement, but the balance to set the limit could be otherwise seen as the acceptable risk that can be considered for exploration. The higher risk with considering higher value of ϵ for $\hat{\mu}_{\mathsf{i}}(\boldsymbol{x}) - \epsilon\hat{\sigma}_{\mathsf{i}}(\boldsymbol{x})$ may reap higher benefits but this could be otherwise, since there is equal probability for $f_{\mathsf{i}}(\boldsymbol{x}) \geq \hat{\mu}_{\mathsf{i}}(\boldsymbol{x}) + \epsilon\hat{\sigma}_{\mathsf{i}}(\boldsymbol{x})$. Hence, this requires the right

[8] We here remind that the expected value can also be otherwise defined as $E(\hat{f}(\boldsymbol{x}))$ in the interval $(-\infty, f(\boldsymbol{x}^{++})]$ (detailed in (6.21)) contrary to EI which is defined as $E(f(\boldsymbol{x}^{++}) - \hat{f}(\boldsymbol{x}))$, but considering $E(\hat{f}(\boldsymbol{x}))$ leads to similar properties as EI in comparing with several reference values

[9] We give the relation in terms of LCB, since for any $f(\boldsymbol{x}^{+}) : \mathcal{P}(f(\boldsymbol{x}) \leq f(\boldsymbol{x}^{+})) \geq \mathcal{P}(f(\boldsymbol{x}) \leq \hat{\mu}(\boldsymbol{x}) - \epsilon\hat{\sigma}(\boldsymbol{x}))$, the following relation holds $f(\boldsymbol{x}^{+}) \geq \hat{\mu}(\boldsymbol{x}) - \epsilon\hat{\sigma}(\boldsymbol{x})$

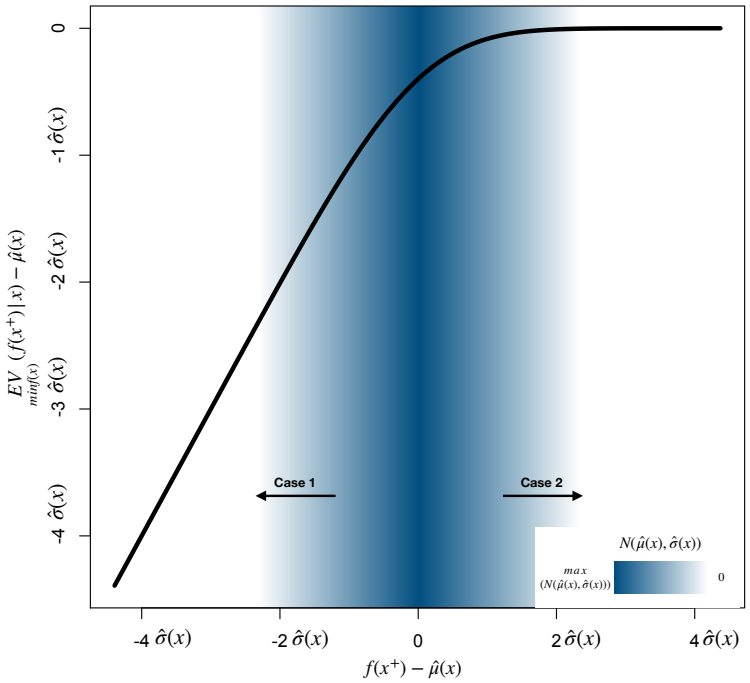

Figure 6.2: Variation of $\underset{min f(\boldsymbol{x})}{EV}(f(\boldsymbol{x}^+)|\boldsymbol{x})$ for change in reference value $f(\boldsymbol{x}^+)$

balance for the choice of ϵ with acceptable risk for exploration.

For MOO, the most feasible improvement that we can look for is with respect to the empirical Pareto-front $f_{\mathrm{i}}(\mathscr{P}_{\mathcal{S}}) := \{f_{\mathrm{i}}(\boldsymbol{p}_1), f_{\mathrm{i}}(\boldsymbol{p}_2), \ldots, f_{\mathrm{i}}(\boldsymbol{p}_{(.)})\}$ of the observed samples. But, there can be multiple $\boldsymbol{p}_{\mathrm{i}} : f_{\mathrm{i}}(\boldsymbol{p}_{\mathrm{i}}) \leq \hat{\mu}_{\mathrm{i}}(\boldsymbol{x}) - \epsilon\hat{\sigma}_{\mathrm{i}}(\boldsymbol{x})$, where we choose the $\boldsymbol{p}_{\mathrm{i}}$ which gives the minimum value of $\underset{min f_{\mathrm{i}}(\boldsymbol{x})}{EV}$. The choice of the minimum value of $\underset{min f_{\mathrm{i}}(\boldsymbol{x})}{EV}$ for a function to be minimised averts **Case 2** which defines the pessimistic choice of reference value, unless it is not possible when no suitable reference value exists. In overall, the above definitions provide the balance between greed and being pessimistic for improvement through the parameter ϵ. The above definitions could be expressed as follows

$$\begin{aligned} \underset{min\, f_{\mathrm{i}}(\boldsymbol{x})}{EV}(\boldsymbol{x}|\mathscr{P}_{\mathcal{S}}, \epsilon) = \underset{\boldsymbol{p}_{\mathrm{i}} \in \mathscr{P}_s}{min}\,(\underset{min f_{\mathrm{i}}(\boldsymbol{x})}{EV}(f_{\mathrm{i}}(\boldsymbol{p}_{\mathrm{i}})|\boldsymbol{x})) \\ \mathscr{P}_s := \{f_{\mathrm{i}}(\boldsymbol{p}_{\mathrm{i}}) \geq \hat{\mu}_{\mathrm{i}}(\boldsymbol{x}) - \epsilon\hat{\sigma}_{\mathrm{i}}(\boldsymbol{x}), \forall \boldsymbol{p}_{\mathrm{i}} \in \mathscr{P}_{\mathcal{S}}\} \end{aligned} \tag{6.36}$$

where the discrete optimisation of $\underset{\boldsymbol{p}_{\mathrm{i}} \in \mathscr{P}_s}{min}\,(\underset{min f_{\mathrm{i}}(\boldsymbol{x})}{EV}(f_{\mathrm{i}}(\boldsymbol{p}_{\mathrm{i}})|\boldsymbol{x}))$ can be implicitly satisfied through defining NDS with $\underset{min\, f_{\mathrm{i}}(\boldsymbol{x})}{EV}(\boldsymbol{x}|\mathscr{P}_{\mathcal{S}}, \epsilon)$, though it may not be a good strategy. Alternatively, from the nature of proportionality for $\underset{min f_{\mathrm{i}}(\boldsymbol{x})}{EV}(f_{\mathrm{i}}(\boldsymbol{p}_{\mathrm{i}})|\boldsymbol{x})) \propto f_{\mathrm{i}}(\boldsymbol{p}_{\mathrm{i}})$, shown

in Fig. 6.2, the most suitable reference value $f_{\mathsf{i}}(\boldsymbol{p}_{\mathsf{i}}^{\star})$ to achieve $\underset{\boldsymbol{p}_{\mathsf{i}}\in\mathscr{P}_s}{min}(\underset{min f_{\mathsf{i}}(\boldsymbol{x})}{EV}(f_{\mathsf{i}}(\boldsymbol{p}_{\mathsf{i}})|\boldsymbol{x}))$ can be simply given as $f(\boldsymbol{p}_{\mathsf{i}}^{\star}) = \underset{\boldsymbol{p}_{\mathsf{i}}\in\mathscr{P}_s}{min} f(\boldsymbol{p}_{\mathsf{i}})$. In short, we define the Eq. (6.36) as EV criterion for the following discussions. In the scope of achieving diversity, for any prediction $\hat{f}_{\mathsf{i}} : \hat{\mu}_{\mathsf{i}}(\boldsymbol{x}) - \epsilon\hat{\sigma}_{\mathsf{i}}(\boldsymbol{x}) > max\, f_{\mathsf{i}}(\mathscr{P}_{\mathcal{S}})$, EV criterion can be adapted as follows $\underset{max f_{\mathsf{i}}(\boldsymbol{x})}{EV}(\boldsymbol{x}|max\, f_{\mathsf{i}}(\mathscr{P}_{\mathcal{S}})) = max\, f_{\mathsf{i}}(\mathscr{P}_{\mathcal{S}}) + \underset{max f_{\mathsf{i}}(\boldsymbol{x})}{EI}(\boldsymbol{x}|max\, f_{\mathsf{i}}(\mathscr{P}_{\mathcal{S}}))$, where the goal is to extend the Pareto-front beyond the inferred Nadir value.

The given definitions allow to define EV criterion in the place of EI, where the problem (6.32) can be defined as follows

$$\underset{\boldsymbol{x}\in\mathcal{X}}{min}\Big[\underset{min\, f_1(\boldsymbol{x})}{EV}(\boldsymbol{x}|\mathscr{P}_{\mathcal{S}},\epsilon)\cdots\underset{min\, f_{\mathsf{m}}(\boldsymbol{x})}{EV}(\boldsymbol{x}|\mathscr{P}_{\mathcal{S}},\epsilon)\Big] \tag{6.37}$$

The MOO can be achieved through NSGA-2, which leads to Pareto-optimal solutions $\mathscr{P}_{\hat{\mathcal{S}}}$. The independent definition of improvement allows to work with only univariate Gaussian distributions and hence, large number of EV criteria can be optimised with relatively ease with a robust multi-objective optimisation tool.

The choice of $f_{\mathsf{i}}(\boldsymbol{p}_{\mathsf{i}}) \in f_{\mathsf{i}}(\mathscr{P}_{\mathcal{S}})$ independently for each $\underset{min\, f_{\mathsf{i}}(\boldsymbol{x})}{EV}(\boldsymbol{x}|\mathscr{P}_{\mathcal{S}},\epsilon)$ means that it can implicitly lead to choosing a reference point $\boldsymbol{g}_o := [f_1(\boldsymbol{p}_{\mathsf{i}}) \in f_1(\mathscr{P}_{\mathcal{S}})\cdots f_{\mathsf{m}}(\boldsymbol{p}_{\mathsf{i}}) \in f_{\mathsf{m}}(\mathscr{P}_{\mathcal{S}})] \in \mathbb{R}^{\mathsf{m}}$ [10] [11] from a grid of points $\mathscr{G} := \{f_1(\mathscr{P}_{\mathcal{S}})\times\cdots\times f_{\mathsf{m}}(\mathscr{P}_{\mathcal{S}})\}$. This means that $\boldsymbol{f}(\mathscr{P}_{\mathcal{S}}) \subset \mathscr{G}$, where $\mathscr{G}$ also contains points dominating or be dominated by points in the set $\boldsymbol{f}(\mathscr{P}_{\mathcal{S}})$, which includes the Utopian point: $\boldsymbol{g}_{\mathsf{o}} \preceq \boldsymbol{f}(\mathscr{P}_{\mathcal{S}})$ and the Nadir point: $\forall \mathsf{i}, \boldsymbol{f}(\boldsymbol{p}_{\mathsf{i}}) \preceq \boldsymbol{g}_{\mathsf{o}}$. The idea of defining improvement $\mathscr{I}_{\boldsymbol{f}(\boldsymbol{p}_{\mathsf{i}})} \in \mathfrak{I}_{\boldsymbol{f}(\boldsymbol{p}_{\mathsf{i}})}$ [12] (Fig. 6.3) is apparent, where the intention is to dominate a given empirical Pareto-front point $\boldsymbol{f}(\boldsymbol{p}_{\mathsf{i}}) \in \boldsymbol{f}(\mathscr{P}_{\mathcal{S}})$. But the implicit definition of a reference point $\boldsymbol{g}_o \in \mathscr{G}$ means that improvements cannot only be defined to dominate $\boldsymbol{f}(\boldsymbol{p}_{\mathsf{i}})$, but multiple Pareto-front points in the set $\boldsymbol{f}(\mathscr{P}_{\mathcal{S}})$, where the ideal goal for domination would be the Utopian point.

With population based evolutionary strategy of NSGA-2, for a given population, the optimisation is simultaneously defined with several reference points in the objective space and hence, individuals in a given generation of NSGA-2 are defined with their respective reference point. Since the improvements are defined as expected values EV in the objective space, comparison can be made to define non-dominated sorting and niching operations. This implicitly models optimisating set of EI functions: $\left\{\underset{\boldsymbol{x}\in\mathcal{X}_{\boldsymbol{g}_1}}{max}\Big[\underset{minf_1(\boldsymbol{x})}{EI}\ \cdots\ \underset{minf_{\mathsf{m}}(\boldsymbol{x})}{EI}\Big]\cdots\underset{\boldsymbol{x}\in\mathcal{X}_{\boldsymbol{g}_{(.)}}}{max}\Big[\underset{minf_1(\boldsymbol{x})}{EI}\ \cdots\ \underset{minf_{\mathsf{m}}(\boldsymbol{x})}{EI}\Big]\right\}$ [13] in the objective

[10] It should be noted that the choice of $\boldsymbol{p}_{\mathsf{i}}$ is independent for each f_{i}

[11] $\boldsymbol{g}_{\mathsf{o}}$ is an arbitrary point in $\mathscr{G}$ with index o

[12] $\mathscr{I}_{\boldsymbol{f}^*}(\boldsymbol{x}) \in \mathfrak{I}_{\boldsymbol{f}^*} = \Big\{\Big[\underset{min\, f_1(\boldsymbol{x})}{EV}(\boldsymbol{x}|f_1^*)\cdots\underset{min\, f_{\mathsf{m}}(\boldsymbol{x})}{EV}(\boldsymbol{x}|f_{\mathsf{m}}^*)\Big]|\forall \mathsf{i}, f_{\mathsf{i}}^* = \underset{\boldsymbol{p}_{\mathsf{i}}\in\mathscr{P}_s}{min} f_{\mathsf{i}}(\boldsymbol{p}_{\mathsf{i}}), \boldsymbol{x} \in \mathcal{X}\Big\}$, $\boldsymbol{f}^* = [f_1^*\cdots f_{\mathsf{m}}^*]$

[13] $\mathcal{X}_{\boldsymbol{g}_o} = \{\boldsymbol{x}|\mathscr{I}_{\boldsymbol{g}_o}(\boldsymbol{x}) \in \mathfrak{I}_{\boldsymbol{g}_o}, \boldsymbol{x}\in\mathcal{X}\}$

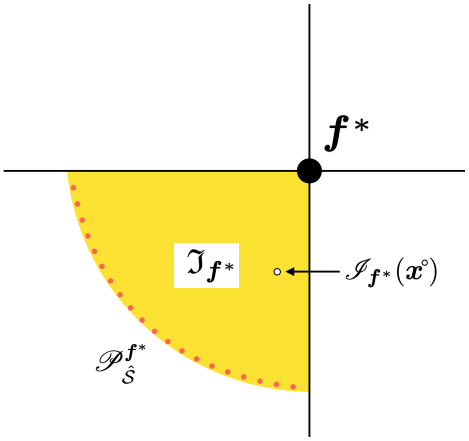

Figure 6.3: Illustration of the set $\mathfrak{I}_{f*}$ and its associated subsets

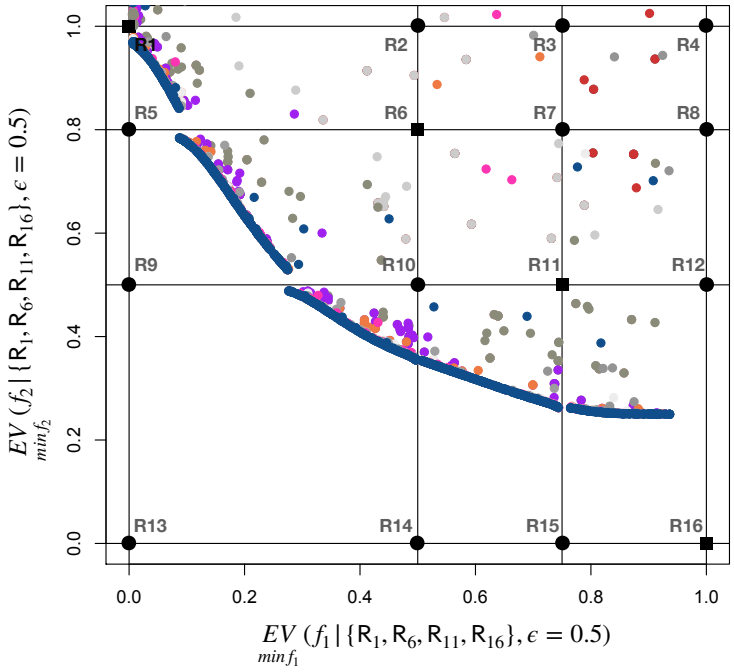

Figure 6.4: An example for optimization of EV

space, with each element: $\underset{\boldsymbol{x}\in\mathcal{X}_{\boldsymbol{g}_o}}{max}\left[\underset{minf_1(\boldsymbol{x})}{EI}\ \cdots\ \underset{minf_{\mathsf{m}}(\boldsymbol{x})}{EI}\right]$ in the set defined with a unique reference point $\boldsymbol{g}_o$, illustrated in Fig.6.5.

An example for the optimisation of (6.37) is shown in Fig. 6.4, for a simple MOO test functions set: ZDT1 of two dimensions ($\mathsf{m}=2$). In this case, $\boldsymbol{f}(\mathscr{P}_{\mathcal{S}}) = \{\mathbf{R}_1, \mathbf{R}_6, \mathbf{R}_{11}, \mathbf{R}_{16}\}$, $\mathscr{G} = \{\mathbf{R}_1, \cdots, \mathbf{R}_{16}\} := \{\mathbf{R}_1 \times \mathbf{R}_6 \times \mathbf{R}_{11} \times \mathbf{R}_{16}\}$. The Pareto front $\boldsymbol{f}(\mathscr{P}_{\hat{\mathcal{S}}})$ is defined by the reference points $\mathbf{R}_2, \mathbf{R}_6, \mathbf{R}_{10}, \mathbf{R}_{11}, \mathbf{R}_{16}$, where two of the reference points $\mathbf{R}_6$ and $\mathbf{R}_{11}$ belong to $\mathscr{P}_{\mathcal{S}}$. This means that $\mathscr{I}_{\mathbf{R}_6} \in \mathfrak{I}_{\mathbf{R}_6}$ and $\mathscr{I}_{\mathbf{R}_{11}} \in \mathfrak{I}_{\mathbf{R}_{11}}$ independently define domination over $\mathbf{R}_6$ and $\mathbf{R}_{11}$ respectively, as $\mathscr{I}_{\mathbf{R}_6} \preceq \mathbf{R}_6$ and $\mathscr{I}_{\mathbf{R}_{11}} \preceq \mathbf{R}_{11}$. For $\mathbf{R}_{10}$, something interesting happens, where $\mathbf{R}_{10} \notin \mathscr{P}_{\mathcal{S}}$ but is purely an outcome of the implicit definition of grid $\mathscr{G}$. In this case, $\mathbf{R}_{10} \preceq \{\mathbf{R}_6, \mathbf{R}_{11}\}$, hence also $\mathscr{I}_{\mathbf{R}_{10}} \preceq \{\mathbf{R}_6, \mathbf{R}_{11}\}$, i.e., any improvement $\mathscr{I}_{\mathbf{R}_{10}} \in \mathfrak{I}_{\mathbf{R}_{10}}$ can dominate the two Pareto-front points $\mathbf{R}_6$ and $\mathbf{R}_{11}$. Hence, $\mathscr{G}$ consists of reference points to define improvement with respect to any $\boldsymbol{f}(\boldsymbol{p}_{\mathsf{i}})$ or combination of several $\boldsymbol{f}(\boldsymbol{p}_{\mathsf{i}}) \in \boldsymbol{f}(\mathscr{P}_{\mathcal{S}})$. $\mathscr{G}$ also contains points $\boldsymbol{g}_{\mathsf{o}} : \boldsymbol{f}(\mathscr{P}_{\mathcal{S}}) \preceq \boldsymbol{g}_{\mathsf{o}}$ where improvement defined with such points are essential in guiding the solutions to define $\mathscr{P}_{\hat{\mathcal{S}}}$. The reference points $\mathbf{R}_2$ and $\mathbf{R}_{12}$ are also weakly dominated by the points in the set $\boldsymbol{f}(\mathscr{P}_{\mathcal{S}})$, where in this case, $\mathscr{I}_{\mathbf{R}_2}$ defines improvement intermediate between $\mathbf{R}_1$ and $\mathbf{R}_6$, and similarly, $\mathscr{I}_{\mathbf{R}_{12}}$ defines improvement intermediate between $\mathbf{R}_{11}$ and $\mathbf{R}_{16}$. In this example, the Utopian point corresponds to $\mathbf{R}_{12} \preceq \boldsymbol{f}(\mathscr{P}_{\mathcal{S}})$ and the Nadir point corresponds to $\mathbf{R}_4$, where all the points in $\mathscr{G}$ dominates $\mathbf{R}_4$.

Once $\mathscr{P}_{\hat{\mathcal{S}}}$ is obtained optimising Eq. (6.37) with NSGA-2, the problem leads to choosing infill points among $\mathscr{P}_{\hat{\mathcal{S}}}$. For the ease of following explanations, we can define a set $\mathscr{G}_{\mathscr{P}_{\hat{\mathcal{S}}}} := \{\boldsymbol{g}_o | \{\mathfrak{I}_{\boldsymbol{g}_o} \cap \boldsymbol{f}(\mathscr{P}_{\hat{\mathcal{S}}})\} \neq \emptyset, \boldsymbol{g}_o \in \mathscr{G}\}$. Firstly, we discuss the preference of choosing $\mathscr{I}_{\boldsymbol{g}_o} \in \mathfrak{I}_{\boldsymbol{g}_o} | \boldsymbol{g}_o \in \mathscr{G}_{\mathscr{P}_{\hat{\mathcal{S}}}}$ since . The part of $\boldsymbol{f}(\mathscr{P}_{\hat{\mathcal{S}}})$ defined by $\boldsymbol{g}_o$ as reference value can hence be expressed as $\boldsymbol{f}(\mathscr{P}_{\hat{\mathcal{S}}}^{\boldsymbol{g}_o}) = \{\mathfrak{I}_{\boldsymbol{g}_o} \cap \boldsymbol{f}(\mathscr{P}_{\hat{\mathcal{S}}})\}$, where the choice of an infill point in the set $\mathfrak{I}_{\boldsymbol{g}_o}$ can be narrowed down to choosing a point $\mathscr{I}_{\boldsymbol{g}_o} \in \boldsymbol{f}(\mathscr{P}_{\hat{\mathcal{S}}}^{\boldsymbol{g}_o})$. A suitable measure to quantify $\mathscr{I}_{\boldsymbol{g}_o}$ with respect to $\boldsymbol{g}_o$ can be given through hypervolume metric as

$$HVI(\mathscr{I}_{\boldsymbol{g}_o} | \boldsymbol{g}_o) = \prod_{\mathsf{i}=1}^{\mathsf{m}} f_{\mathsf{i}}^* - \underset{min\ f_{\mathsf{i}}(\boldsymbol{x})}{EV}(\boldsymbol{x} | f_{\mathsf{i}}^*) \tag{6.38}$$

where the calculation of HVI is simply given by product of EI in each objective, since $f_{\mathsf{i}}^* - \underset{min\ f_{\mathsf{i}}(\boldsymbol{x})}{EV}(\boldsymbol{x} | f_{\mathsf{i}}^*) = \underset{min\ f_{\mathsf{i}}(\boldsymbol{x})}{EI}(\boldsymbol{x} | f_{\mathsf{i}}^*)$, which is analytical irrespective of the dimensions. In this case, $HVI(\mathscr{I}_{\boldsymbol{g}_o} | \boldsymbol{g}_o)$ is equivalent to $EHVI(\boldsymbol{x} | \boldsymbol{g}_o)$ which is also similar to mEI. Hence, the most suitable choice of $\mathscr{I}_{\boldsymbol{g}_o} \in \boldsymbol{f}(\mathscr{P}_{\hat{\mathcal{S}}}^{\boldsymbol{g}_o})$ is which maximises $HVI(\mathscr{I}_{\boldsymbol{g}_o} | \boldsymbol{g}_o)$, expressed as $\underset{\mathscr{I}_{\boldsymbol{g}_o}\in\mathfrak{I}_{\boldsymbol{g}_o}}{max}\ HVI(\mathscr{I}_{\boldsymbol{g}_o} | \boldsymbol{g}_o)$[14].

[14] $\underset{\mathscr{I}_{\boldsymbol{g}_o}\in\mathfrak{I}_{\boldsymbol{g}_o}}{max}\ HVI(\mathscr{I}_{\boldsymbol{g}_o} | \boldsymbol{g}_o) = \underset{\mathscr{I}_{\boldsymbol{g}_o}\in\boldsymbol{f}(\mathscr{P}_{\hat{\mathcal{S}}}^{\boldsymbol{g}_o})}{max}\ HVI(\mathscr{I}_{\boldsymbol{g}_o} | \boldsymbol{g}_o)$

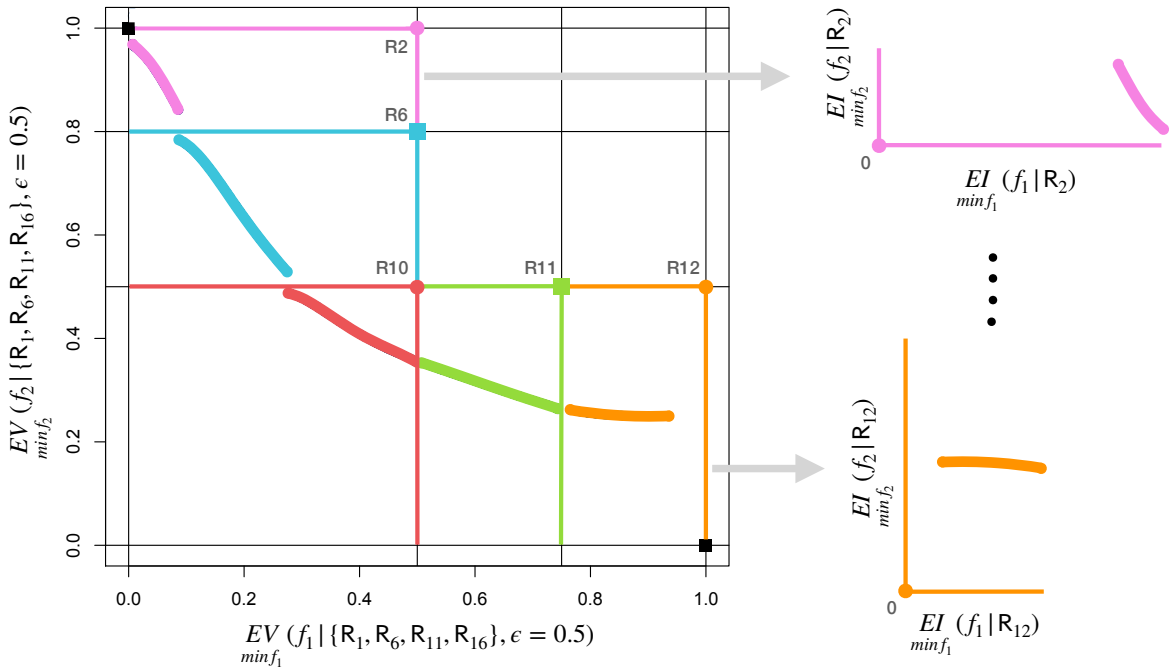

Figure 6.5: Interpretation of optimising EV criterion as multiple EI criteria with distinct reference points

The definition of $\boldsymbol{f}(\mathscr{P}_{\hat{\mathcal{S}}})$ with respect to several reference points makes it suitable for multipoint selection, where a point can be selected from $\mathfrak{I}_{\boldsymbol{g}_o} \forall \boldsymbol{g}_o \in \mathscr{G}_{\mathscr{P}_{\hat{\mathcal{S}}}}$ with $\underset{\mathscr{I}_{\boldsymbol{g}_o} \in \mathfrak{I}_{\boldsymbol{g}_o}}{max}\ HVI(\mathscr{I}_{\boldsymbol{g}_o}|\boldsymbol{g}_o)$. This can be impractical for parallelization, since typically the size of $\mathscr{G}_{\mathscr{P}_{\hat{\mathcal{S}}}}$ can grow rapidly and also the improvement with respect to some points can be very low to bring any considerable HVI. But to make choice among $g_o \in \mathscr{G}_{\mathscr{P}_{\hat{\mathcal{S}}}}$ for a limited number of parallelisation requires definition of improvement with respect to $\boldsymbol{f}(\mathscr{P}_{\mathcal{S}})$. The choice of $\underset{\mathscr{I}_{\boldsymbol{g}_o} \in \mathfrak{I}_{\boldsymbol{g}_o}}{max}\ HVI(\mathscr{I}_{\boldsymbol{g}_o}|\boldsymbol{g}_o)$ expresses the best HVI with respect to $\boldsymbol{g}_o$, but it makes no relation of HVI relative to $\boldsymbol{f}(\mathscr{P}_{\mathcal{S}})$. While HVI relative to $\boldsymbol{f}(\mathscr{P}_{\mathcal{S}})$ can simply be expressed as $HVI(\mathscr{I}|\boldsymbol{f}(\mathscr{P}_{\mathcal{S}}), \mathbf{R})$[15], this is quite an expensive strategy to pick an infill point from $\mathscr{P}_{\hat{\mathcal{S}}}$, since this requires evaluation of $HVI(\mathscr{I}|\boldsymbol{f}(\mathscr{P}_{\mathcal{S}}), \mathbf{R})$ for all $\mathscr{I} \in \mathscr{P}_{\hat{\mathcal{S}}}$. But with the edge of defining $\mathscr{I}$ with respect to a reference value $\boldsymbol{g}_o$ as $\mathscr{I}_{\boldsymbol{g}_o}$, it can be said that the relation of $\mathscr{I}_{\boldsymbol{g}_o}$ with respect to $\boldsymbol{f}(\mathscr{P}_{\mathcal{S}})$ can be defined by counting the $HVI(\boldsymbol{g}_o|\boldsymbol{f}(\mathscr{P}_{\mathcal{S}}), \mathbf{R})$ with $HVI(\mathscr{I}_{\boldsymbol{g}_o}|\boldsymbol{g}_o)$, expressed as

$$HVI_{\uplus}(\mathscr{I}_{\boldsymbol{g}_o}|\boldsymbol{f}(\mathscr{P}_{\mathcal{S}}), \mathbf{R}) = HVI(\mathscr{I}_{\boldsymbol{g}_o}|\boldsymbol{g}_o) + HVI(\boldsymbol{g}_o|\boldsymbol{f}(\mathscr{P}_{\mathcal{S}}), \mathbf{R}) \tag{6.39}$$

The idea is that instead of defining $HVI(\mathscr{I}|\boldsymbol{f}(\mathscr{P}_{\mathcal{S}}), \mathbf{R})$ for all $\mathscr{I} \in \mathscr{P}_{\hat{\mathcal{S}}}$, the computation of higher complexity $HVI((.)|\boldsymbol{f}(\mathscr{P}_{\mathcal{S}}), \mathbf{R})$ is limited to the reference points $\boldsymbol{g}_o \in \mathscr{G}_{\mathscr{P}_{\hat{\mathcal{S}}}}$. Hence, with the definition of $HVI((.)|\boldsymbol{f}(\mathscr{P}_{\mathcal{S}}), \mathbf{R})$ for a $\boldsymbol{g}_o \in \mathscr{G}_{\mathscr{P}_{\hat{\mathcal{S}}}}$, the definition of HVI for any improvement $\mathscr{I}_{\boldsymbol{g}_o} \in \mathfrak{I}_{\boldsymbol{g}_o}$ is given by product relation in (6.38). For sequential selection, the infill point from $\mathscr{P}_{\hat{\mathcal{S}}}$ to define the maximum HVI relative to $\boldsymbol{f}(\mathscr{P}_{\mathcal{S}})$ can be expressed as

$$\boldsymbol{x}^{\iota} = \underset{\boldsymbol{x} \in \mathcal{X}}{arg\,max}\Big\{HVI_{\uplus}(\mathscr{I}_{\boldsymbol{g}_o}(\boldsymbol{x})|\boldsymbol{f}(\mathscr{P}_{\mathcal{S}}), \mathbf{R})|\boldsymbol{g}_o \in \mathscr{G}_{\mathscr{P}_{\hat{\mathcal{S}}}}, \boldsymbol{x} \in \mathcal{X}\Big\} \tag{6.40}$$

For v multipoint selection, given that number of points in the set $\mathscr{G}_{\mathscr{P}_{\hat{\mathcal{S}}}}$ is greater than v, the first v maximum in the set: $\Big\{\underset{\mathscr{I}_{\boldsymbol{g}_o} \in \mathfrak{I}_{\boldsymbol{g}_o}}{max}\ HVI_{\uplus}(\mathscr{I}_{\boldsymbol{g}_o}|\boldsymbol{f}(\mathscr{P}_{\mathcal{S}}), \mathbf{R}), \boldsymbol{g}_o \in \mathscr{G}_{\mathscr{P}_{\hat{\mathcal{S}}}}\Big\}$ can be chosen. Choosing $\underset{\mathscr{I}_{\boldsymbol{g}_o} \in \mathfrak{I}_{\boldsymbol{g}_o}}{max}\ HVI_{\uplus}(\mathscr{I}_{\boldsymbol{g}_o}|\boldsymbol{f}(\mathscr{P}_{\mathcal{S}}), \mathbf{R})$ with respect to each reference point can implicitly achieve diversity. But to be even more specific with diversity, $\mathscr{P}_{\hat{\mathcal{S}}}$ can be clustered through K-means and a point can be sampled from each cluster for $max\, HVI_{\uplus}(\mathscr{I}|\boldsymbol{f}(\mathscr{P}_{\mathcal{S}})$, such that points sampled from each cluster are defined by unique reference points. If points sampled from different cluster share the same reference point, then in this case, a different mechanism has to be adapted to sample more than one point with respect to a given reference point, which we do not focus here.

The other simple approach can be defined also by clustering improvements in $\mathscr{P}_{\hat{\mathcal{S}}}$ through K-means and a point can be sampled from each cluster considering uncertainty, given by sum of uncertainty of the $\mathcal{GP}$ models. Hence, this strategy tries to reduce uncertainty on the $\mathcal{GP}$ meta-models for the points in $\mathscr{P}_{\hat{\mathcal{S}}}$, rather than to seek

[15] $\mathscr{I}$ is an arbitrary improvement point where we do not focus on the reference point with which it is defined, contrary to $\mathscr{I}_{\boldsymbol{g}_o}$

improvement through quality indicators. But care should be taken, since adjacent points between adjacent clusters can have the same measure of uncertainty and hence can lead to samples for parallelization from the same part of the design space.

Effect of ϵ in choosing reference values

We show the effect of ϵ through the following plots, where the idea is to show the behaviour for a range of predictions. The range is defined for $\hat{\mu}(\boldsymbol{x}) \in [50, 200]$, distinguished with color scale and $\hat{\sigma}(\boldsymbol{x}) \in [5, 50]$ defined on the vertical axis. The horizontal axis defines the EV criteria with four possible reference values $\{62.5, 75, 100, 150\}$ to choose for any prediction. Firstly, to have a general idea, we give the plot of $\hat{\mu}(\boldsymbol{x})$ against $\hat{\sigma}(\boldsymbol{x})$.

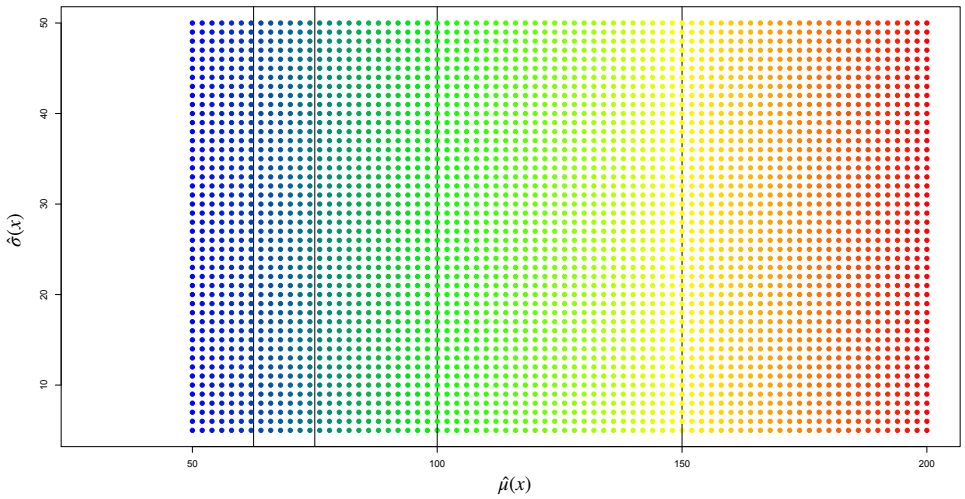

Figure 6.6: Plot of $\hat{\mu}(\boldsymbol{x})$ against $\hat{\sigma}(\boldsymbol{x})$

As it can be seen in Fig.6.6, a property in 6.4.1 cannot be achieved with choosing $\hat{\mu}(\boldsymbol{x})$ for improvement since $\hat{\mu}_{\mathsf{i}} = \hat{\mu}_{\mathsf{i}}{}' \wedge \hat{\sigma}_{\mathsf{i}} > \hat{\sigma}_{\mathsf{i}}{}' \implies EI(\hat{f}_{\mathsf{i}}) \not> EI(\hat{f}_{\mathsf{i}}')$. With EV criterion, as shown in Figs. 6.4.1,6.4.1, the properties are satisfied. It should be that, ϵ only influences the choice of reference value but not the magnitude of improvement. Nevertheless, the role of ϵ in choosing a reference value implicit effect in defining improvement. From the discontinuities, it can be observed that for lower ϵ values, the points were pessimistic in choosing its respective reference value, where the points became more optimistic with higher values of ϵ. This can be inferred with the reference value 62.5, where for any given $\hat{\sigma}_{\mathsf{i}}$ more points were considered as ϵ increases. It should be noted that as ϵ increases, only choice of the reference value changes. This can be better observed with the blue points which are largely defined by 62.5 as reference value, is nearly unchanging for any value of ϵ.

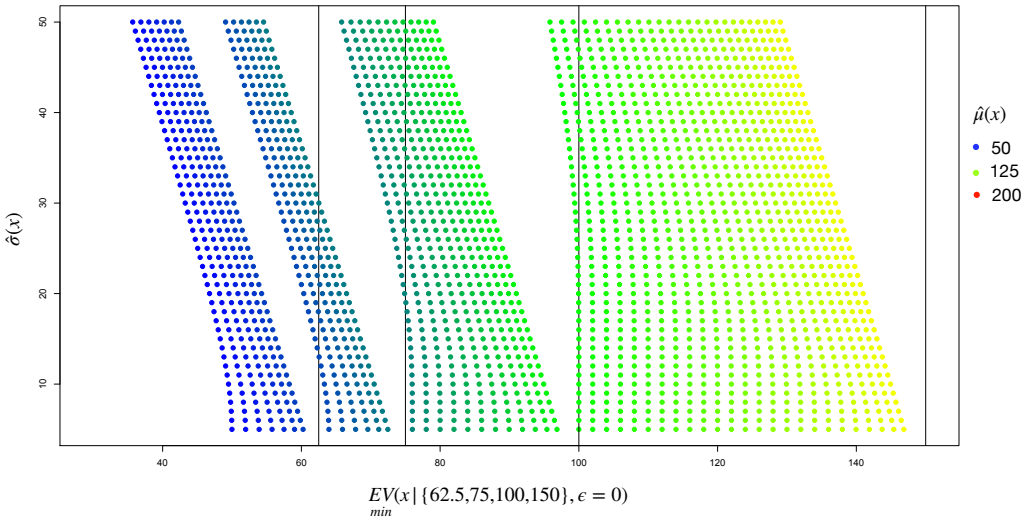

(a) $\epsilon = 0$

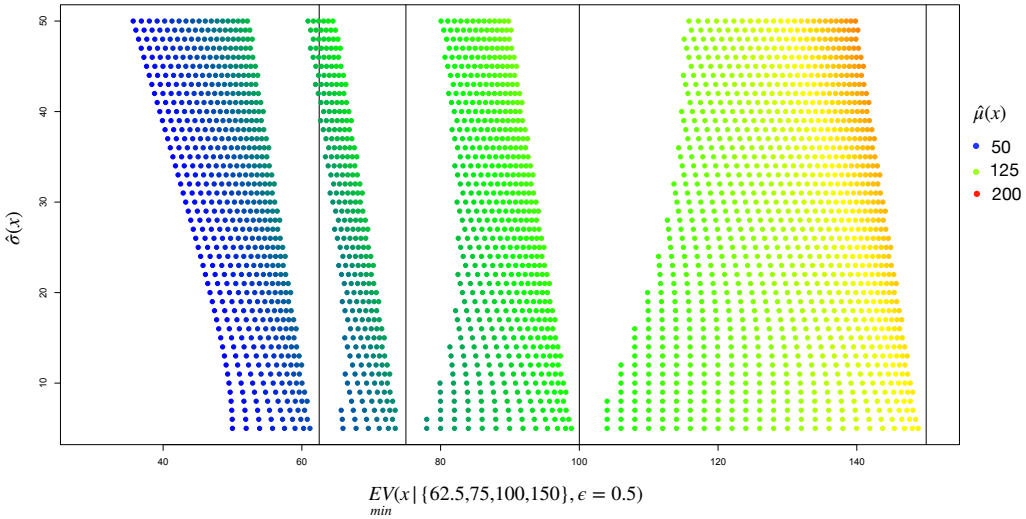

(b) $\epsilon = 0.5$

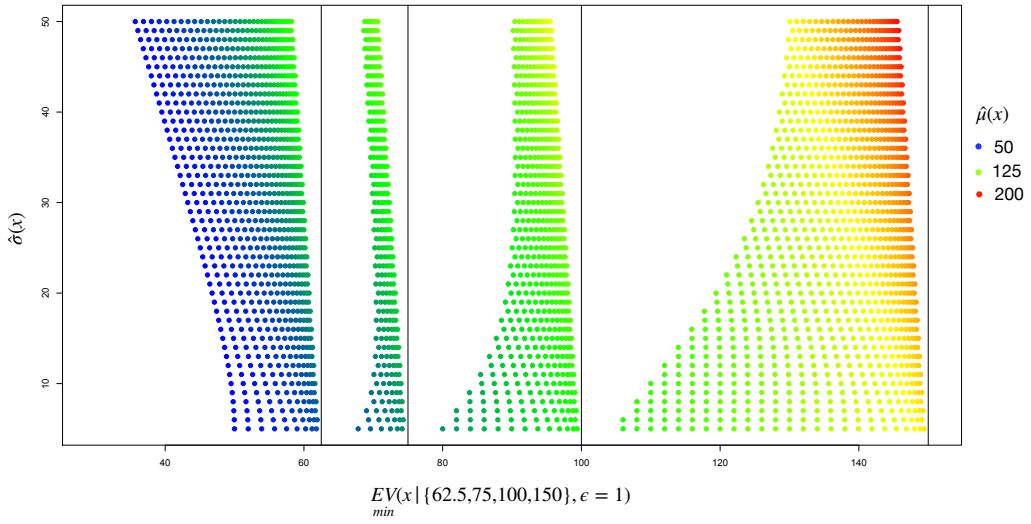

(a) $\epsilon = 1$

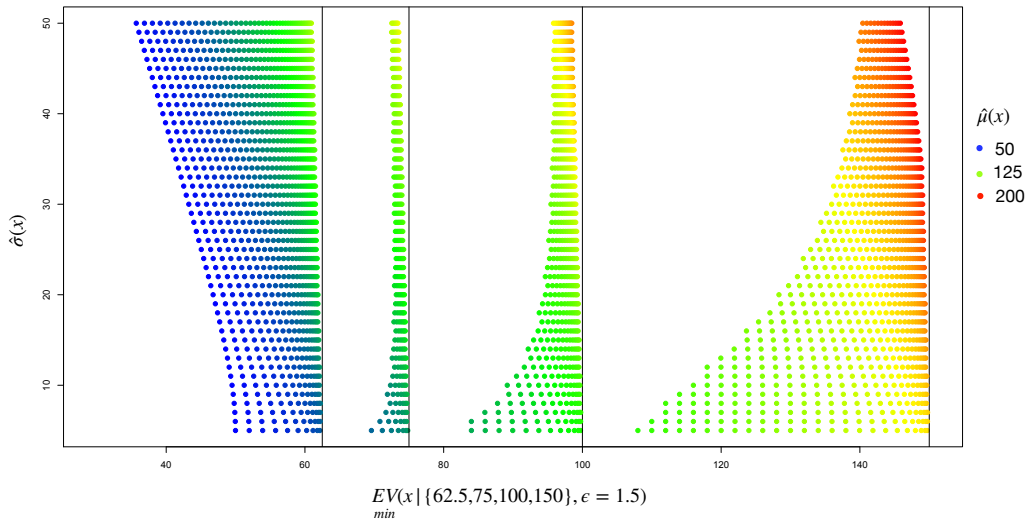

(b) $\epsilon = 1.5$

Some of the special cases where it converges to Utopian value and Nadir value as reference is shown in Figs. 6.7 and 6.8.

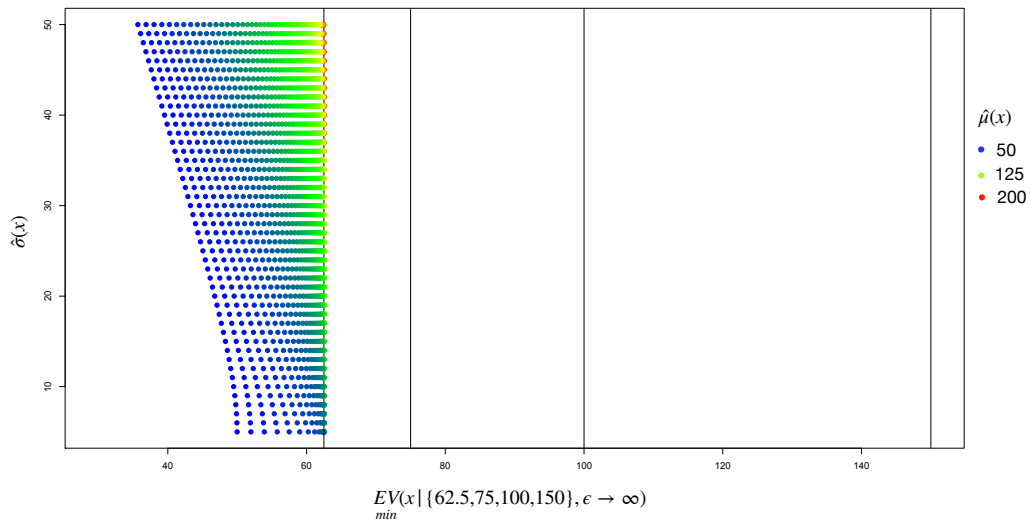

Figure 6.7: $\epsilon \to \infty$, which is equivalent to optimising with Utopian value as reference

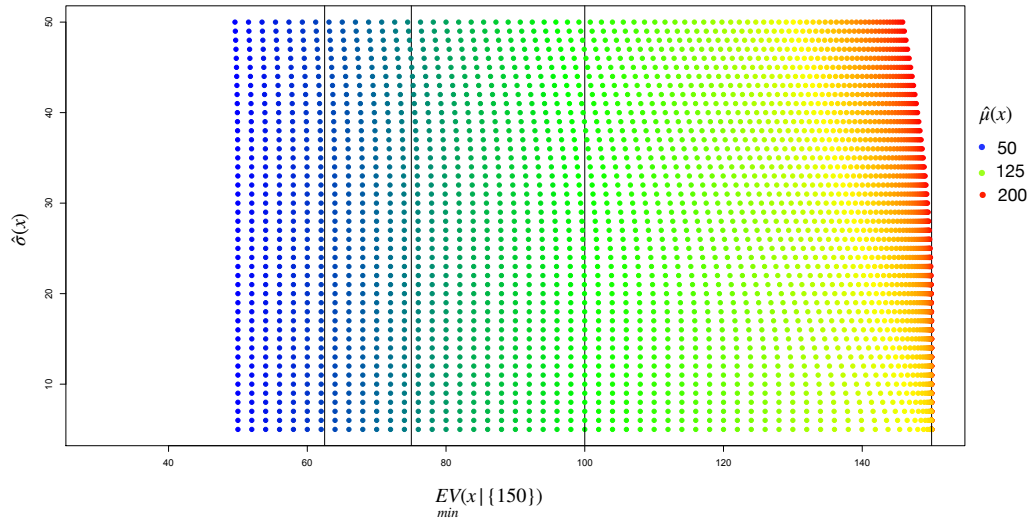

Figure 6.8: EV with Nadir value as reference

7 Shape optimisation of disc-pad system

All the results presented in the following discussion were obtained for the objectives defined in §5.1. The $\mathcal{GP}$ meta-model was defined for the computationally expensive objective function C_{s} where we used a linear polynomial trend function to define the prior mean and the covariance function was defined by Matern 5/2 kernel considering anisotropic spatial correlation. Hence, in the context of MOBO, the infill points were determined primarily for the evaluation of the function C_{s}. Even though in our case, the $\mathcal{GP}$ model for MOBO was defined only for one of the objectives, it can be extended for MOBO with multiple $\mathcal{GP}$s.

We present a brief description on the characteristics of the Pareto-front obtained for MOBO through an *EV* criterion. The discontinuities appear in the Pareto-front of Figure 7.1 due to local definition of improvement, since the optimization is defined with multiple reference values where the discontinuities occur, but with in the same optimization setting to define NDS through NSGA-2. This means that the individuals in a given generation of NSGA-2 are defined with their respective reference values to seek improvement, but the non-dominated sorting and niching are defined on the objective space as a whole –which is less computationally expensive given the simultaneous definition of improvement which use several reference values.

The optimization for the infill points through NSGA-2 was defined with the following parameters:

- Population size: 200
- No. of generations: 50
- Crossover definition: Simulated Binary crossover (SBX)
- SBX distribution index: 8
- Crossover probability: 0.9
- Mutation definition: Polynomial Mutation
- Polynomial Mutation index: 20
- Mutation probability: 0.2

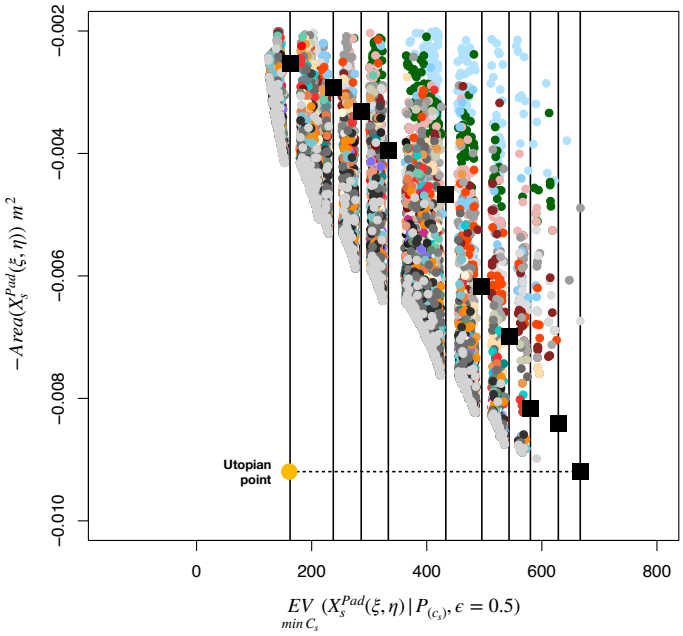

Figure 7.1: Optimization for infill points with EV criterion and $-Area(\check{\boldsymbol{X}}_s^{\mathrm{p}})$. The colored points represent the population, with each color representing a generation obtained through NSGA-2. The black squared points are the empirical Pareto-front points ($\mathbf{P}_{(C_s)}$) in the objective space and the vertical lines correspond to the empirical Pareto-front points which are used as reference values for the EV criterion. (We here remind that the coordinates of the EV criterion correspond to the coordinates of the objective space)

Mutation probability was restricted due to more probability for failure with constraints in defining $\check{\boldsymbol{X}}_s^{\mathrm{p}}$. This is balanced with increase in the population size and the number of generations for convergence.

In general, with EV criterion, the initial generation starts with largely individuals whose eligibility for reference value will be far from the Utopian value –where the eligibility depends on the parameter ϵ in (6.36)– and through the progression of the generations will reach the individuals which will be eligible for improvement regarding the Utopian value. This is shown in Figure 7.3 for the EV criterion with $\epsilon = 1$, along with comparison for EI criterion in Figure 7.2 with Utopian value as reference, where a same $\mathcal{GP}$ model was used for both the cases.

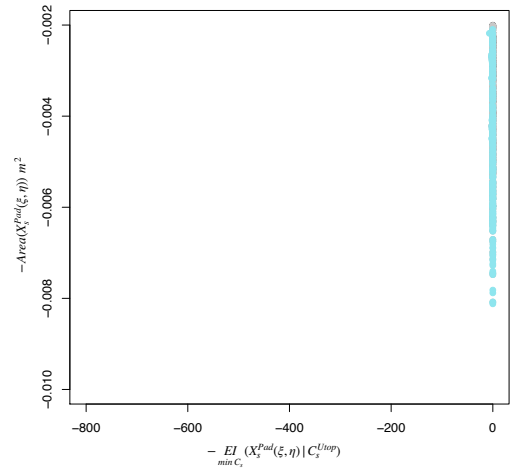

(a) Iteration 4:

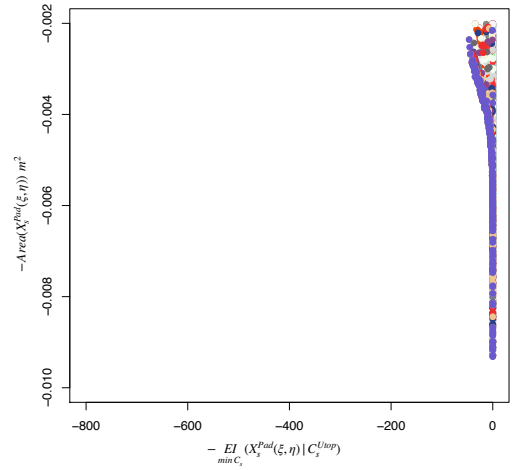

(b) Iteration 22:

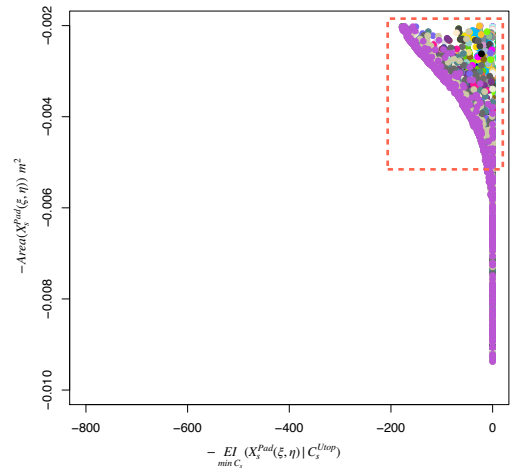

(c) Iteration 50:

Figure 7.2: Optimization for infill points with EI criterion and $-Area(\check{\boldsymbol{X}}_s^{\mathrm{p}})$. The colored points represent the population with each color representing a generation obtained through NSGA-2.The red highlight at the iteration 50 is to be compared with the iteration 50 from figure 7.3.

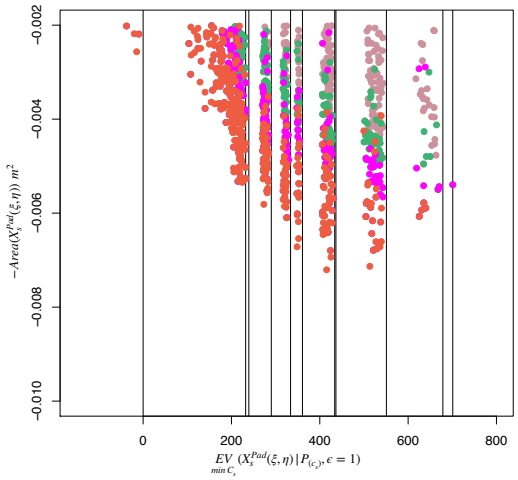

(a) Iteration 4:

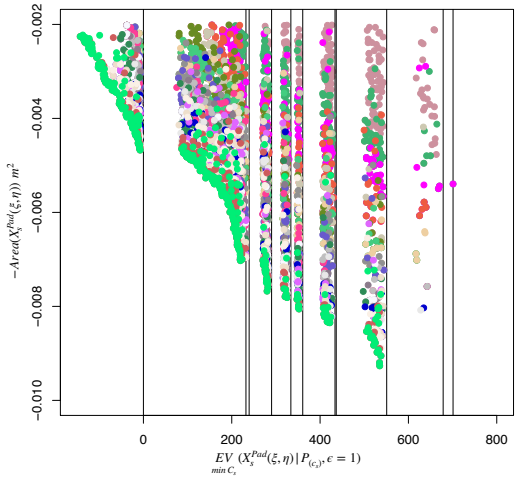

(b) Iteration 22:

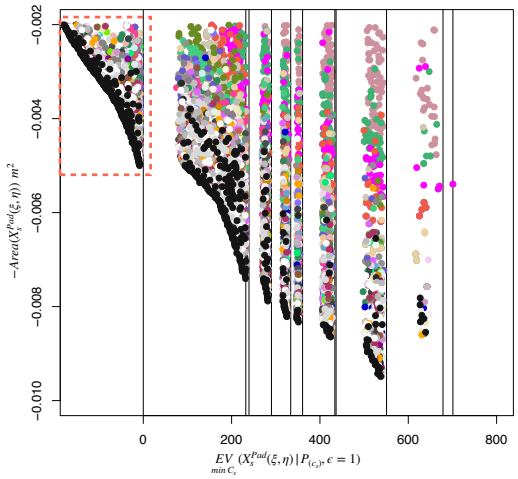

(c) Iteration 50:

Figure 7.3: Optimization for infill points with EV criterion and $-Area(\check{\boldsymbol{X}}_s^{\mathrm{p}})$. Optimization of acquisition function defined by EV criterion to determine infill points. Population with each color representing a generation obtained through NSGA-2 for Min. EV. The red highlight at the iteration 50 is to be compared with the iteration 50 from figure 7.2.

When comparing Figure 7.2 and Figure 7.3, the optimization of EI with Utopian value as reference has some correspondance to the optimization of EV with Utopian value as one of the reference values, which can be seen at the Iteration 50 for both the cases. This is quite expected since the improvement related to the Utopian value is the same for both the criteria atleast in the region where some probability for improvement exists given through the parameter ϵ for the EV criterion. In the region where improvement was not possible to be defined for the EV given an Utopian value, the resolution for EI was very poor, which happens as $Area(\check{\boldsymbol{X}}_s^{\mathrm{p}})$ increases. But for the EV, for a larger $Area(\check{\boldsymbol{X}}_s^{\mathrm{p}})$, the optimization was defined with a reference value more probable. The above comparison shows the limitation of defining improvement based on a single reference value where we chose Utopian value to define the EI criterion, and hence justifies the definition of improvement with EV criterion in our application. The limitation of a single reference value can also be shown through Nadir value which we did not expose here, but a theoretical justification to this limitation was given in .

Though in the above case there was a possibility to define some improvement linked with the Utopian value for the EI criterion, but it cannot be in general. This is possible when the Utopian value may correspond to the extremum of the function, where the EI with Utopian value as reference can fail to define improvement completely since there can be no possibility to define improvement related to a given extremum. But the EV criterion can adapt to define improvement with respect to the next possible reference value.

Though we have not provided results to show the effect of the parameter ϵ, it is also possible to infer through (6.36) that the discontinuities in the NDS will become stronger with increase in the value of ϵ and converges to the case similar to EI with Utopian value as reference, except in different coordinates. The opposite is true with decrease in ϵ where the EV converges to EI with Nadir value as reference.

We discussed the optimization to determine the infill points and now we show its consequence in the objective space for improvement in NDS of the sampled arguments. The improvement of the NDS for the sampled arguments in the objective space through the progression of iterations for MOBO with the EV criterion is shown in the Figure 7.4.

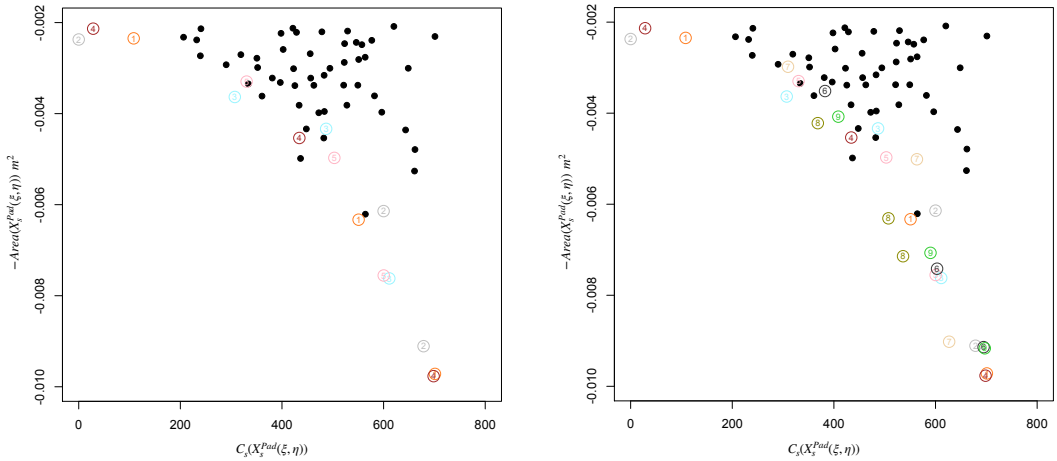

(a) Iterations 1-4:

(b) Iterations 1-8:

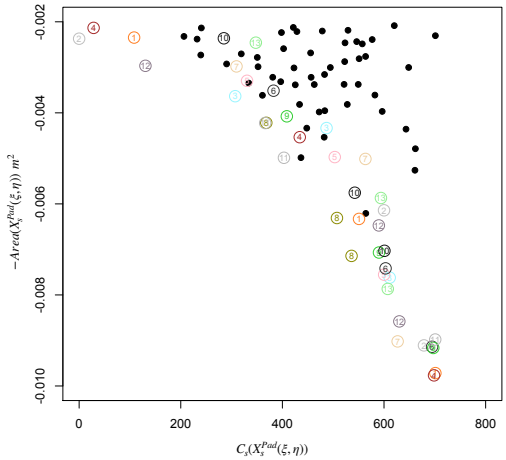

(c) Iterations 1-12:

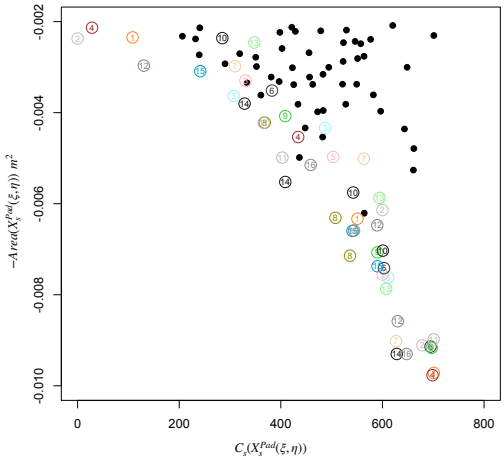

(d) Iterations 1-16:

Figure 7.4: Objective space : $C_{\mathsf{s}}(\check{\boldsymbol{X}}_s^{\mathrm{p}}) \,|\, \Im(\boldsymbol{\Lambda}(\check{\boldsymbol{X}}_s^{\mathrm{p}})) \in [10KHz, 13KHz]$ and $-Area(\check{\boldsymbol{X}}_s^{\mathrm{p}})$. Addition of infill points with progression of iteration for MOBO with EV criterion. Black points represent the initial samples. The colored circles represent the Infill points, with 3 infill points per iteration, where each color represents an iteration with the iteration number.

The MOBO optimization (shown in Figure 7.4) was initiated with an initial sample size of 50 which satisfy the constraints after Latin-Hypercube sampling (LHS) and an addition of 48 infill points were added, with 3 points per iteration for a total of 16 iterations. As it can be seen, the initial samples did not cover any designs with larger $Area(\check{\boldsymbol{X}}_s^{\mathrm{p}})$, which is due to very few designs in this region and hence, all the designs with larger $Area(\check{\boldsymbol{X}}_s^{\mathrm{p}})$ were purely obtained in the process of optimization. The improvement in the NDS can also be seen where all the NDS in the final iteration were obtained through the infill points. We also see some overlap of infill points but clustering through K-means in the design space shows that the overlapping points mostly correspond to completely different clusters, as seen in Figure 7.5, which also indicates the multi-modality of the function $C_{\mathtt{s}}$. The multi-modality maybe also due to the redundancies in the design space as explained in section . The overlapping can also be attributed to the choice of infill points from the NDS obtained for the optimization of the infill points, where we did not choose any metric for diversification but with the metric of uncertainity..

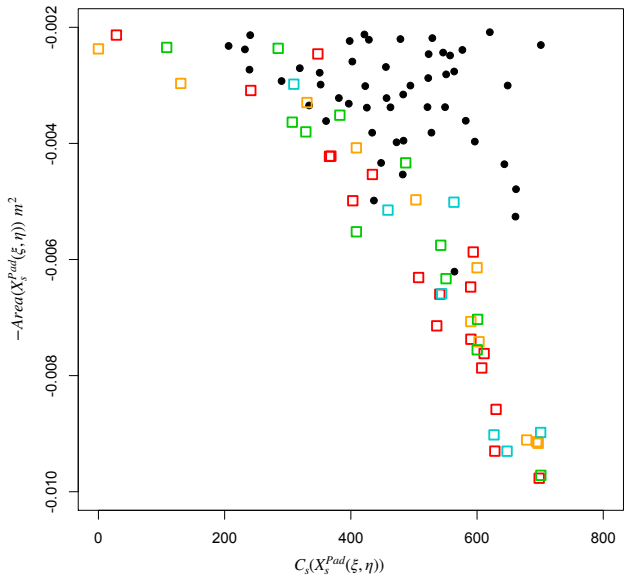

Figure 7.5: Objective space : $C_{\mathtt{s}}(\check{\boldsymbol{X}}_s^{\mathrm{p}}) \,|\, \Im(\boldsymbol{\Lambda}(\check{\boldsymbol{X}}_s^{\mathrm{p}})) \in [10KHz, 13KHz]$ vs $-Area(\check{\boldsymbol{X}}_s^{\mathrm{p}})$. Clustering of the infill points, with each color representing a cluster and black points representing the initial samples

The following measures of time are given in an approximate sense for a general notion of the time involved in the given MOBO. We used a 10 physical cores ($x86\_64$) machine, equipped with $252GB$ of ECC RAM. It took a total of 53 hours to reach the given empirical Pareto-front, for which 36 hours were spent on optimisation of the infill points, which was necessary given the design space and the constraints involved. Each iteration of NSGA-2 took approximately 150 seconds, where most of the time was spent on constraint evaluation, and hence 50 iterations in NSGA-2 took 2 hours to find the converged pareto-front for MOO of the infill points. The evaluation of the stability criteria C_s took around 22 minutes with parallelization, where the parallelization was initialized for 20 friction coefficients between 0 to 1. With the availability of 10 cores, the parallelization was achieved in two batches, with a minute taken for each batch. This would have otherwise taken an additional 20 minutes to evaluate C_s. Since the parallelization was defined for the evaluation of C_s, this restricted the use of parallelization in MOBO, at least given the resources. After analysis of the time involved in each step of the MOBO, we realized that it would have been better to utilize parallelization for MOBO rather than evaluating C_s, since it would have cut time in our case to 47 hours, given that three infill points were chosen for evaluation of C_s per iteration in MOBO.

We expose some of the shapes from the objective space in Figure 7.6. It can be observed that, largely for a given $Area(\check{\boldsymbol{X}}_s^{\mathrm{p}})$ to achieve a low value of $C_{\mathsf{s}}(\check{\boldsymbol{X}}_s^{\mathrm{p}})$, the pad shapes prefer to align more radially to the the disc than rather tangentially. It also seems that the pad shapes prefer to achieve a shape with three vertices, even though the shapes are defined with four vertices i.e., four curves of C^0 continuity between them, where one of the vertices is smoothed out with some continuity or one of the edges was defined to be very small to mimic a three vertices configuration. The existence of very few solutions when $Area(\check{\boldsymbol{X}}_s^{\mathrm{p}})$ is larger can be attributed to lack of design space where this explains the lack of improvement related to $C_{\mathsf{s}}(\check{\boldsymbol{X}}_s^{\mathrm{p}})$ in this region. While, in the region of the objective space for smaller $Area(\check{\boldsymbol{X}}_s^{\mathrm{p}})$, there is more flexibility in defining the pad designs $\check{\boldsymbol{X}}_s^{\mathrm{p}}$ and hence, better improvement in solutions relative to $C_{\mathsf{s}}(\check{\boldsymbol{X}}_s^{\mathrm{p}})$ were obtained. We also obtained an interesting solution from this region with no instability as it can be observed, i.e., $C_{\mathsf{s}}(\check{\boldsymbol{X}}_s^{\mathrm{p}}) \,|\, \Im(\Lambda(\check{\boldsymbol{X}}_s^{\mathrm{p}})) \in [10KHz, 13KHz] = 0$.

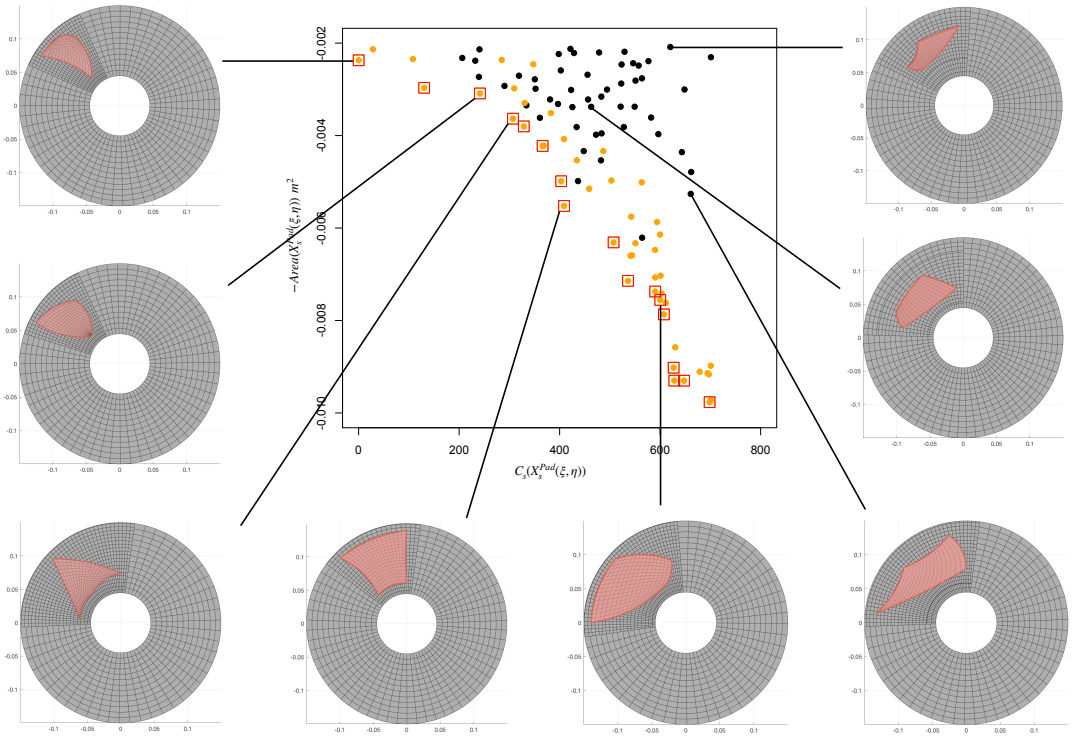

Figure 7.6: A sample of shapes from the objective space are shown. Black points represent the initial samples, Orange points represent the infill points and the NDS obtained after 16 iterations of MOBO are highlighted in red.

For a given initial sample, we provide a comparison in the objective space for the infill points obtained with the EV criterion against the same number of infill points obtained through the EI criterion, given in the Figure 7.7, where more NDS were found to be obtained through the EV criterion. The hypervolume comparison between the two cases corresponds to sample 1 in Figure 7.8, which was considered with infill points from 15 iterations.

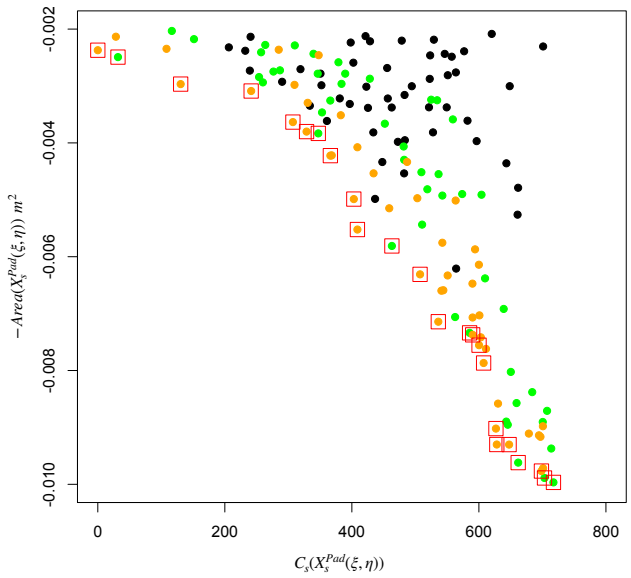

Figure 7.7: Objective space : $C_{\mathbf{s}}(\check{\boldsymbol{X}}_s^{\mathrm{p}}) \,|\, \Im(\boldsymbol{\Lambda}(\check{\boldsymbol{X}}_s^{\mathrm{p}})) \in [10KHz, 13KHz]$ vs $-Area(\check{\boldsymbol{X}}_s^{\mathrm{p}})$. Comparison of infill points obtained between EV and EI criteria for an initial sample. Black points represent the initial samples. Orange and green points represent infill points obtained by EV and EI respectively, with red highlights for the NDS.

In order to show the effect of initial samples to the improvement achieved through MOBO with EI and EV criteria in the objective space, the optimisation was performed with 5 different initial samples for 15 iterations, with 3 infill points per iteration. The hypervolume improvement comparison is shown in Figure 7.8 where EV criterion outperforms for all initial samples. We here remind that the infill points were chosen not with the goal of HVI but to reduce the uncertainty of the solutions from each cluster of the NDS obtained for the optimization of infill points, but consequently, this shows better improvement with EV criterion because of better resolution in defining the NDS. Further, the overall variation of the dominated hypervolume for each criterion, with comparison between the criteria are shown in Figure 7.9.

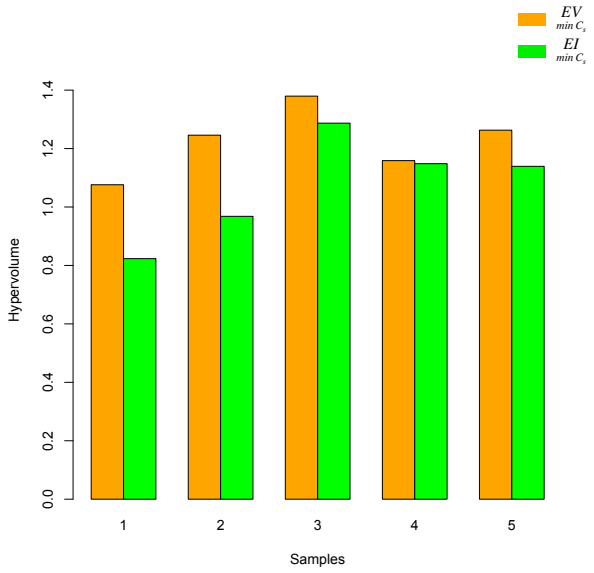

Figure 7.8: Comparison between EV and EI criteria for hypervolume improvement of NDS linked with the NDS of the initial samples, shown for a five set of initial samples.

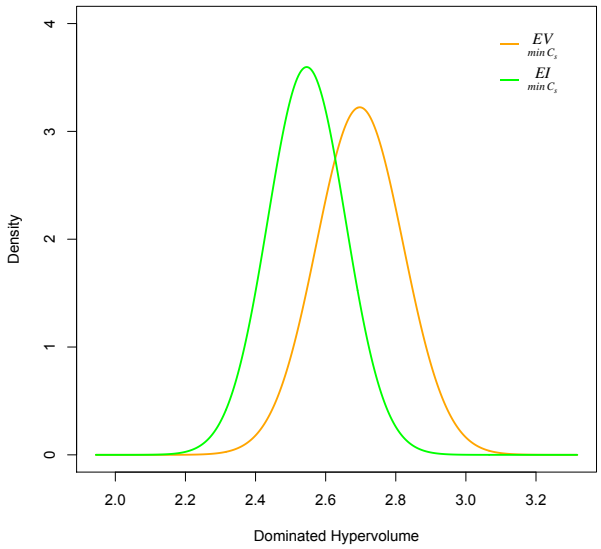

Figure 7.9: The variation of the dominated hypervolume for the NDS with initializing samples, obtained for the same set of initial samples in Figure 7.8.

8 Conclusion

We proposed an efficient strategy to deal with the shape optimization of brake systems through a simple disc-pad representation for squeal noise reduction. The weak formulation of contact and friction specific for modelling friction induced instabilities through CEA was defined with isogeometric approach for discretisation. This kind of study may be considered for braking systems as found in automotive or aeronautic industry, but also for other applications with friction phenomena, such as clutch. Through CEA, the stability criterion C_{s} was defined as a black-box function to characterize the instabilities independent of friction coefficient for the shape optimization, where parallel computation and dynamic model reduction techniques were used to reduce the computational cost of the stability criterion.

In parameterizing the computational domain for the disc-pad system with NURBS, a multi-patch parameterization strategy was realized for the disc domain to achieve local refinement at the contact interface. While, the parameterization of the pad shapes was achieved through the discrete Coon's patch method. Hence, the design space in shape optimization was constrained to the pad shapes for which injective parametrization exists with the Coon's patch method. This was found to provide satisfactory shapes which are less conceptual for a pad design at the reduced cost of more advanced parameterization techniques which require expensive optimization, though we are interested in such conceptual shapes for future works. The injective parameterization obtained through the Coon's patch method was also found to have a good quality parameterization required for CEA, where it can be difficult to define a robust meshing for even such shapes with the classical finite elements without severe element distortion. Though we are aware that the meshing can be achieved irrespective of the domain with the classical finite elements when robustness is not questioned, which is simply not possible with the body-fitted NURBS parameterization. Nevertheless, provided an intial parameterization for a design description, the sub-sequent analysis-suitable parameterization can be easily achieved which is the underpinning of the Isogeometric approach, but defining an injective initial parameterization can be cumbersome at least for a shape optimization with arbitrary definition of shapes, or given a parameterization scheme, the question also arises for the bounds of the design space where a good quality parameterization exists.

Moving on to MOBO, the expensive stability criterion was approximated through a $\mathcal{GP}$ meta-model and a MOO was defined for minimizing the instability and maximizing the contact area. The NDS were obtained through MOBO for a given number of iterations where a new criterion EV was defined as an extension of the classical EI

criterion for better resolution in MOO. The infill points obtained at each iteration of the MOBO were observed to provide consistent improvement in the NDS. Further, the hypervolume metric of the NDS was found to be better with the EV criterion compared to the EI criterion for the considered MOO, where the comparison was made with five random initializations. Some of the shapes from the NDS and the worst performing shapes were shown for comparison, where some empirical observations were discussed. It was also clear from the optimization that the instabilities at some narrow frequency range as much as 3 KHz can be reduced or completely eliminated through shape optimization irrespective of the friction coefficient. We are aware that real-life braking systems can involve more complex non-linearities, with more complex domain rather than a simple disc-pad representation which can effect the understanding of the dynamics. Nevertheless, the above frame work with CEA and the disc-pad system can be used for preliminary understanding of the dynamics purely linked with shapes in a design process, where CEA is already widely used in industries for squeal analyses. The optimization framework of MOBO could also be extended with more complex considerations for which the meta-heuristic approach is more generic irrespective of the objective functions and the constraints present, where we only tested for a bi-objective case with $\mathcal{GP}$ meta-modelisation for one of the objectives.

For future scope, it is important to consider experimental validation of contact stiffness and sensitivity of the characteristics to be inferred in relation to modelling contact and friction. It can be a good starting to expand the optimisation with robustness consideration, given that suitable parameterisation strategy is developed with in the scope of body-fitted Isogeometric approach to achieve any possible shape variation. Typical geometries in application are far more complex and in the scope of defining a generic parameterisation scheme, Immersed method seem to be a more viable approach or even defining a generic strategy to decompose a topology with multiple patches. This is especially useful to capture design features such as holes which can sometimes be sensitive to the defined application. We tested the Bayesian optimisation for the prescribed only for biobjective problem

9 Annexe

9.1 Mesh sensitivity for Node-to-Node contact

In relation to the expensive evaluation of the stability criteria, mesh convergence study was performed for the influence of mesh at the contact interface and outside the contact interface. The eigenmodes reflecting maximum instability as predicted by the maximum positive real part of the complex eigenvalues are only of interest to us and hence taken in to account to check for convergence. It should be noted that contact formulation can have some influence on mesh convergence with CEA, where no clear studies has been performed. In this case, we define convergence with node-to-node contact formulation.

The dynamic properties with respect to maximum instability show little variation for change in mesh size out of the contact region for a given shape and number of contact points. The comparison is shown through a model with highly coarse mesh as in Fig. 9.1 against a model with the same shape but for a relatively fine mesh as in Fig. 9.2, while maintaining the same number and position for the contact points. The mismatch in frequencies between the models is shown in Fig. 9.3 where the range for frequency is zoomed to a pair of frequencies which induce mode coalescence predicted to cause the maximum instability. The shift in unstable frequencies and the point of bifurcation of the maximum real part as shown in Fig. 9.4 are observed to be very low for change in mesh size.

Though the variation of the mesh out of the contact interface is shown to have a little influence on the maximum instability, the variation of mesh at the contact interface is observed to have a considerable effect on the dynamic properties. This can be seen by comparing results of the models in Fig. 9.1 and Fig. 9.2 against the models in Fig. 9.5 and Fig. 9.6 which are of the same shape. Hence, it is intuitive to assume a large number of contact points, since the contact interface is a continuum after all. The convergence is shown with large number of contact points in Fig. 9.5 and Fig. 9.6 with plot for bifurcation of the real part in Fig. 9.8) and frequencies inducing maximum instability in Fig. 9.7.

The definition of the contact points can be observed to have significant influence on the maximum real part of the complex eigenvalues and hence also the stability criteria, which demands a good mesh definition to define a robust stability criteria in optimisation. For this reason, we defined a structured mesh as in Fig. 9.9 where

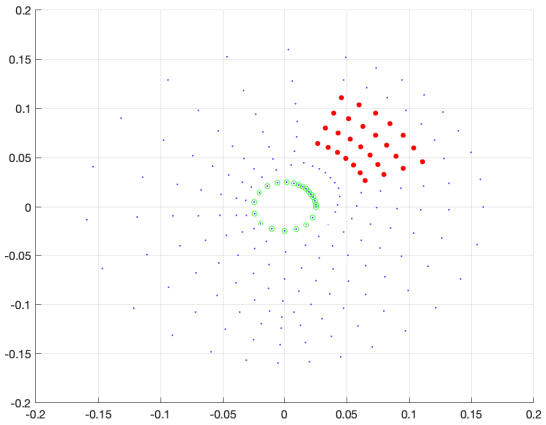

Figure 9.1: Node plot for a coarse mesh of the disc geometry with contact nodes represented in red

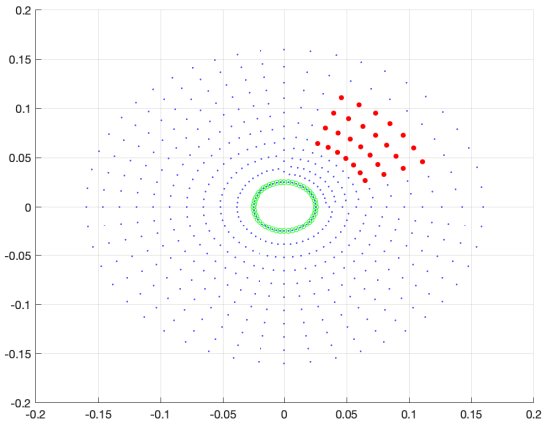

Figure 9.2: Node plot for a relatively fine structured mesh of the disc geometry with contact nodes represented in red

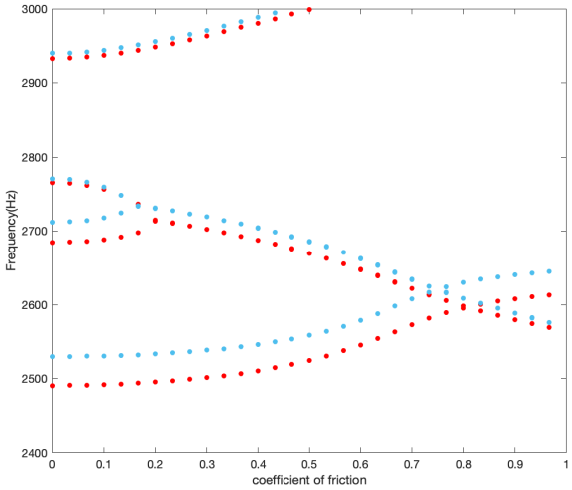

Figure 9.3: Plot of Frequency vs Friction coefficient, of modes showing maximum instability; Blue represents for the model in 9.1; Red represents for the model in 9.2

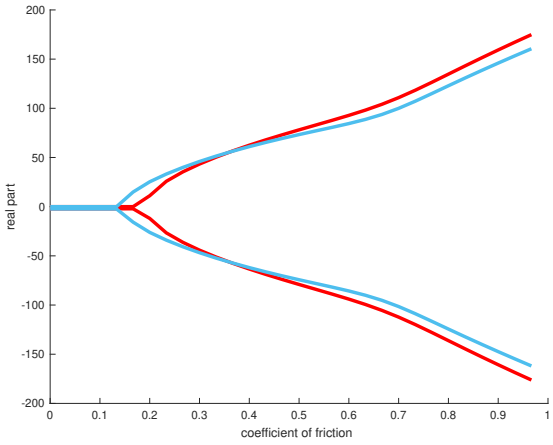

Figure 9.4: Plot of Real part of the complex eigenvalues vs Friction coefficient, of modes showing maximum instability; Blue represents for the model in 9.1; Red represents for the model in 9.2

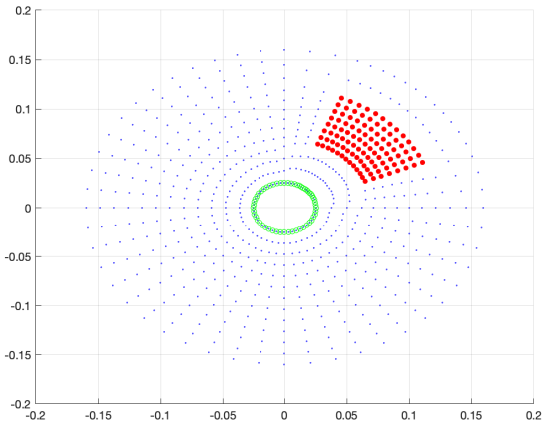

Figure 9.5: Node plot for a fine mesh with contact nodes represented in red

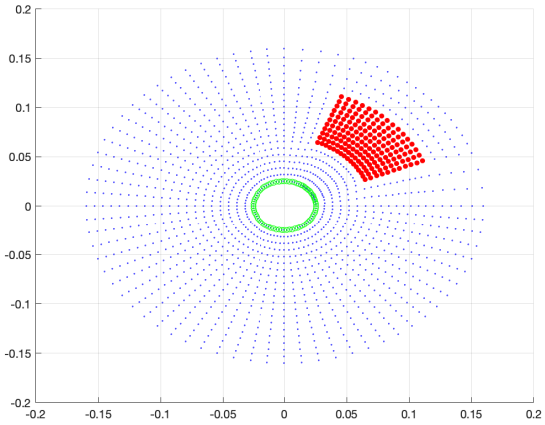

Figure 9.6: Node plot for a relatively finer mesh compared to 9.5, especially on the contact interface with contact nodes represented in red

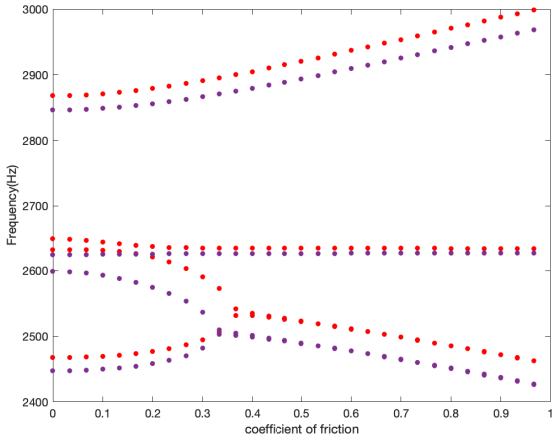

Figure 9.7: Plot of Frequency vs Friction coefficient, of modes showing maximum instability; Red represents the plot for the model in 9.5; Violet represents the plot for the model in 9.6

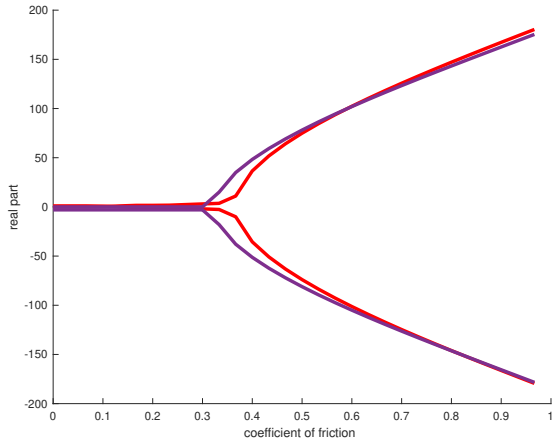

Figure 9.8: Plot of Real part of the complex eigenvalues vs Friction coefficient, of modes showing maximum instability; Red represents the plot for the model in 9.5; Violet represents the plot for the model in 9.6

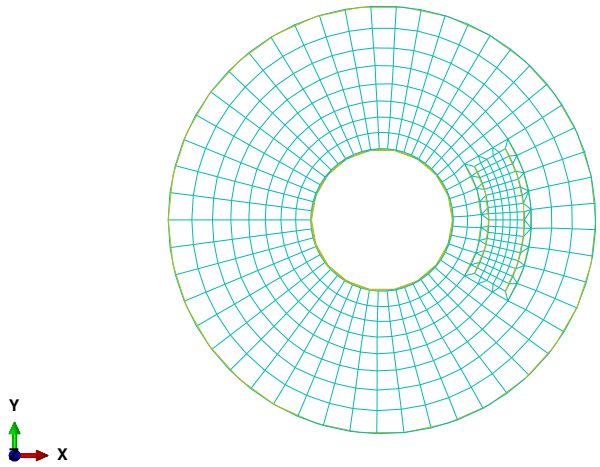

Figure 9.9: Considered mesh definition

linear hexahedral elements are largely used through out the model with smaller elements at the contact interface, while the region outside of contact interface is defined by larger elements. The difference in mesh density is compromised by introducing 3D wedge elements to maintain a structured mesh.

Bibliography

[1] Grégoire Allaire, François Jouve, and Anca-Maria Toader. Structural optimization using sensitivity analysis and a level-set method. Journal of Computational Physics, 194(1):363–393, 2004.

[2] J. Simon. Differentiation with respect to the domain in boundary value problems. Numerical Functional Analysis and Optimization, 2(7-8):649–687, 1980.

[3] Kohei Shintani and Hideyuki Azegami. Shape optimization for suppressing brake squeal. Structural and Multidisciplinary Optimization, 50(6):1127–1135, Dec 2014.

[4] A Francavilla, C V Ramakrishnan, and O C Zienkiewicz. Optimization of shape to minimize stress concentration. Journal of Strain Analysis, 10(2):63–70, 1975.

[5] V. Braibant and C. Fleury. Shape optimal design using b-splines. Computer Methods in Applied Mechanics and Engineering, 44(3):247–267, 1984.

[6] R. Haftka and R. Grandhi. Structural shape optimization — a survey. Applied Mechanics and Engineering, 57:91–106, 1986.

[7] R. Salomon. Evolutionary algorithms and gradient search: similarities and differences. IEEE Transactions on Evolutionary Computation, 2(2):45–55, 1998.

[8] Thomas Bäck and Hans-Paul Schwefel. An overview of evolutionary algorithms for parameter optimization. Evolutionary Computation, 1(1):1–23, 1993.

[9] P. Frazier. A tutorial on bayesian optimization. ArXiv, abs/1807.02811, 2018.

[10] B. Shahriari, K. Swersky, Z. Wang, R. P. Adams, and N. de Freitas. Taking the human out of the loop: A review of bayesian optimization. Proceedings of the IEEE, 104(1):148–175, 2016.

[11] K. Deb, A. Pratap, S. Agarwal, and T. Meyarivan. A fast and elitist multiobjective genetic algorithm: Nsga-ii. IEEE Transactions on Evolutionary Computation, 6(2):182–197, 2002.

[12] E. Zitzler and L. Thiele. Multiobjective evolutionary algorithms: a comparative case study and the strength pareto approach. IEEE Trans. Evol. Comput., 3:257–271, 1999.

[13] C.M. Fonseca and P.J. Fleming. Multiobjective optimization and multiple constraint handling with evolutionary algorithms. i. a unified formulation. IEEE Transactions on Systems, Man, and Cybernetics - Part A: Systems and Humans, 28(1):26–37, 1998.

[14] C.M. Fonseca and P.J. Fleming. Multiobjective optimization and multiple constraint handling with evolutionary algorithms. ii. application example. IEEE Transactions on Systems, Man, and Cybernetics - Part A: Systems and Humans, 28(1):38–47, 1998.

[15] Brian Prasad and Raphael Haftka. Optimal structural design with plate finite elements. Journal of the Structural Division, American Society of Civil Engineers (ASCE), 105:2367–2382, 11 1979.

[16] S.S. Bhavikatti and C.V. Ramakrishnan. Shape optimization of structural systems using finite elements and sequential linear programming. In ALVIN WEXLER, editor, Large Engineering Systems, pages 224–235. Pergamon, 1977.

[17] L. Piegl and W. Tiller. The NURBS Book. Monographs in Visual Communication. Springer Berlin Heidelberg, 1996.

[18] T.J.R. Hughes, J.A. Cottrell, and Y. Bazilevs. Isogeometric analysis: Cad, finite elements, nurbs, exact geometry and mesh refinement. Computer Methods in Applied Mechanics and Engineering, 194(39):4135–4195, 2005.

[19] E. Cohen, T. Martin, R.M. Kirby, T. Lyche, and R.F. Riesenfeld. Analysis-aware modeling: Understanding quality considerations in modeling for isogeometric analysis. Computer Methods in Applied Mechanics and Engineering, 199(5):334–356, 2010. Computational Geometry and Analysis.

[20] Leslie A Piegl and Arnaud M Richard. Tessellating trimmed nurbs surfaces. Computer-Aided Design, 27(1):16–26, 1995.

[21] Dominik Schillinger, Luca Dede, Michael Scott, John Evans, Michael Borden, Ernst Rank, and Thomas Hughes. An isogeometric design-through-analysis methodology based on adaptive hierarchical refinement of nurbs, immersed boundary methods, and t-spline cad surfaces. Computer Methods in Applied Mechanics and Engineering, s 249–252:116–150, 12 2012.

[22] Ernst Rank, Martin Ruess, Stefan Kollmannsberger, Dominik Schillinger, and Alexander Düster. Geometric modeling, isogeometric analysis and the finite cell method. Computer Methods in Applied Mechanics and Engineering, s 249–252:104–115, 12 2012.

[23] Gang Xu, Bernard Mourrain, Régis Duvigneau, and André Galligo. Parametrization of computational domain in isogeometric analysis: methods and comparison. Computer Methods in Applied Mechanics and Engineering, 200(23-24):2021–2031, April 2011.

[24] A Limkilde, A Evgrafov, J Gravesen, and Angelos Mantzaflaris. Practical isogeometric shape optimization: Parameterization by means of regularization. Journal of computational design and engineering, January 2021.

[25] Florian Buchegger and Bert Jüttler. Planar multi-patch domain parameterization via patch adjacency graphs. Computer-Aided Design, 82:2–12, 2017. Isogeometric Design and Analysis.

[26] T. Maquart, Y. Wenfeng, T. Elguedj, A. Gravouil, and M. Rochette. 3d volumetric isotopological meshing for finite element and isogeometric based reduced order modeling. Computer Methods in Applied Mechanics and Engineering, 362:112809, 2020.

[27] Gerald Farin and Dianne Hansford. Discrete coons patches. Computer Aided Geometric Design, 16(7):691–700, 1999.

[28] K. Miettinen. Nonlinear multiobjective optimization. In International series in operations research and management science, 1998.

[29] J. Koski. Defectiveness of weighting method in multicriterion optimization of structures. Communications in Applied Numerical Methods, 1:333–337, 1985.

[30] T. Athan and P. Papalambros. A note on weighted criteria methods for compromise solutions in multi-objective optimization. Engineering Optimization, 27:155–176, 1996.

[31] H. Ishibuchi, Yuji Sakane, N. Tsukamoto, and Y. Nojima. Simultaneous use of different scalarizing functions in moea/d. In GECCO '10, 2010.

[32] Yutao Qi, X. Ma, F. Liu, L. Jiao, J. Sun, and Jianshe Wu. Moea/d with adaptive weight adjustment. Evolutionary Computation, 22:231–264, 2014.

[33] E. Hughes. Evolutionary many-objective optimisation: many once or one many? 2005 IEEE Congress on Evolutionary Computation, 1:222–227 Vol.1, 2005.

[34] C. K. Williams and C. Rasmussen. Gaussian processes for regression. In NIPS, 1995.

[35] J. Kleijnen. Kriging metamodeling in simulation: A review. Eur. J. Oper. Res., 192:707–716, 2009.

[36] Donald Jones, Matthias Schonlau, and William Welch. Efficient global optimization of expensive black-box functions. Journal of Global Optimization, 13:455–492, 12 1998.

[37] Tobias Wagner, Michael Emmerich, André Deutz, and Wolfgang Ponweiser. On expected-improvement criteria for model-based multi-objective optimization. In International Conference on Parallel Problem Solving from Nature, pages 718–727, 01 2011.

[38] Michael T. M. Emmerich, André H. Deutz, and Jan Willem Klinkenberg. Hypervolume-based expected improvement: Monotonicity properties and exact computation. In 2011 IEEE Congress of Evolutionary Computation (CEC), pages 2147–2154, 2011.

[39] Andreia P. Guerreiro, C. Fonseca, and Luís Paquete. The hypervolume indicator: Problems and algorithms. ArXiv, abs/2005.00515, 2020.

[40] Shinkyu Jeong and Shigeru Obayashi. Multi-objective optimization using kriging model and data mining. International Journal of Aeronautical and Space Sciences, 7:1–12, 06 2006.

[41] MR North. Disc brake squeal: a theoretical model. MIRA Noneaton, 1972.

[42] A. Akay. Acoustics of friction. The Journal of the Acoustical Society of America, 111:1525–48, 05 2002.

[43] R. A. Ibrahim. Friction-Induced Vibration, Chatter, Squeal, and Chaos—Part I: Mechanics of Contact and Friction. Applied Mechanics Reviews, 47(7):209–226, 07 1994.

[44] R. A. Ibrahim. Friction-Induced Vibration, Chatter, Squeal, and Chaos—Part II: Dynamics and Modeling. Applied Mechanics Reviews, 47(7):227–253, 07 1994.

[45] Quoc Nguyen and Franck Moirot. Brake squeal: A problem of flutter instability of the steady sliding solution? Archives of Mechanics, 4:645–662, 01 2000.

[46] H. D. Hibbit. Some follower forces and load stiffness. International Journal for Numerical Methods in Engineering, 14(6):937–941, 1979.

[47] G. Herrmann. Dynamics and Stability of Mechanical Systems with Follower Forces. NASA Contractor Report. National Aeronautics and Space Administration, 1971.

[48] A. R. Abu-Bakar and H Ouyang. Complex eigenvalue analysis and dynamic transient analysis in predicting disc brake squeal. International Journal of Vehicle Noise and Vibration, 2, 01 2006.

[49] J. E. Mottershead and S. N. Chan. Flutter Instability of Circular Discs with Frictional Follower Loads. Journal of Vibration and Acoustics, 117(1):161–163, 01 1995.

[50] J.A.C. Martins, S. Barbarin, M. Raous, and A. Pinto da Costa. Dynamic stability of finite dimensional linearly elastic systems with unilateral contact and coulomb friction. Computer Methods in Applied Mechanics and Engineering, 177(3):289 – 328, 1999.

[51] E. Denimal, L. Nechak, J.-J. Sinou, and S Nacivet. A novel hybrid surrogate model and its application on a mechanical system subjected to friction-induced vibration. Journal of Sound and Vibration, 434:456–474, 2018.

[52] L. Nechak, S. Besset, and J.-J. Sinou. Robustness of stochastic expansions for the stability of uncertain nonlinear dynamical systems – application to brake squeal. Mechanical Systems and Signal Processing, 111:194–209, 2018.

[53] Gaetano Fichera. Existence Theorems in Elasticity, pages 347–389. Springer Berlin Heidelberg, Berlin, Heidelberg, 1973.

[54] Gaetano Fichera. Boundary Value Problems of Elasticity with Unilateral Constraints. In Linear Theories of Elasticity and Thermoelasticity, pages 391–424. Springer Berlin Heidelberg, 1973.

[55] N. Kikuchi and J.T. Oden. Contact Problems in Elasticity: A Study of Variational Inequalities and Finite Element Methods. Studies in Applied Mathematics. Society for Industrial and Applied Mathematics, 1988.

[56] Marius Cocu. Existence of solutions of signorini problems with friction. International Journal of Engineering Science, 22(5):567–575, 1984.

[57] J.A.C. Martins and J.T. Oden. Existence and uniqueness results for dynamic contact problems with nonlinear normal and friction interface laws. Nonlinear Analysis: Theory, Methods & Applications, 11(3):407–428, 1987.

[58] G. Duvaut and J.L. Lions. Inequalities in Mechanics and Physics. Grundlehren der mathematischen Wissenschaften in Einzeldarstellungen mit besonderer Berücksichtigung der Anwendungsgebiete. Springer-Verlag, 1976.

[59] J. J. Moreau and P. D. Panagiotopoulos. Unilateral Contact and Dry Friction in Finite Freedom Dynamics, pages 1–82. Springer Vienna, Vienna, 1988.

[60] J.T. Oden and J.A.C. Martins. Models and computational methods for dynamic friction phenomena. Computer Methods in Applied Mechanics and Engineering, 52(1):527–634, 1985.

[61] S.H. Strogatz and M. Dichter. Nonlinear Dynamics and Chaos, 2nd ed. SET with Student Solutions Manual. Studies in Nonlinearity. Avalon Publishing, 2016.

[62] A. Klarbring, A. Mikelić, and M. Shillor. Frictional contact problems with normal compliance. International Journal of Engineering Science, 26(8):811–832, 1988.

[63] P. Rabier, J.A.C. Martins, J.T. Oden, and L. Campos. Existence and local uniqueness of solutions to contact problems in elasticity with nonlinear friction laws. International Journal of Engineering Science, 24(11):1755–1768, 1986.

[64] Lars-Eric Andersson. A quasistatic frictional problem with normal compliance. Nonlinear Analysis: Theory, Methods & Applications, 16(4):347–369, 1991.

[65] Roy R Craig and Mervyn C C Bampton. Coupling of Substructures for Dynamic Analyses. AIAA Journal, 6(7):1313–1319, 1968.

[66] Norbert Hoffmann, Michael Fischer, Ralph Allgaier, and Lothar Gaul. A minimal model for studying properties of the mode-coupling type instability in friction induced oscillations. Mechanics Research Communications, 29:197–205, 07 2002.

[67] Davide Bigoni and Giovanni Noselli. Experimental evidence of flutter and divergence instabilities induced by dry friction. Journal of the Mechanics and Physics of Solids, 59:2208–2226, 10 2011.

[68] Jean-Jacques Sinou and Louis Jézéquel. Mode coupling instability in friction-induced vibrations and its dependency on system parameters including damping. European Journal of Mechanics - A/Solids, 26(1):106 – 122, 2007.

[69] Y. Bazilevs, V.M. Calo, J.A. Cottrell, J.A. Evans, T.J.R. Hughes, S. Lipton, M.A. Scott, and T.W. Sederberg. Isogeometric analysis using t-splines. Computer Methods in Applied Mechanics and Engineering, 199(5):229 – 263, 2010. Computational Geometry and Analysis.

[70] TJR Hughes, JA Cottrell, and Y Bazilevs. Isogeometric analysis: Cad, finite elements, nurbs, exact geometry and mesh refinement. Computer Methods in Applied Mechanics and Engineering, 194(39-41):4135–4195, 2005.

[71] Peter Wriggers. Finite element algorithms for contact problems. Archives of Computational Methods in Engineering, 2:1–49, 12 1995.

[72] İ. Temizer, P. Wriggers, and T.J.R. Hughes. Contact treatment in isogeometric analysis with nurbs. Computer Methods in Applied Mechanics and Engineering, 200(9):1100–1112, 2011.

[73] M.E. Matzen, T. Cichosz, and M. Bischoff. A point to segment contact formulation for isogeometric, nurbs based finite elements. Computer Methods in Applied Mechanics and Engineering, 255:27–39, 2013.

[74] L. Lorenzis, P. Wriggers, and T. Hughes. Isogeometric contact: a review. Gamm-mitteilungen, 37:85–123, 2014.

[75] B. Yang, T. Laursen, and X. Meng. Two dimensional mortar contact methods for large deformation frictional sliding. International Journal for Numerical Methods in Engineering, 62:1183–1225, 2005.

[76] Ericka Brivadis, Annalisa Buffa, Barbara Wohlmuth, and Linus Wunderlich. Isogeometric mortar methods. Computer Methods in Applied Mechanics and Engineering, 284:292–319, 2015. Isogeometric Analysis Special Issue.

[77] M.E. Matzen and M. Bischoff. A weighted point-based formulation for isogeometric contact. Computer Methods in Applied Mechanics and Engineering, 308:73–95, 2016.

[78] I.M Sobol′. Global sensitivity indices for nonlinear mathematical models and their monte carlo estimates. Mathematics and Computers in Simulation, 55(1):271 – 280, 2001. The Second IMACS Seminar on Monte Carlo Methods.

[79] Hervé Monod, C Naud, and David Makowski. Uncertainty and sensitivity analysis for crop models. Working with Dynamic Crop Models, pages 55–100, 01 2006.

[80] Carlotta Giannelli, Bert Jüttler, and Hendrik Speleers. Thb-splines: The truncated basis for hierarchical splines. Computer Aided Geometric Design, 29(7):485 – 498, 2012.

[81] J. Mockus. Application of bayesian approach to numerical methods of global and stochastic optimization. Journal of Global Optimization, 4:347–365, 1994.

[82] J. Knowles. Parego: a hybrid algorithm with on-line landscape approximation for expensive multiobjective optimization problems. IEEE Transactions on Evolutionary Computation, 10(1):50–66, 2006.

[83] Wudong Liu, Qingfu Zhang, Edward Tsang, Cao Liu, and Botond Virginas. On the performance of metamodel assisted moea/d. In Lishan Kang, Yong Liu, and Sanyou Zeng, editors, Advances in Computation and Intelligence, pages 547–557, Berlin, Heidelberg, 2007. Springer Berlin Heidelberg.

[84] Michael Emmerich, Kyriakos Giannakoglou, and Boris Naujoks. Single- and multiobjective evolutionary optimization assisted by gaussian random field metamodels. Evolutionary Computation, IEEE Transactions on, 10:421 – 439, 09 2006.

[85] Nicola Hochstrate, Boris Naujoks, and Michael Emmerich. Sms-emoa: Multiobjective selection based on dominated hypervolume. European Journal of Operational Research, 181:1653–1669, 02 2007.

[86] Anne Auger, Johannes Bader, Dimo Brockhoff, and Eckart Zitzler. Articulating User Preferences in Many-Objective Problems by Sampling the Weighted Hypervolume. In Genetic and Evolutionary Computation Conference (GECCO 2009), pages 555–562, Montreal, Canada, July 2009.

[87] Pramudita Satria Palar, Kaifeng Yang, Koji Shimoyama, Michael Emmerich, and Thomas Bäck. Multi-objective aerodynamic design with user preference using truncated expected hypervolume improvement. In Proceedings of the Genetic and Evolutionary Computation Conference, GECCO '18, page 1333–1340, New York, NY, USA, 2018. Association for Computing Machinery.

[88] Andy Keane. Statistical improvement criteria for use in multiobjective design optimisation. AIAA Journal, 44:879–891, 01 2006.

[89] Shinkyu Jeong, Youichi Minemura, and Shigeru Obayashi. Optimization of combustion chamber for diesel engine using kriging model. Journal of Fluid Science and Technology, 1(2):138–146, 2006.